2023

Anteromedial Thalamus Gates the Selection & Stabilization of Long-Term Memories

Andrew Toader

ANTEROMEDIAL THALAMUS GATES THE SELECTION & STABILIZATION OF LONG-TERM MEMORIES

A Dissertation

Presented to the Faculty of the David Rockefeller Graduate Program

in Biosciences

in Partial Fulfillment of the Requirements for the Degree of

Doctor of Philosophy

by

Andrew Toader

November 2022

ANTEROMEDIAL THALAMUS GATES THE SELECTION & STABILIZATION OF LONG-TERM MEMORIES

Andrew Toader, The Rockefeller University, 2022

The hippocampus is necessary for the initial encoding and recent storage of memories. Under the standard model of systems consolidation, it is thought that the memory trace eventually reorganizes from the hippocampus to a distributed cortical network, with the anterior cingulate cortex playing a central role in remote memory retrieval. However, little is known about the mechanisms responsible for coordinating this process. Additionally, the intermediate memory representations in the brain and the circuits that might gate and select memories for permanent storage remain unknown. To facilitate the longitudinal tracking of memory circuits in the brain, we first developed a novel virtual reality-based behavioral task for mice. We used fiber photometry to record neural activity from multiple regions across the brain throughout consolidation and identified a unique and significant neural correlate of memory in anterior thalamus that emerged in training and persisted for weeks. Inhibition of the anteromedial thalamus to anterior cingulate cortex projections during training resulted in substantial memory consolidation deficits, whereas excitation of the same projection drove the consolidation of otherwise unconsolidated memories. To gain mechanistic understanding into the role of anteromedial thalamus during consolidation, we developed a technique for imaging three brain regions simultaneously with single-cell resolution in the behaving mouse. Using this technology, we uncovered that the anteromedial thalamus rapidly forms preferential tuning to consolidated memories, and establishes inter-regional correlations that are causally required for synchronizing and stabilizing cortical representations to achieve successful memory consolidation.

Biographical Sketch

Andrew Toader was born on May 22, 1994 in Kalamzoo, Michigan. In 2016, he graduated *magna cum laude* from Duke University with a dual degree in Biomedical Engineering and Electrical and Computer Engineering. After graduating, he worked for a year at the National Institutde for Neurological Disorders and Stroke in the laboratory of Dr. Eric Wassermann, where he studied the ability of transcranial magnetic stimulation to modulate functional brain connectivity and memory. In 2017, he began at the Tri-Institutional MD-PhD program at Weill Cornell/Rockefeller/Sloan-Kettering. After two years of medical school and several laboratory rotations, he began his PhD work under the mentorship of Dr. Priyamvada Rajasethupathy at The Rockefeller University. His work aims to discover and characterize the circuits that gate and facilitate the process of memory consolidation.

Acknowledgements

I have been incredibly fortunate to have studied at The Rockefeller University, a highly collaborative scientific community full of researches at the top of their fields. In particular, I am thankful to have had the honor and privilege of working under Dr. Priya Rajasethupathy, a mentor whose passion and skill for scientific inquiry is eclipsed only by her dedication to mentorship. When I was just a rotation student in her lab, Priya would set aside hours to simply chat about life, science, and any ideas that we both found fascinating. This excitement never wavered through the years, from big picture discussion at our regular meetings, to sitting down and combing through details of various imaging techniques or analyses - regardless of how busy she was. I owe who I am as a scientist to Priya, and I am so grateful to have had to opportunity to work with her.

Additionally, I would like to thank the rest of the Rajasethupathy Lab for their constant support and expertise. Without Josue Regalado, my co-author and partner in lab since day one, none of this work would be possible. To Vivian, thank you for your undying support even when things were not going according to plan. Alessandra, you have been a foundation of support for me and the everyone in the lab; thank you for all that you do for us. And thank you to the rest of the rest of the lab, both former and present members - Nakul, Andrea, Zach, James, Jak, Andrew, Yujin, Sloane, Chelsea, Milli, Suraj, and more - you've made the laboratory a wonderful place to do science.

I am also very grateful for my thesis committee, Dr Leslie Vosshall, Dr. Charles Gilbert, and Dr. Conor Liston, for investing time and effort toward shaping my project and my

growth as a scientist. Your feedback and support has been crucial to the development of this thesis.

I would also like to thank my family for their unconditional love and support throughout my educational career. And finally to my friends, who have been with me through my highs and my lows, thank you for being you.

Table of Contents

List of Figures

Chapter 1

Introduction

1.1 The history of memory consolidation

Our lives are built up of a constant stream of information, some of which persists as memories that can be stored and retrieved for days-to-years later. This remarkable ability of the brain to create what is an essentially permanent imprint of experience is central to our lives, and provides stability to our identify. This is glaringly obvious in cases of individuals that have lost this ability, who are forever stuck in the present. Why is it though that in most of us, some memories - such as what one had for lunch last Tuesday - fade, while others - such as the layout of one's childhood home - may last a lifetime ?

The idea that memory strength changes over time is an old one, dating back at least to the ancient Romans. In his series of of writings, *Institutio Oratoria*, rhetorician Quintillian stated: "...the power of recollection...undergoes a process of ripening and maturing during the time which intervenes." (Quintillian, First Century A.D.) Despite little documentation, this idea likely persisted through the middle ages and resurfaced occasionally,

such as when philosopher David Hartley proposed that dreaming may alter the strength of associative memories (Hartley, 1791). However, it was not until the late 1800's when the field of experimental psychology emerged that memory research became a quantitative science. German psychologist Herman Ebbinghaus believed that memory was the result of a physical process instantiated by the brain, and that this process could be measured (Ebbinghaus, 1885). In his experiments, Ebbinghaus generated a list of hundreds of syllabus which he then recited and attempted to recall in a consistent fashion. Among other things, he quantified the number of repetitions needed to attain a high accuracy, and identified what is known as the "forgetting curve", describing the decline in memory retention over time. With this approach, Ebbinghaus laid the foundation for future experiments on memory in both humans and animals.

One such set of experiments was carried out soon after Ebbinghaus by Müller and Pilzecker around the turn of the 19th century (Müller and Pilzecker, 1900). Similar to Ebbinghaus, Müller and Pilzecker used a list of nonsense syllables, this time in pairs, and tested subjects on their accuracy for syllable-pair recall after a fixed number of trials. When testing recall at specific time intervals, they found that errors made by subjects tended to be other syllables from the same list, rather than unrelated syllables. Notably, this effect appeared strongest in the first 10 minutes after training, but not later. Subjects also reported anecdotally that syllable pairs entered their mind intrusively in the time between trials. Müller and Pilzecker labeled this effect "preservation", and suggested that it may be caused by transient activity in the brain that is necessary to strengthen the formed associations in memory. To test this claim, they designed a new set of experiments aimed at disrupting preservation. First, subjects were to memorize a list of syllable pairs (List A). After a short delay, a second list of syllable pairs was presented (List X). After a longer interval of 6 minutes, memory for list A was tested. Separately, subjects were trained on a third list (List B), and then tested after 6 minutes without an intervening list. Memory

recall for list A was significantly worse than for list B, suggesting that engaging with list X while list A had recently been learned disrupted the memory for list A, an effect they termed ”retroactive inhibition” (Figure 1.1). They found evidence for retroactive inhibition even if list X was instead replaced with a completely unrelated set of stimuli. To explain these effects of preservation and retroactive inhibition, Müller and Pilzecker concluded that in the minutes following a learned association, the memory is ”consolidated” to strengthen the association, and during consolidation, memory is particularly sensitive to disruption.

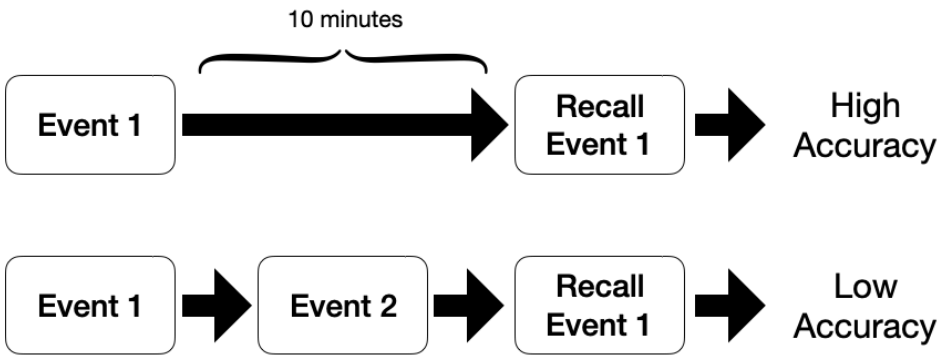

Figure 1.1 | **Retroactive Inhibition.** General principle of retroactive inhibition. There is a critical window in the minutes after an event where intervening stimuli can disrupt recall for the original event, suggesting that memories are ”consolidated” during this time.

Other researches soon realized that memory consolidation could explain certain cases of retrograde amnesia following brain injury or electroconvulsive shock (Ribot, 1883, Duncan, 1949). As William Bunham in his 1903 article suggested, “The fixing of an impression depends upon a physiological process. It takes time for an impression to become so fixed that it can be reproduced after a long interval; for it to become part of a permanent store of memory considerable time may be necessary” (Burnham, 1903). Thus, the field of psychology had opened the door to understanding what we call ”memory consolidation”, but what of the biological underpinnings of this process?

1.2 The biological basis of memory consolidation

It is now believed that memory consolidation occurs in two phases: synaptic consolidation in the minutes-to-hours after memory formation, and systems consolidation in the days, weeks, and even years after. Evidence for synaptic consolidation first started with the early studies on the cellular basis of memory. At the turn of the 20th century, Santiago Ramon Y Cajal first hypothesized that memories are formed at the connections, or synapses, between cells (Ramón y Cajal, 1894). This idea gained much support, but it was not until mid century and the works of Jerzy Konorski (Konorski, 1948), Donald Hebb, and others, that the field had a working model for learning and memory in biological networks. Hebb proposed the dual-trace theory, whereby short term memory was held in reverberations in the connections between neurons (echoing Müller and Pilzecker's preservation theory), and structural changes in these connections led to long-term memory (Hebb, 1949). Evidence for these structural changes came from studies demonstrating the necessity of protein synthesis after learning for memory formation (Flexner et al., 1963, Barondes and Cohen, 1966). In the 1970's Eric Kandel and colleagues meticulously described the sequence of molecular and cellular changes occurring during behaviorally relevant memory formation in invertebrates (Bailey and Kandel, 1993) which would end up being the predominate model for synaptic plasticity across the animal kingdom. Several key proteins have been identified as central to the induction and maintenance of long-term memory such as CREB (Dash et al., 1990), CaMKII (Lisman et al., 2002), and PKMζ (Serrano et al., 2008). Synaptic consolidation thus refers to these processes, which involve a cascade of transcriptional and translational programs occurring in neurons, and which are particularly sensitive to disruption in these early moments. However, as stated above, there is a second, slower form of consolidation that is thought to occur in the brain, which will be the focus of the remainder of this thesis.

Evidence for a slow consolidation initially came from brain-injury patients with a temporally-graded retrograde amnesia (Burnham, 1903). These patients reported preserved memory for remote events, but were unable to recall from experiences occurring close in time to the lesion. This pattern suggested to neurologists that memory might be localized to a particular area of the brain, and that these memories take a while (months, sometimes years) to consolidate. However, the diffuse nature of these injuries and the otherwise resilience of memory to lesions (Lashley, 1950) made identifying the site of memory storage difficult to localize.

A major breakthrough came in the 1950's when Brenda Milner and William Scoville published a report on patient H.M. who had a curious case of amnesia (Scoville and Milner, 1957). H.M. had had a bilateral removal of his hippocampus, along with surrounding parts of his medial temporal lobe, for treatment of intractable epilepsy. Despite the benefit toward his epilepsy, the surgery left patient H.M. with severe memory deficits. Just as the patients mentioned above, he had a temporally-graded retrograde amnesia as well as a profound anterograde amnesia - he was unable to form new memories. Due to the focal nature of his lesion, Scoville and Milner were able to attribute his memory deficits with the hippocampus and associated structures for the first time. Through their careful psychological testing, they and others were able to conclude that the hippocampus is required for the initial formation and temporary recall of episodic memories, but after some time (months to years), these memories appear to become independent of the hippocampus and are consolidated elsewhere in the brain. These findings were replicated in other cases of patients with hippocampal damage (Russell and Nathan, 1946, Zola-Morgan et al., 1986, Sanders and Warrington, 1971, Teng and Squire, 1999). Furthermore, the role of the hippocampus in the initial encoding of memory was generalizable to other mammals such as rodents in the case of such tasks as contextual fear conditioning (Kim and Fanselow, 1992), socially acquired food preference (Winocur, 1990), and spatial

learning (Morris et al., 1982), as well as in nonhuman primates with object discrimination (Salmon et al., 1987). This role was further bolstered by functional studies such as the discovery of long-term potentiaion in the rabbit hippocampus by Bliss and Lomo (Bliss and Lømo, 1973), and the local identification single-neuron signals for learned associations (Wirth et al., 2003, 2009, Rutishauser et al., 2006). However, if memories only initially depend on the hippocampus, where do they end up?

1.3 Models of systems consolidation

The neuroscientist David Marr was among the first to propose a theory for systems consolidation in the early 1970's (Marr, 1970, 1971). Under this model, the hippocampus forms rapid associations as memories, and over time trains the neocortex to store the memory more permanently. Through the process of consolidation, the cortex is thought to extract semantics and schema from memories (Winocur et al., 2010). This model was further developed by Larry Squire and others (Squire and Alvarez, 1995), and grew into what is now referred to as Standard Systems Consolidation Theory. The primary purpose of this model was to explain the temporally graded retrograde amnesia exhibited by patient H.M. and others with selective hippocampal lesion, though where exactly memory resided in the longer-term remained an open question.

Research in animal models revealed that remote memory retrieval appeared to activate a widely distributed cortical network in both animals and humans (Bontempi et al., 1999, Wiltgen et al., 2004, Maviel et al., 2004, Smith et al., 2010). Certain areas, such as the prefrontal and retrosplenial cortices reliably showed increased responsiveness to the recall of remote but not recent memories. Within a cortical region, the activity pattern also shift from layers V-VI to more the superficial layers II-III, where most cortico-cortico

projections terminate. One area in particular seemed to have the strongest reactivation to remote memories - the anterior cingulate cortex (ACC) (Frankland et al., 2004). The ACC is reciprocally connected to sensory, motor, and limbic areas of the brain, supporting its role in integrating information from many sources. The role of the ACC in remote memory retrieval was confirmed by several inactivation or lesion studies in animals (Takehara et al., 2003, Vetere et al., 2011). Though likely working in concert with other areas, the ACC appears to be a major site of memory recall after systems consolidation.

Under standard systems consolidation theory, memory is thought to reach the cortex through repeated activations of hippocampal-cortical networks (O'Reilly and Rudy, 2000, Buzsáki, 1989). This can happen through active recall, but also likely happens during sleep, spefically during non-rapid eye movement sleep (Rothschild, 2019). During this period of time, it has been found that the hippocampus exhibits patterns of strong, synchronous activation of many neurons. This firing can be detected in the local electrical field potential and is referred to as a sharp-wave ripple (SWR), a high amplitude, 150-250 Hz depolarization (Joo and Frank, 2018). Though the SWR occurs most frequently during sleep, though it can occur in the awake state, usually during periods of quiet rest. Interestingly, SWRs contain sequences of neural activity that repeat those seen during a prior experience. During a SWR, hippocampal "place cells" that represent a path traversed through space during wake are compactly reactivated in sequence, either forward or reverse (Pfeiffer and Foster, 2013, Foster and Wilson, 2006, Wu and Foster, 2014). Thus they represent a neural correlate of hippocampal replay. Crucially, disrupting SWRs during sleep impairs memory performance (Girardeau et al., 2009), but cortical stimulation immediately following a SWR improves hippocampal-cortical coordination alongside memory performance (Maingret et al., 2016). In fact, the SWR co-activates extrahippocampal cortical regions (including the ACC), suggesting a neural mechanism for the reorganization of information during systems consolidation (Siapas and Wilson, 1998, Wang and

Ikemoto, 2016, Remondes and Wilson, 2015, Atherton et al., 2015).

Direct connections between the hippocampus and ACC are sparse (Jay et al., 1992), so which circuits might be involved during systems consolidation? The entorhinal cortex, part of the medial temporal lobe structure, functions anatomically as one of the main input-output gateways between the hippocampus and the rest of the cortex (Witter et al., 2017), and thus may play a role in facilitating consolidation. Disrupting the entorhinal cortex during memory encoding produces a temporally-graded amnesia similar to hippocampal lesions, disrupting the recall of remote but not recent memories (Cho et al., 1993). This region also appears to facilitate long-term cortical memory encoding by strengthening hippocampal-cortical communication (Cho et al., 1993, Robinson et al., 2017). Furthermore, recently formed memories are associated with increased functional connectivity between hippocampus and entorhinal cortex, while older memories are associated with increased entorhinal cortex – ACC connectivity(Takehara-Nishiuchi et al., 2012). A recent study showed that cortical memory representations and remote recall were disrupted if entorhinal input to ACC was inhibited during training (Kitamura et al., 2017). While a major step forward, the small effect sizes suggest contributions from other areas as well. Thus many open questions remain (Takehara-Nishiuchi, 2014), but clearly much can be learned by analyzing circuits intermediate to the hippocampus and cortex.

It should be noted that significant evidence suggests that the cortex is likely engaged not just late but also early on during memory formation (Barker and Warburton, 2008, Bero et al., 2014, Rajasethupathy et al., 2015, Ito et al., 2015), especially when integrating prior knowledge into existing information (Tse et al., 2011). In these cases, the rate of memory consolidation may be facilitated by binding information to connecting neurons representing existing ”schemas”. Additionally, learning is thought to ”tag” certain cortical neurons that may eventually become part of the consolidated memory trace (Les-

burguères et al., 2011). Thus, models of standard system consolidation theory typically state that early memory representations are stored in both the hippocampus and cortex, and the hippocampal-dependency fades, while the cortical representations are maintained or strengthed (Figure 1.2).

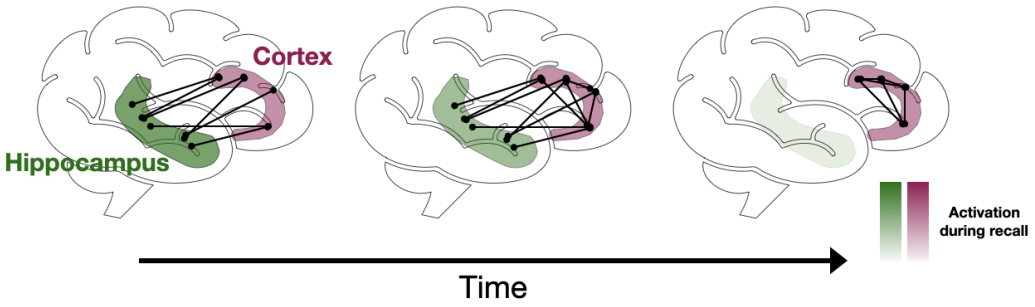

Figure 1.2 | **Standard systems consolidation theory.** Under the standard theory of systems consolidation, the hippocampus rapidly forms the associations necessary for the initial encoding and retrieval of memories. Over time through repeated interactions, the cortex is eventually able to recall memory independently of the hippocampus

Alternatives to standard systems consolidation theory have also been proposed. The most prominent of these being Multiple Trace Theory (MTT), put forward by Nadel and Moscovitch (Nadel and Moscovitch, 1997). MTT proposes that the hippocampus is always involved in memory retrieval, particularly in the case of detail-rich episodic memories. In this model, the hippocampus acts as a pointer and each reactivation of a memory creates a new pointer (hence "multiple trace"). This model evolved in response to multiple clinical cases of patients exhibiting a flat (equal loss of remote and recent memory), or a particularly prolonged retrograde amnesia after hippocampal lesions (Tulving et al., 1988, Rempel-Clower et al., 1996, Kapur, 1997, Viskontas et al., 2002, Cipolotti et al., 2001). MTT further posits that the cortex is particularly specialized for retaining semantic memory (versus episodic), and thus the memory for facts may persist despite hippocampal damage. Aside from MTT, other theories are still regularly put forward to explain variations in the amnesias exhibited by patients (Yonelinas et al., 2019). However, the many cases of temporally graded retrograde amnesia observed in both humans

and animal studies are undeniable (Zola-Morgan and Squire, 1990, Winocur, 1990, Kim and Fanselow, 1992, Anagnostaras et al., 1999, Kitamura et al., 2017, Gilmore et al., 2021, Vetere et al., 2021).

1.4 Summary

Decades of work have led us to a model of systems consolidation, whereby the initial encoding and recent storage of memories occurs in the hippocampus, but long-term memory eventually becomes hippocampal-independent, likely relying on particular regions of the neocortex for retrieval. What though, are the cellular and circuit-level mechanisms that drive this process? This question remains to be explored in longitudinal studies utilizing both large-scale neural recordings and circuit manipulations. Little is still known about the mechanisms enabling the reorganization of information from the hippocampus to the cortex, or how specific memories are selected to enter permanent storage. A new approach is needed to look across and beyond hippocampal-cortical circuits to identify intermediate brain regions that might play a role in gating and facilitating the process of consolidation. The aim of the present work is to apply these novel techniques to study distributed dynamics of memory across the brain, from their inception through to remote timepoints, and identify key nodes in the brain during systems consolidation.

One such node we identified was a subnucleus of the anterior thalamus, namely the anteromedial thalamus, of which little is still known functionally. However, converging anatomical, physiological, and behavioral data suggest it may be ideally positioned to mediate memory consolidation. In the next section I will briefly review this evidence to provide context and biological plausibility to our findings.

Chapter 2

The anteromedial thalamus and its role in memory

2.1 Anatomy and connectivity

The anteromedial thalamus (AM) is an anatomically and functionally defined region lying along the midline of the anterior nucleus of the thalamus. The anterior thalamus itself has been long known as part of what is called the ”limbic system” of the brain, first described by Thomas Willis in 1664 (Willis, 1664). Historically thought to regulate the experience and expression of emotion, its structure and function was further characterized by anatomist James Papez, who traced out a complete circuit that would eventually bear his name (Papez, 1937). This circuit (Figure 2.1) begins at the hippocampus and follows its main output, the fornix, from the subiculum to both the mammillary bodies at the base of the brain, and the anterior thalamic nuclei. The mamillary bodies themselves send further strong axonal projections to the anterior thalamus in the form of the mam-

millothalamic tract. The anterior thalamus (specifically the AM) then sends projections to the ACC, which in turn projects back to the entorhinal cortex through the cingulum bundle. Finally, the entorhinal cortex interacts strongly with the hippocampus, completing the circuit. The Papez circuit and its intermediate components (between the hippocampus and cingulate cortex) have received little attention in recent decades, though they are now believed to be involved more in memory and spatial processing rather than emotion (Vann and Nelson, 2015, Jankowski et al., 2013). This section will thus focus on reviewing what is currently known about the anterior thalamus - with a focus on AM.

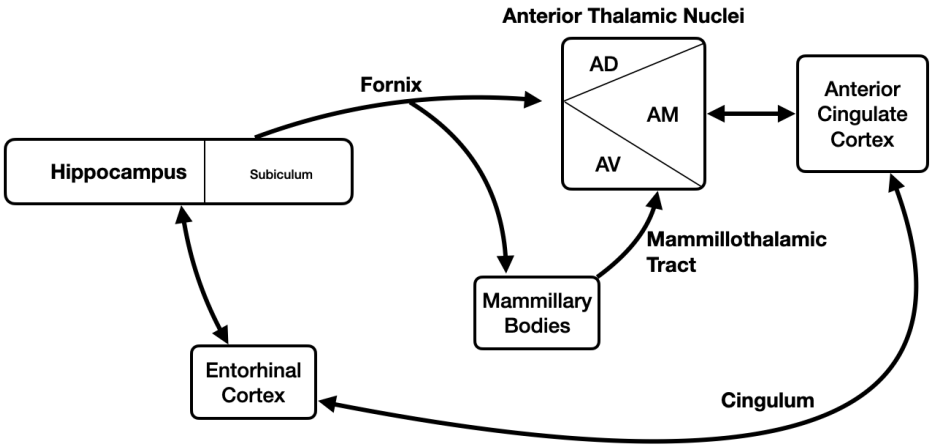

Figure 2.1 | **The Papez Circuit.** Overall anatomical structure and connectivity of the Papez circuit

In addition to the AM, the anterior nucleus of the thalamus also consists of an anterodorsal (AD) and anteroventral (AV) region. As stated above, primary inputs to the anterior thalamic nuclei primarily come either directly from the hippocampus (specifically, the subiculum subregion) through the fornix, or indirectly from the hippocampus via the dense mammillothalamic tract. Additional input is received from the pre- and post- subiculum as well as the retrosplenial cortex (Wright et al., 2010). Within the mammillothalamic tract, medial mammillary bodies project to AM and AV while lateral mammillary bodies project to AD, suggesting complementary functional roles along the medial-lateral axis (Vann and Aggleton, 2004). The primary outputs of the anterior nu-

clei are reciprocal projections back to the hippocampal formation and retrosplenial cortex (Jankowski et al., 2013). Additionally, the AM thalamus appears to uniquely send and receive strong, reciprocal projections to ACC (Shibata and Naito, 2005).

2.2 Functional role in memory

In the 1880's Sergei Korsakoff described a series of cases of patients with severe memory dysfunction, the majority of which were associated with chronic alcohol abuse (Korsakoff, 1887, 1889). It is now known that this syndrome occurs due to an encephalopathy brought on by thiamine deficiency, often in alcoholics. In all cases, damage to the mammillary bodies was implicated. Interestingly, patients who experienced a persistent memory deficit had further damage to the anterior thalamic nuclei (Harding et al., 2000). Other lesions of the anterior thalamic nucleus in particular seem to cause a severe and persistent anterograde amnesia (Aggleton and Sahgal, 1993).However, it is difficult to find cases in patients where the lesion is focally located to just the anterior thalamus and lesions are also likely to damage passing fiber tracts.

More precise studies in animals have allowed us to get a more complete picture of its function. For example, it has been shown that in rodents, the anterior thalamus is active during both encoding and recall of contextual memories (Roy et al., 2022) (corroborated by functional imaging studies in humans, see Geier et al., 2020 and Pergola et al., 2013), and it is required for the remembering of the temporal order of events (Wolff et al., 2006). Furthermore, stimulation of AM thalamus in particular enhances both short and long-term memory (Liu et al., 2021, Chamaa et al., 2021). Other studies have also found a role for spatial processing and spatial memory in the anterior thalamus (Moreau et al., 2013, Mair et al., 2003), often to an even greater degree than the hippocampus. Interestingly, one

recent study found that the AM-ACC is required for attention, specifically in cases with high-interference information (Bubb et al., 2021). Thus, it appears the anterior thalamus - the AM in particular - is well positioned to gate the selection of memories for long-term storage in the cortex, though this remains to be tested.

Little is currently known about individual cellular responses in any of the anterior nuclei during behavior and/or memory formation. From what has been observed, there seems to be coherence with hippocampal theta rhythm, with roughly 40%, 22%, and 6% of AD, AV, and AM cells, respectively, exhibiting theta synchrony (Albo et al., 2003). Theta oscillations are fluctuations in the local field potential in the brain around 6-10 Hz and most frequently observed in the hippocampus, and are thought to be associated with memory and spatial processing. Recordings of theta oscillations in surgical patients from the anterior thalamus suggest they play a role in memory retrieval (Bauch et al., 2018, Tsanov et al., 2011). The other major finding in anterior thalamus is the presence of spatial coding. Though primarily located in AD versus the other two nuclei, ”head direction” cells can be found that code for the direction an animal is facing and might act as an internal compass during navigation (Taube, 1995, 2007). These cells play a causal role in supporting other navigation-related signals in the brain such as head direction cells and grid cells in the parahippocampal cortex, and act independently of hippocampal place cells. (Goodridge and Taube, 1997, Winter et al., 2015, Golob and Taube, 1997).

2.3 Summary

The anteromedial thalamus is a region of the thalamus located intermediately between the hippocampus and prefrontal cortex. Thus, it is unsurprising that converging evidence from multiple sources suggests that it and surrounding nuclei play a role in both memory

processing and spatial navigation. However, much of what we know about this region comes from relatively nonspecific lesion studies in humans and animal models. There is still little-to-no research on the function of the AM thalamus on the level of cells and circuits during behavior. In chapters 3-4, I discuss the exploratory experiments that led us to further investigate activity in the anterior thalamus during memory encoding and retrieval. In chapter 5, I will provide causal evidence for the role of AM thalamus in memory consolidation. Finally, in chapter 6, I detail the first simultaneous live imaging of AM cells alongside hippocampus and cortex, and propose a mechanism for the selection and stabilization of long-term memories in cortex by AM.

Chapter 3

A virtual reality-based task to study memory consolidation

3.1 Introduction

Several different types of behavioral tasks have been used to study hippocampal-dependent memory in animal models, each with their advantages and limitations. In rodents, these are typically divided into two main categories - contextual fear conditioning (for examples, see Kim and Fanselow, 1992, Anagnostaras et al., 1999, Shimizu et al., 2000) and spatial learning (Morris et al., 1982, Cho et al., 1993, Remondes and Schuman, 2004). The primary advantage of these approaches is the ease with which animals are able to learn the tasks, as well as the straightforward behavioral readouts of memory recall (for example, percent freezing as a measure of conditioned fear memory). However, these readouts can be highly variable and typically do not allow for repeated probing of memory strength over the duration of consolidation (Tipps et al., 2014). Building on these

efforts, we sought to develop a new task that is complex and explicitly hippocampus-dependent, undergoes consolidation, and that would allow us to simultaneously manipulate and record from circuits across the brain during behavior.

Virtual reality-based behaviors offer a way to precisely control sensory stimuli and record behavioral outputs time locked to neural events (Holscher et al., 2005). Rodents are able to explore virtual environments effectively, and the neural activity responses evoked mimic those seen in freely navigating animals (Harvey et al., 2009, Radvansky and Dombeck, 2018). Here, I will detail the development and testing of a novel virtual reality-based behavior for mice in order to study memory consolidation. We then validated that the task is both dependent on the hippocampus for initial acquisition and recall, and furthermore, that the task undergoes consolidation.

3.2 Results

3.2.1 Virtual reality-based behavior

We designed a 1-dimensional virtual reality environment for head-fixed mice, adapted from previous approaches (Rajasethupathy et al., 2015, Harvey et al., 2012). This task requires self-initiated trials, special navigation, and contextual discrimination using multiple sensory modalities (Figure 3.1A). The setup consists of a styrofoam ball rotating around an axial rod, with motion tracked by an optical computer mouse. The mice were head-restrained with a headplate mount directly above the ball. In front of the mouse was a rounded screen onto which the virtual environment was projected. The mice had free access to a lick port through which reward was selectively delivered, and to which was connected a capacitive touch sensor for recording lick events. A plastic tube blew a

constant flow of air into the nostrils of the mouse, with solenoids gating the delivery of odorants - alpha-pinene or isoamyl acetate. A speaker was used to deliver either a 7 kHz or 13 kHz tone. Finally, an additional plastic tube connected to a solenoid-gated high pressure air source was pointed at the eye of the mouse to selectively deliver an aversive air puff. The entire setup was built within a light- and sound-proofed container to minimize any influence from external stimuli. The virtual environment was designed in MATLAB using ViRMEn (Virtual Reality MATLAB Engine, 2016 release).

The mice were trained to run down a linear virtual track, beginning in a "start zone". Once they initiated running, they entered a "cue zone", drawn from one of two pseudo-randomly selected contexts (Reward or Aversive). In the cue zone, the mice would be presented a combination of visual, auditory, and olfactory cues, with each set of cues unique to a given context (e.g. blue triangles, alpha-pinene scent and 13kHz tone for the Reward context). If the mice reached the end of the cue zone (50 cm) within a time limit, they were placed in the "outcome zone", receiving either sucrose water (Reward context) or an aversive puff of air (Aversive context). Thus, mice would learn to run in the Reward context to receive sucrose reward and stop in the Aversive context to avoid punishment (Figure 3.1B). To quantify learning and memory retrieval, we tracked both run speed during cue presentation and lick rate. Mice were first habituated to running on the ball in a cue-free track for one week (Figure A.1A). They were then trained over five days and then subsequently probed with "retrieval" sessions, where neither reinforcement outcome was given, at weekly sessions up to seven weeks following the end of training. Re-training sessions followed each retrieval sessions to minimize memory extinction. On each day, once a session was initiated, the task was entirely automated, requiring no human intervention.

Mice were successfully trained in this paradigm and were able to maintain high per-

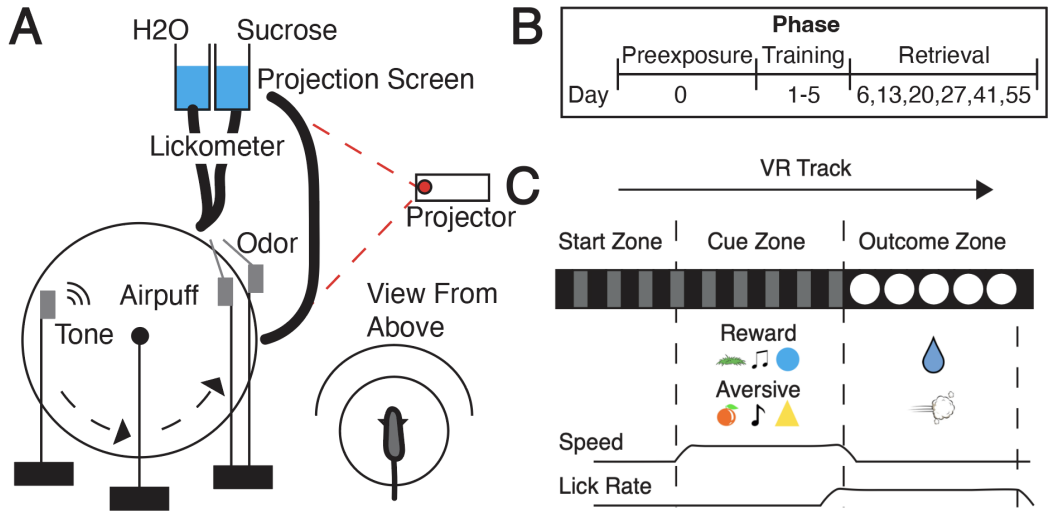

Figure 3.1 | **Virtual reality behavior setup and task design.** (A) Schematic of virtual reality experimental setup. (B) Timeline of behavioral task from preexposure (day 0), through training (days 1-5), and retrieval (probe trials on days 6, 13, 20, 27, 41, and 55). A single retraining session occurs after each retrieval session. (C) Virtual reality linear track with start, cue, and outcome zones, and example behavioral parameters (speed, lick rate) tracked. Reinforcements are provided in the outcome zone during training but omitted during retrieval probes.

formance on a months-long timescale. By employing appropriate shaping procedures, we observed high task engagement, learning, and memory that persisted for weeks to months (Figures 3.2A-C). While in the cue zone, animals demonstrated learning and memory by reliably decreasing their speed and anticipatory licking when cues predicted aversive airpuff, while increasing speed and anticipatory lick rate when cues predicted sucrose reward (Figures 3.2A-B, A.1C and A.1F). On average, mice demonstrated a high degree of learning and memory, quantified by their discrimination of anticipatory lick behavior between the two contexts (2.5Hz vs 0.2 Hz lick rate in reward vs aversive context on day 55, discrimination index of 0.85; $p<0.01$, two-way ANOVA with repeated measures; see Methods for calculation of discrimination index).

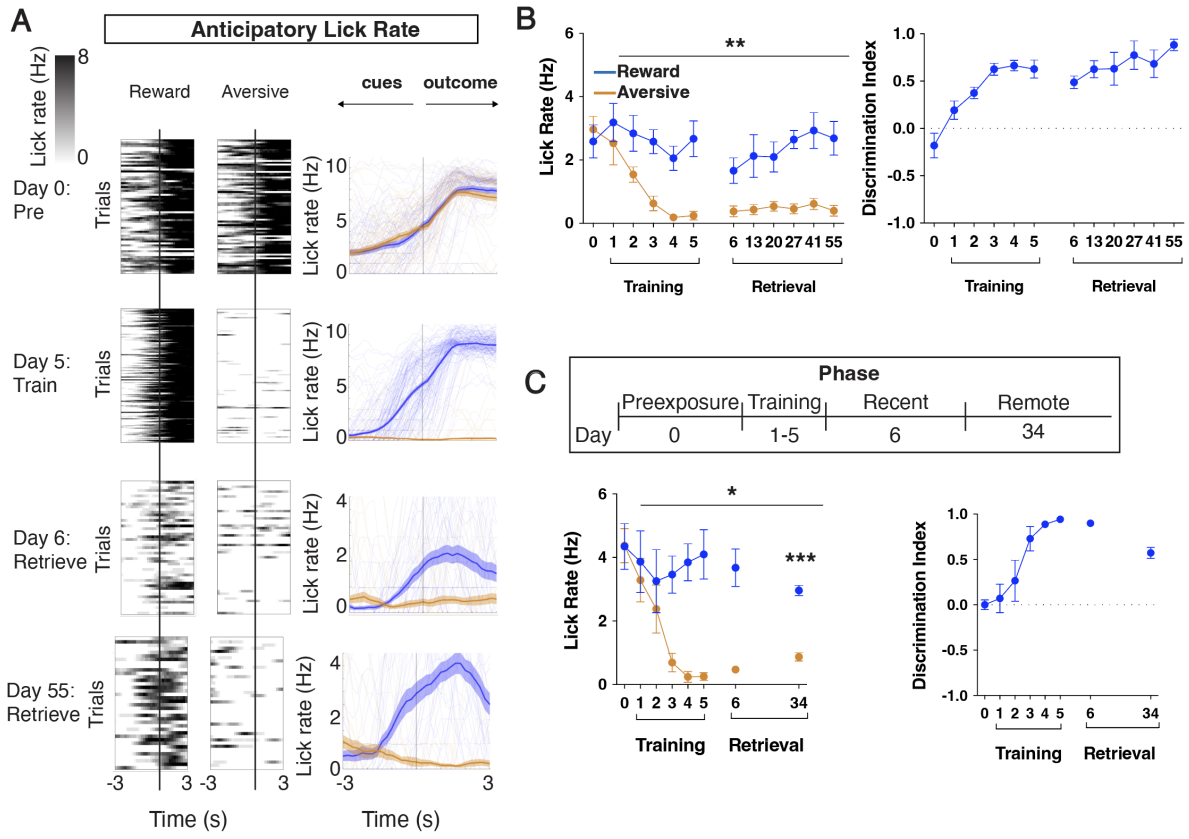

Figure 3.2 | **Performance on VR memory task.** (A) Raster of individual trials and plot of trial averages. Anticipatory lick rate (Hz) is described as the lick rate prior to the outcome zone. Also shown is lick rate 3 seconds into the outcome zone. N=5 mice, 8 trials/context/session during training, 4 trials/context/session during retrieval. (B) Left: average anticipatory lick rate (Hz) in each context during preexposure, training, and weekly retrieval sessions throughout consolidation. Right: quantification of discrimination index (difference of anticipatory lick rates in reward and aversive context divided by their sum). N=5 mice, **p<0.01, Two way ANOVA with repeated measures, data are mean ± s.e.m. (C) Same as (B), but without weekly retrieval sessions, and testing only recent (day 6) and remote (day 34) retrieval, N=4 mice, *p<0.05, Two way ANOVA with repeated measures, data are mean ± s.e.m. ***p<0.001 for R34, Bonferroni corrected for multiple comparisons, data are mean ± s.e.m.

Importantly, neither sets of cues, in the absence of paired reinforcement were inherently rewarding or aversive (Figure 3.2A, Day 0). To minimize extinction due to repeated longitudinal retrieval sessions, we performed minimal retraining, which we confirmed yields comparable performance to a single remote retrieval session (Figure 3.2C), without loss of motivation when reward is again provided (Figure A.1D). To determine whether mice use all three of the different sensory modalities when learning the task, we trained a cohort as described above, and then tested them on a version of the task where every combination of one, two, or all three sensory cues were presented on a given trial. We found that context discrimination reliably increased with increasing number of cues (Figure A.1E), suggesting mice integrate sensory cues to optimize performance.

3.2.2 Learning and recent memory recall require the hippocampus

We next wanted to verify that memory for this task is indeed dependent on the hippocampus initially. To do so, we expressed the inhibitory opsin stGtACR2 (Mahn et al., 2018) in excitatory neurons of the hippocampus in a cohort of mice and trained them on the task while light was delivered throughout the cue and outcome zone (Figure 3.3A). We found that inhibiting the hippocampus prevented the normal learning of context discrimination through five training days and when memory was tested one day after training with a retrieval session (Figures 3.3B-C). Furthermore, when mice were trained without inhibition, but then tested with a retrieval session with inhibition (Figure 3.3D), mice were unable to successfully recall (Figures 3.3E-F). Thus, the hippocampus is required for both normal memory acquisition and recent memory retrieval.

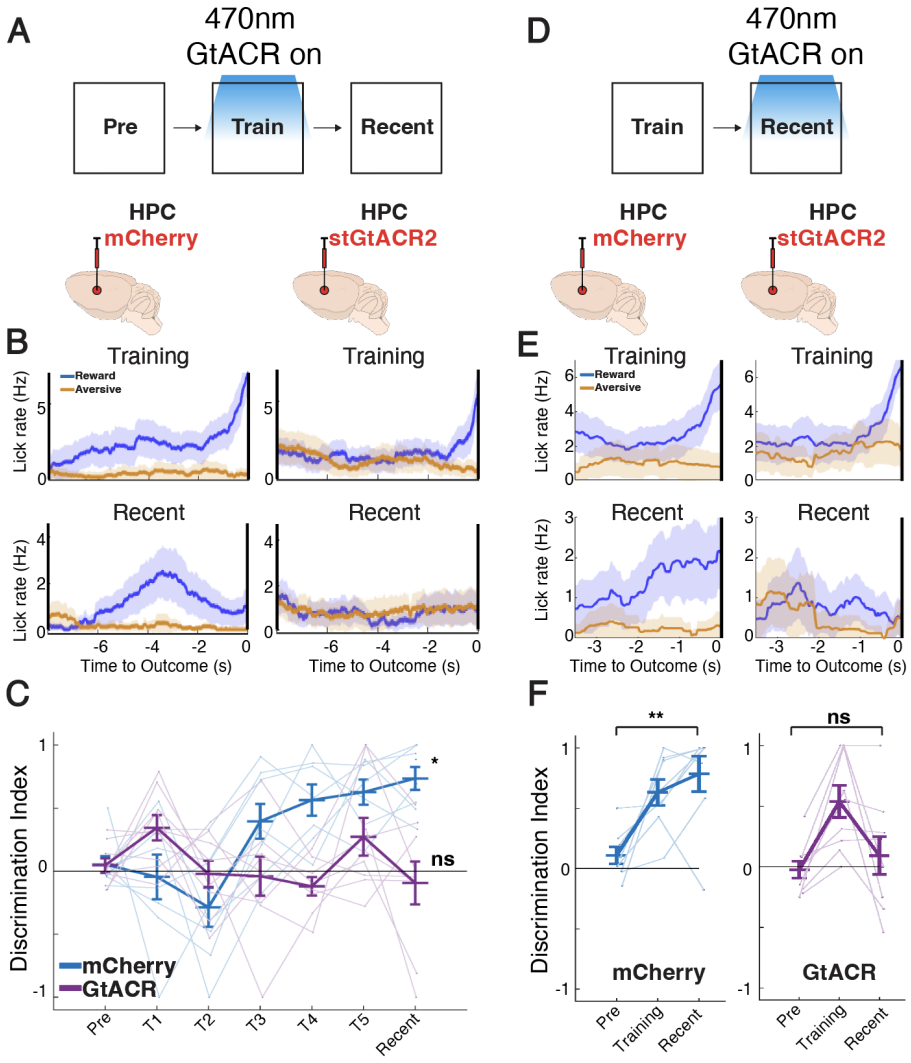

Figure 3.3 | **Learning and recent memory recall require the hippocampus.** (A) Schematic of experimental design: stGtACR2-based optogenetic inhibition during training (T1-T5), followed by a test of recent memory. (B) Raw lick rate traces for mCherry (left control, N=8) and GtACR (right; HPC with opsin, N=8) in each context during training and recent retrieval sessions, data are mean (solid line) ± s.e.m (shaded area).(C) Quantification of discrimination between reward and aversive lick rates per mouse cohort on preexposure, training, and recent retrieval sessions. *$p<0.05$ between pre-exposure and recent. (D) Schematic of experimental design: GtACR-based optogenetic inhibition during recent memory in animals that were trained without optogenetic inhibition.(E) Raw lick rate traces for mCherry (left) and GtACR (right) in each context during training and recent retrieval sessions, data are mean (solid line) ± s.e.m (shaded area). (F) Quantification of discrimination between reward and aversive lick rates per mouse cohort on preexposure, training, and recent retrieval sessions. **$p<0.01$ for between pre-exposure and recent. Statistical tests are one-way repeated measures ANOVA with post-hoc Tukey's multiple comparison test. Individual data points shown, with mean ± s.e.m.

3.2.3 Remote recall depends on anterior cingulate cortex, but not hippocampus

Finally, we sought to determine whether the memories formed for this task are cortically consolidated to the ACC and become HPC-independent (Frankland and Bontempi, 2005). To do this, we habituated and trained three separate cohorts of mice on the task. One cohort would express the inhibitory chemogenetic receptor hM4D(Gi) (Armbruster et al., 2007) in excitatory cells of the hippocampus, another would express hM4D(Gi) in the ACC, and the third would express a control fluorophore tag in either HPC or ACC (Figure 3.4A). After 3 weeks, we tested the mice on retrieval for the task after injecting CNO (the biologically inert ligand for hM4D(Gi)) 45 minutes prior to testing. We opted for a chemogenetic approach (rather optogenetic) to ensure broader anatomical coverage and sustained inhibition throughout the retrieval.

When tested, we found that only inhibition of ACC, but not HPC or control, resulted in a significant decrease in contextual discrimination for the remote time point (Figure 3.4B-C). Thus, combined with the prior result of hippocampal dependence during training and early retrieval, we can conclude that memory for this task undergoes consolidation.

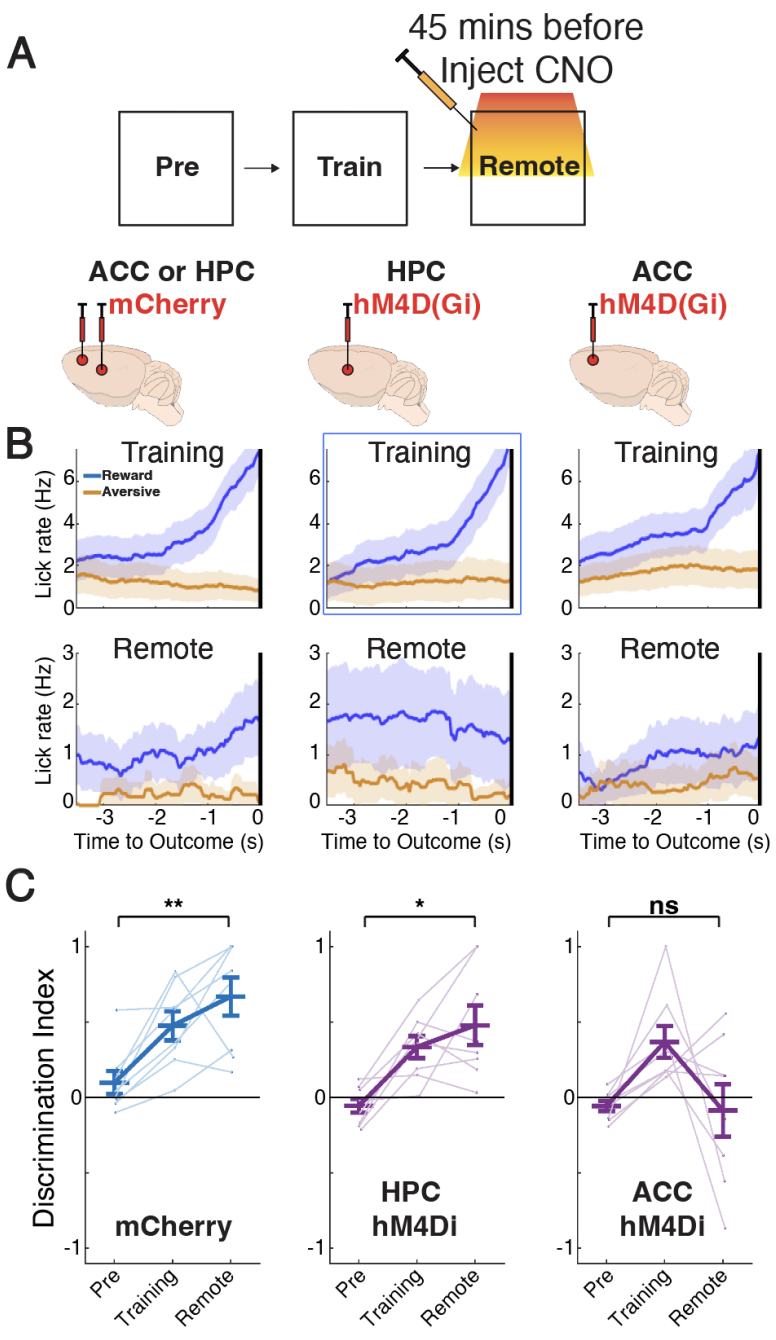

Figure 3.4 | **Remote recall depends on ACC but not HPC.** (A) Schematic of experimental design: DREADDS-based chemogenetic inhibition during remote memory in trained animals. CNO was administered 45 minutes prior to the remote retrieval session. (B) Raw lick traces for mCherry (left; ACC or HPC with no hM4Di, N=8), HPC hM4Di (middle; HPC with hM4Di, N=8), ACC hM4Di (right; ACC with hM4Di, N=8) in each context during training and recent retrieval sessions, data are mean (solid line) ± s.e.m (shaded area). (C) Quantification of discrimination between reward and aversive lick rates per mouse cohort on preexposure, training, and remote retrieval sessions. **p<0.01 for mCherry between preexposure and remote, *p<0.05 for HPC hM4Di, p=0.945 for ACC hM4Di, one-way repeated measure ANOVA with post-hoc Tukey's multiple comparison test. Individual data points shown, with mean ± s.e.m..

3.3 Discussion

In this section I discussed the development of a novel virtual reality-based contextual memory task that is 1) dependent on the hippocampus for acquisition and early retrieval, 2) consolidated to cortex over weeks to become independent of the hippocampus, and 3) allows us to reliably track memory recall repeatedly and up to 55 days after initial training.

Our findings that hippocampus is required for the initial acquisition and recall of memory is in line with prior studies in rodents studying different modalities such as contextual fear conditioning (Kim and Fanselow, 1992) and the Morris water maze (Morris et al., 1982). Additionally, the finding that after about a month, memory recall becomes independent of the hippocampus lends support for standard systems consolidation theory, versus competing theories such as multiple trace theory.

Though we cannot rule out the involvement of other regions of the brain, we did confirm a role for the ACC in remote memory retrieval, as has been reported previously (Takehara et al., 2003, Vetere et al., 2011). In addition to memory retrieval, the ACC is known to serve multiple other functions relating to integrating sensory, motivational, decision-making, and higher-level cognitive signals from across the brain (Devinsky et al., 1995). It is possible that through its highly central role in cognition, ACC is capable of driving recall by activating a widely distributed cortical network (Frankland et al., 2004), rather than containing the entirety of the memory trace.

How does the ACC acquire the ability to drive recall independently of the HPC after weeks? In the next section, I will discuss potential pathways from HPC to ACC, and analyze their responses to long-term memory acquisition and retrieval to identify potential sites of gating and interaction with cortex.

Chapter 4

Longitudinal fiber photometry recordings reveals a neural correlate of memory in anterior thalamus

4.1 Introduction

How do the hippocampus and anterior cingulate cortex interact throughout memory consolidation? The ACC receives few direction projections from dorsal HPC (Jay et al., 1992) (though the reverse projections exist (Rajasethupathy et al., 2015)), while the ventral HPC (involved more in emotional processing rather than memory) provides the majority of connections between the structures. Thus, it might be insightful to search for intermediate brain regions that could gate the flow of memory-related information between dorsal HPC and ACC. To do this, we opted for a retrograde viral tracing approach (Xu et al., 2020) to identify candidate circuits to investigate.

To search for neural correlates of memory consolidation, we used fiber photometry to record ongoing neural activity from genetically defined cell populations (Cui et al., 2013).

The technique uses fiber optics to collect neural-activity-dependent fluorescence changes within a local area of the brain, and can be used with either head-fixed or freely-moving behavior. A major strength of the technique is its temporal resolution and scalability to multiple simultaneous regions (Kim et al., 2016). The aim of this chapter is thus to identify a brain region that is both intermediate to HPC and ACC anatomically, and also contains memory-associated activity that aligns with the timeline of consolidation.

4.2 Results

4.2.1 Anatomical tracing from ACC using retrograde tracers

To identify brain regions that send projections to ACC, we injected a retrograde tracer, AAVrg-tdTomato unilaterally in ACC. This virus is taken up by synaptic terminals and travels retrogradely by axonal transport to express the fluorophore (tdT) in the cell bodies (Figure 4.1A). We scanned the brain through the rostral-caudal axis and identified regions with prominent tdT expression. From this, we found three well-defined candidate regions: basolateral amygdala (BLA), entorhinal cortex (EC), and anterior thalamus (ANT) (Figure 4.1B). Each of these has known inputs from hippocampus (BLA, (Yang and Wang, 2017); EC, (Naber et al., 2001); ANT, (Wright et al., 2010)). With these three candidate regions identified, we next sought to record from this entire HPC-ACC network (Figure 4.1C) simultaneously during behavior in order to identify neural correlates of memory.

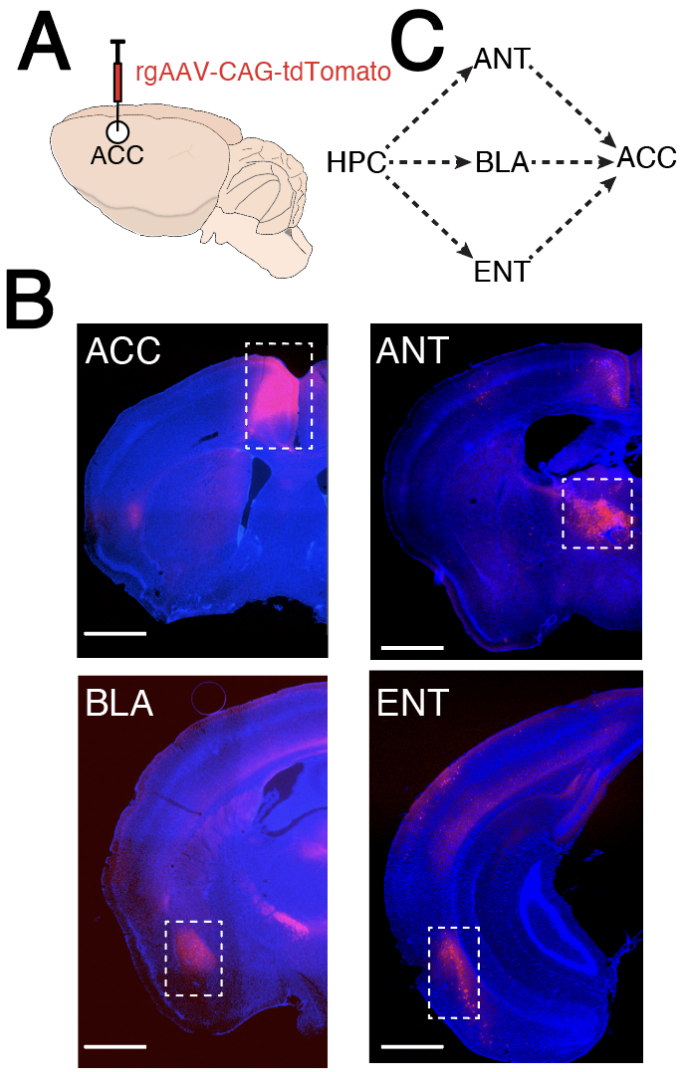

Figure 4.1 | **Retrograde tracing from anterior cingulate cortex.** (A) rgAAV-CAG-tdTomato was injected into ACC, (B) revealing retrogradely labeled neurons in anterior thalamus (ANT), basolateral amygdala (BLA), and entorhinal cortex (ENT) among other regions. (C) Each of ANT (via mammillary bodies), BLA, and ENT receive input from the dorsal hippocampus (HPC). Scale: 1mm.

4.2.2 Multi-region fiber photometry during behavior reveals mixed coding of task-relevant features

We injected the genetically encoded calcium indicator GCaMP6f in ACC, HPC, ANT, BLA, and ENT, implanted optical fibers above each region, and recorded neural activity during the task daily during training or weekly thereafter by multi-fiber photometry (Kim et al., 2016). The injection coordinates (Methods) were optimized to target the area of ANT, BLA, and ENT that contained direct projections to ACC. Neural activity recordings from each brain region of a given animal were then frame projected onto a camera sensor (Figure 4.2A), and custom MATLAB scripts (Methods) were used to extract time-series data, regress out motion-related artifacts and align to behavioral data at 100-ms resolution (Figure 4.2B, Methods).

Several steps were taken to ensure high-quality data. There are many factors that might affect signal quality such as GCaMP expression, distance from implant to expressing cells, and motion artifacts. Examples of recordings with different levels of noise are provided in Figure A.3B. Because the photometry signal tends to contain large, slow ($<$1 Hz) activity, signal fidelity can be estimated by dividing the peak amplitude by the power contained in the high frequency content of the signal. First we characterized the distribution of all of the recordings' peak-to-noise ratios and excluded recordings below a statistically defined threshold (Figures A.3C; Methods). The total number of "high quality" signals included in all analysis from each region is shown in figure A.3D.

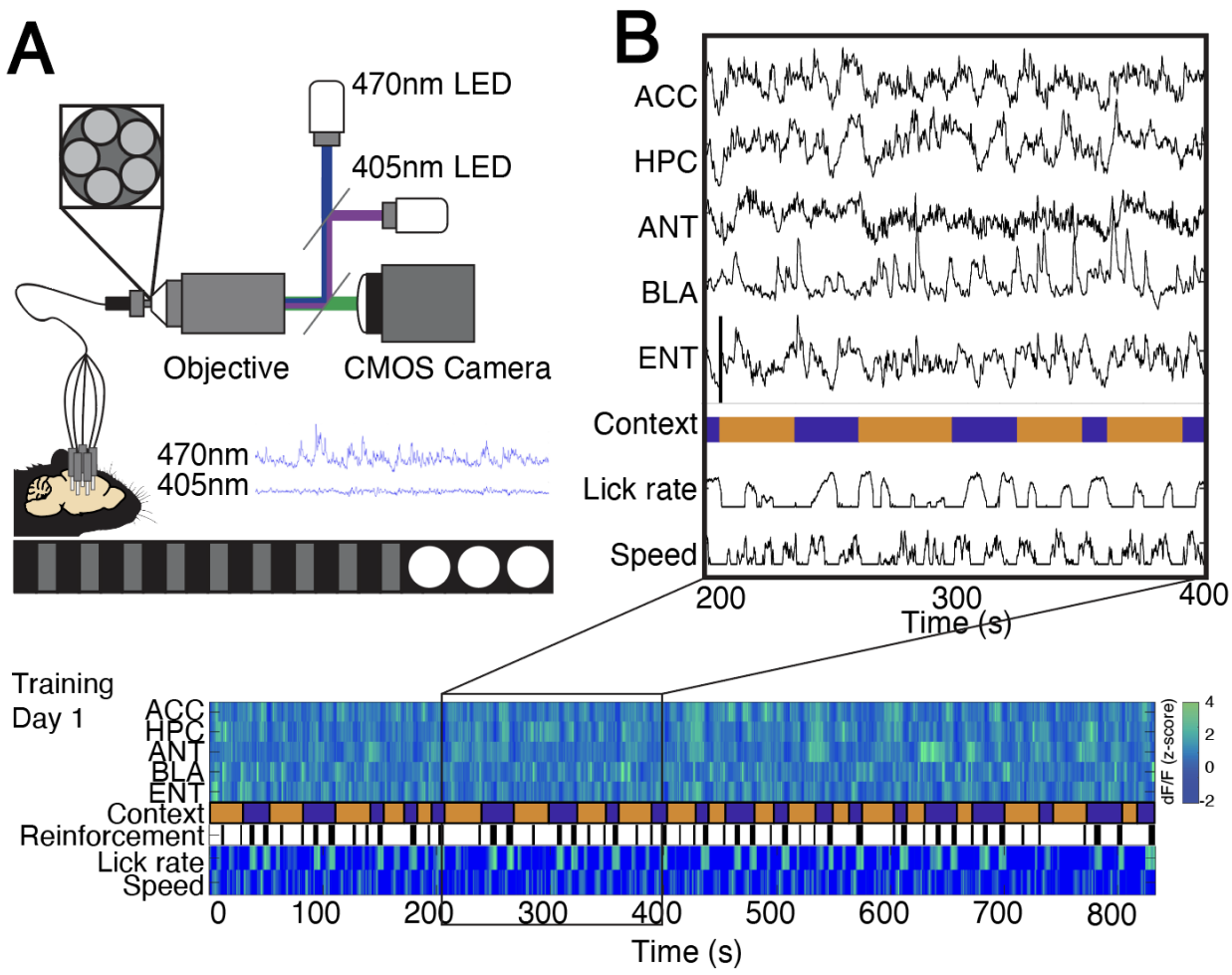

Figure 4.2 | **Approach for multi-region fiber photometry during virtual reality behavior.** (A) Photometry setup. Excitation light is delivered through fiber optic cables placed above the five implanted cannulas, and emitted fluorescence is projected back onto a CMOS camera. The calcium-dependent fluorescence from GCaMP6f is normalized by the calcium-independent fluorescence to correct for movement artifacts and calculate $\Delta F/F$. (B): Example traces of $\Delta F/F$ from one mouse on training day 1 from all five regions aligned to task and behavioral variables.

We then asked whether we could identify neural signals in these regions that were tuned to task-relevant features. We observed several types of neural responses including those that were time locked to onset of reinforcement, including air puff and sucrose (Figure 4.3A). Given that most brain regions encoded multiple variables simultaneously, we developed an encoding model, a generalized linear model (see Methods), to isolate signals related to each measured task variable, including task zone, sensory cues, reinforcement, elapsed time, as well as the continuous behavioral variables including run speed and lick rate. The model reliably predicted neural activity time series on held-out trials across regions and across days (Figures 4.3B and A.4A). Using this model, we calculated the variance explained in the predicted activity by each task variable (Methods). We observed that multi-modal information existed in all regions, some of which were modulated by learning and time. For instance, air puff representations diminished in all five regions across days, while sucrose representations increased in BLA (Figure 4.3A). Notably, a significant cue representation, relative to the start zone inter-trial interval, and independent of running or licking, uniquely emerged in ANT on days 3-5 of training (Figure 4.3C, arrows). Further characterization revealed that these changes in task-related tuning were not due to changes in the overall magnitude or rate of neural population activity (Figures A.4B-D), but rather changes in the relative timing to contextual and behavioral variables.

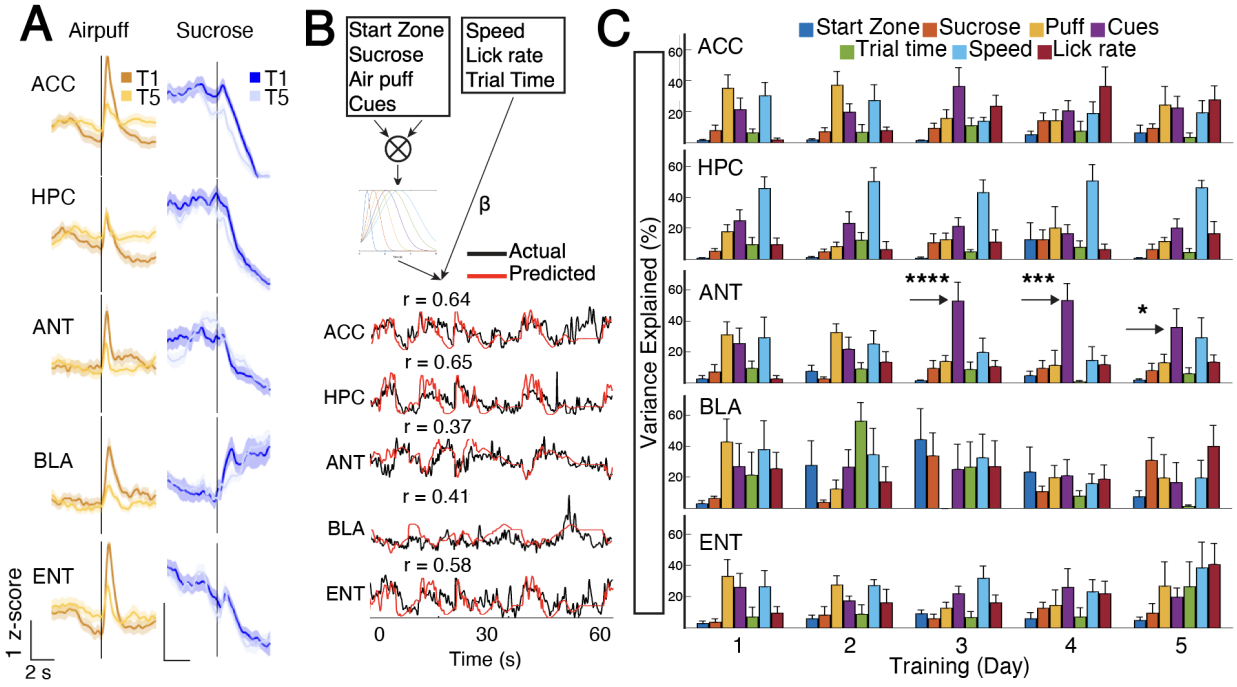

Figure 4.3 | **Longitudinal photometry recordings with distributed and mixed coding of task-relevant features.** (A) Robust trial-averaged responses to reinforcement (airpuff or sucrose) on training day 1 (T1) and 5 (T5). N=7 mice. Data are mean (dark line) and s.e.m. (shaded area). Photometry scale: x/y: 2s/1z. (B) Schematic of the generalized linear used to predict bulk neural activity from task and behavioral variables, with example model outputs from each region shown below (see methods). (C) Percentage of variance explained in the model by each variable throughout training (T1-T5) for each region. N=7 mice. Arrows: One-way ANOVA with Tukey's multiple comparison test between inter-trial interval (start zone) and cue zone for T3 (****$p<0.0001$), T4 (***$p<0.001$), and T5 (*$p<0.05$). Data are mean ± s.e.m.

4.2.3 A neural correlate to conditioned stimulus and response in ANT

We proceeded to identify the emergence and evolution of "memory-related" neural activity patterns by focusing on neural activity that tracks both the conditioned stimulus, i.e., cues, and conditioned response, i.e., anticipatory lick rate. We found that neural activity in ANT contained prominent signals for both (Figure 4.4). Specifically, ANT contained cue-related signals that were distinct for each context, which emerged in training and persisted through consolidation, and which were not explained by changes in animal speed (Figures 4.4A and B). Importantly, these signals emerged late in training, around T4-T5, demonstrating that they are not a sensory signal, but rather a representation of the learned association. Strikingly, ANT also contained a prominent neural activity signal tracking the conditioned response, i.e., anticipatory lick, when aligned to outcome zone, that persisted through consolidation (Figures 4.4C and 4.4D). Again, of note, these neural signals emerged on later sessions than the learned anticipatory lick behavior (Figure A.4E), and within the cue zone preceded the onset of licking (Figure 4.4C), which together support that it represents the cognitive process of memory retrieval rather than the motor process of licking. Such memory related signals tracking the conditioned stimulus and conditioned response were not observed in BLA and ENT.

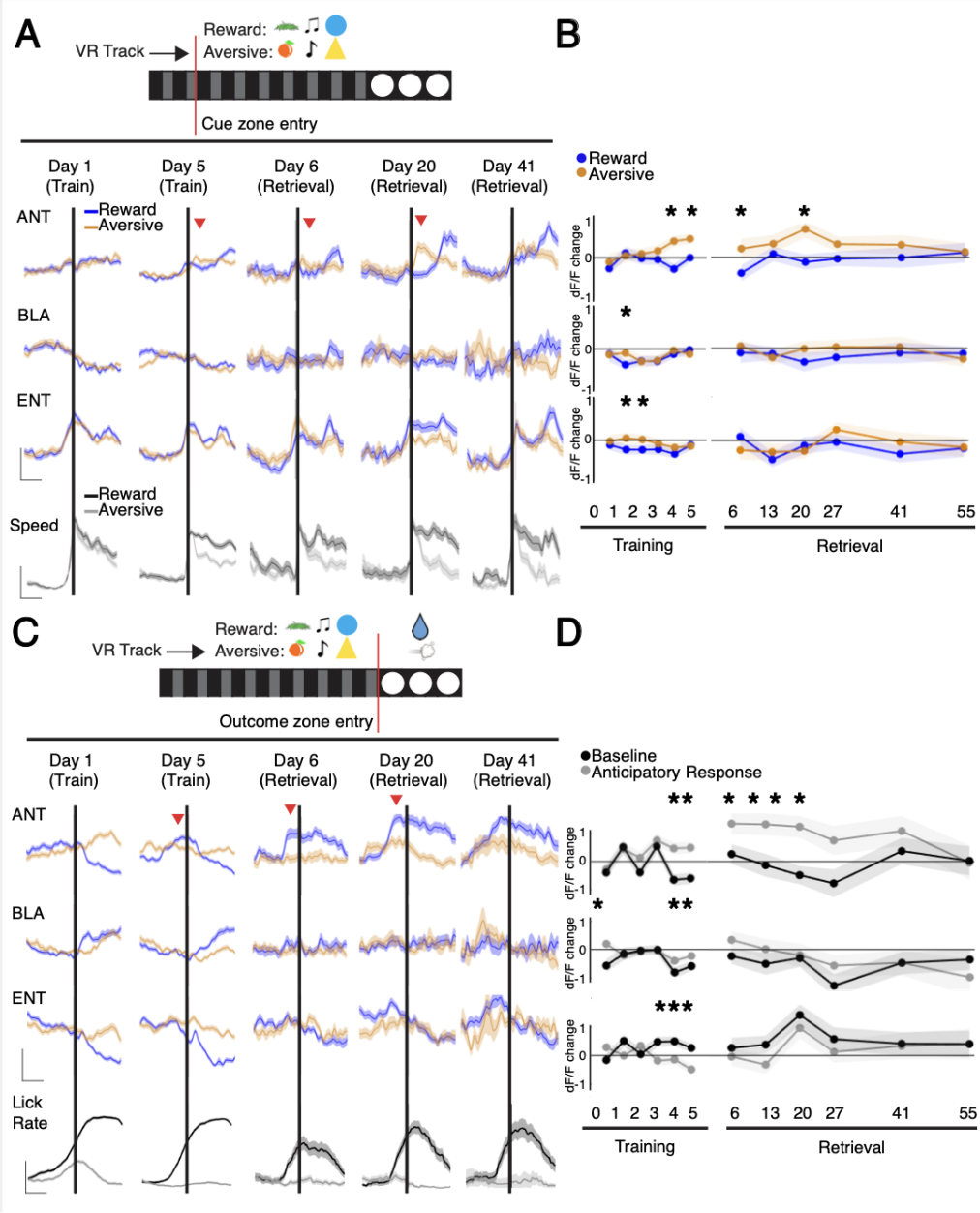

Figure 4.4 | **A neural correlate of memory in anterior thalamus throughout the consolidation window..** (A) Top: schematic of VR track with cue zone entry in red. Bottom: Mean dF/F in ANT, BLA and ENT aligned to cue zone entry for both contexts (blue vs orange). Bottom row: animal speed aligned to cue zone entry. Red arrow signifies AM signals quantified in 4B (see Methods). N=7 mice. Data are mean (dark line) with s.e.m. (shaded area). Photometry scale: x/y: 2s/1z. Speed scale: x/y: 2s/0.5z. (B) Quantification of mean change in dF/F at 1s vs. 0s in cue zone, assessed separately for each context. N=7 mice, *p<0.05, paired t-test. (C) Same as (A), but aligned to outcome zone entry. Photometry scale: x/y: 2s/1z. Lick rate scale: x/y: 2s/5Hz. Red arrow signifies AM signals quantified in 4D (see Methods). (D) Quantification of the mean difference in dF/F between contexts prior to outcome zone entry (anticipatory) compared to cue zone entry (baseline). N=7 mice, *p<0.05, paired t-test.

4.3 Discussion

In this chapter, I detailed the identification of three different brain regions that lie intermediate to hippocampus and anterior cingulate cortex - the basolateral amygdala (BLA), the entorhinal cortex (EC), and the anterior thalamus (ANT). Each of these regions have been implicated in memory processing and may serve parallel roles in memory consolidation. The BLA is involved in both fear and reward memory formation as well as decision making (Ghods-Sharifi et al., 2009, Wassum and Izquierdo, 2015), and has previously implicated in mediating synaptic plasticity across the brain during memory consolidation (Paré, 2003). The EC is thought to facilitate long-term cortical memory encoding by strengthening hippocampal-cortical communication (Cho et al., 1993, Robinson et al., 2017). The ANT is also thought to play a role in long-term memory (reviewed in Chapter 2), though this is the first time its activity during memory formation and retrieval has been recorded longitudinally.

These findings highlight two neural signatures in ANT that together represent a learned association, which is cognitive in nature, rather than sensory or motor. These signals consist of reliably divergent neural activity patterns at different times throughout the trial, suggesting two different representations emerged through learning. I do not dismiss functional roles of BLA and ENT in memory consolidation because bulk neural activity recordings often obscure fine scale computations; however, given the unique and prominent signals identified in ANT, we proceeded to further characterize its yet unknown contributions during memory consolidation through causal manipulations (Chapter 5) and cellular resolution neural activity recordings (Chapter 6).

Chapter 5

Bi-directional gating of memory consoldiation by AM thalamus

5.1 Introduction

Within the anterior thalamus, we conjectured that the anteromedial thalamus (AM) is anatomically positioned to function in consolidation because it receives direct inputs from the hippocampus (Wright et al., 2010), and indirect inputs via the mammillary bodies (i.e., Papez circuit), in turn sending the most prominent direct projections to anterior cingulate cortex. If AM is necessary for systems consolidation, we expect that inhibition of this circuit prior to or during consolidation should prevent the eventual recall of remote, but not recently formed memories. In this chapter, we will test this hypothesis directly with an optogenetic approach.

In addition to assessing the necessity of AM during consolidation, we also wanted to determine whether AM activity was *sufficient* to drive the consolidation of memories.

To test this, we needed a way to modulate the degree to which a memory was consolidated. We opted to do this by varying the salience of contextual memories. Whether aversive or rewarding, more salient experiences are more likely to be stored in long-term memory (Hamann et al., 1999). This is thought to occur through dopaminergic signaling at the time of learning (Lisman et al., 2011, Shohamy and Adcock, 2010). For example, one study found that dopaminergic activity at the time of encoding predicted successful memory retrieval three weeks out (Wittmann et al., 2005). The AM receives input from neuromodulatory regions of the brain (Harris et al., 2019), lending plausibility to its role in salience selection. Thus, we chose to adapt our virtual-reality based task to include a context that has low salience, such that a mouse is less likely to recall successfully it at remote time points. If AM can selectively support the consolidation of memories to cortex, increasing its activity during encoding of a low-salience context should enhance eventual recall after weeks.

5.2 Results and Discussion

5.2.1 AM-ACC is necessary for memory consolidation

We first confirmed that AM in particular anatomically connects hippocampal circuits with ACC using a transsynaptic viral tracing technique (Schwarz et al., 2015) and identified cells in the mamillary bodies that are directly pre-synaptic to AM-ACC projecting cells (Figure A.2A). To assess whether the AM thalamus is required for memory consolidation, we performed projection-defined optogenetic inhibition of the AM-to-ACC circuit during training. We expressed the soma-targeted inhibitory opsin stGtACR2 by injecting retroAAV- Cre in ACC and floxed-stGtACR2 (or floxed-mCherry for control) in AM

thalamus and implanted optical fibers bilaterally above AM thalamus. Importantly, at this dorsal location, no other anterior thalamic nuclei project to ACC, and thus we can confirm an AM-to-ACC specific manipulation. Expression and accurate implantation at the injection site were verified by histology (Figure A.5A). We observed that bilateral inhibition of AM-to-ACC during the cue and outcome zone of training sessions (Figures 5A) resulted in no significant learning or recent memory deficit, but a significant deficit in remote memory retrieval in the stGtACR cohort compared with the control mCherry cohort (Figures 5B-5D). This was not due to significant changes in how the mice valued the reward or were motivated to lick, because in a subsequent re-training session following memory retrieval, the amount of licking in the reward context outcome zone matched that of the control cohort (Figure A.5C).

To ensure our results were not confounded by the intervening early retrieval with re-training, we repeated this experiment while only testing the mice at remote time (Figure A.6A). We found no learning impairment in mice inhibited during training, but again observed impaired memory recall at remote timepoints (Figures SB-D). To test whether this disruption of consolidation generalizes to other types of hippocampal-dependent memory, we subjected mice to contextual fear conditioning, while inhibiting the same AM-to-ACC projections during conditioning (Figure 2E). We again found a deficit during remote, but not recent memory retrieval in the inhibited mice when compared to control mice (Figure 2F). Taken together, these optogenetic and behavioral results are consistent with a sustained requirement for AM-to-ACC activity beginning at the time of learning to ensure consolidation and memory recall at remote time.

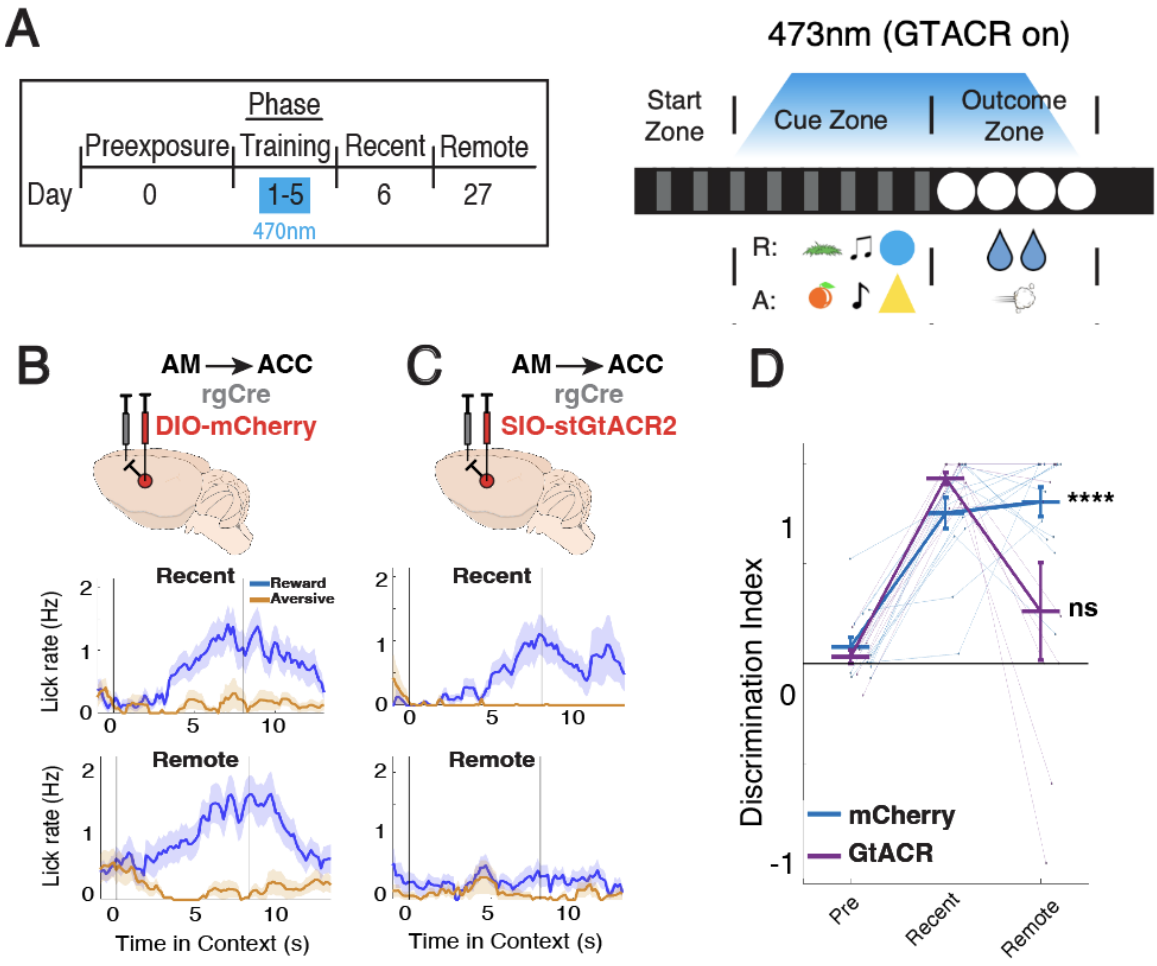

Figure 5.1 | **Inhibition of AM-ACC during training disrupts recall for remote, but not recent memory.** (A) Schematic of experimental design: stGtACR2-based optogenetic inhibition during training (T1-T5), followed by a test of recent (R6) and remote (R27) memory. Light was delivered during cue and outcome periods of the trial. See also Fig. A.6 for optogenetic inhibition during training followed by a direct test of remote memory. (B,C) Injection strategy for targeting anteromedial thalamus (AM) projections to ACC (AM-ACC) in mCherry control and stGtACR2 opsin cohorts. Raw lick traces are shown for each mouse in each context on recent and remote retrieval sessions, data are mean (solid line) ± s.e.m (shaded area). (D) Quantification of discrimination between reward and aversive lick rates per mouse on preexposure, recent, and remote retrieval sessions; mCherry (AM-ACC no opsin control, N=13), GtACR (AM-ACC with opsin, N=9). ****$p<0.0001$ for mCherry between Preexposure and Remote, $p>0.05$ for GtACR, one-way repeated measures ANOVA with post-hoc Tukey's multiple comparison test. Individual data points shown, with mean ± s.e.m.

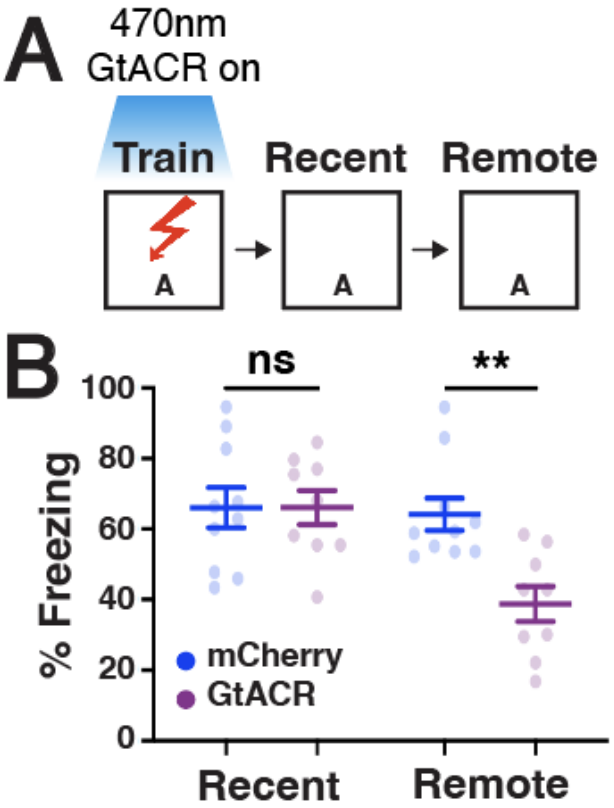

Figure 5.2 | **Inhibition of AM-ACC during contextual fear conditioning disrupts consolidation.** (A) Contextual fear conditioning protocol. Mice are placed in the conditioning chamber on day one where they receive foot shocks while laser light is delivered to AM. They are subsequently returned and tested for freezing behavior after 1 day (Recent) or 3 weeks (Remote) (B) Quantification of freezing behavior in training and remote retrieval sessions in mCherry (AM-ACC no opsin control, N=11) and GtACR (AM-ACC with opsin, N=9). **p<0.01 between mCherry and GtACR cohorts on remote, unpaired t-test. Individual data points shown, with mean ± s.e.m.

We next asked whether enhancing the natural excitability of the AM-to-ACC circuit during training could facilitate consolidation of a memory that otherwise would not be consolidated. To test this, we extended the current behavioral task to include two reward contexts, with non-overlapping sets of sensory cues, where one was associated with high reward and the other with a less salient, low reward outcome (Figure 5.3, Methods). Several rounds of pilot studies were run in order to optimize this task so that, on average,

mice would learn the two context-associations equally (and recall early) but consolidate only the high reward context.

Figure 5.3 | **Updated virtual reality behavior to test consolidation.**

To facilitate activity in the AM-ACC circuit in a manner that modulates the excitability of ongoing activity without exogenously driving spiking activity, we used a stabilized step function opsin (SSFO) (Yizhar et al., 2011). We injected retroAAV-Cre bilaterally in ACC, and floxed-SSFO-eYFP (or floxed-eYFP for control) bilaterally in AM thalamus, followed by implantation of optical fibers bilaterally in AM (Figure 5.4B-C). As an additional control, we expressed floxed-SSFO in another memory-related circuit with direct projections to ACC, the retrosplenial cortex (RSP), in an analogous manner. Blue light was delivered for 5 seconds immediately prior to beginning the task on training days. After each training session was completed, yellow light was delivered for 5 seconds to ensure inactivation of the SSFO.

Strikingly, we found that enhancing AM-ACC excitability during training uniquely and significantly enhanced remote memory retrieval of the low reward context, effectively recalling both HR and LR at remote time (Figures 5.4E-F; AM SSFO DI = 0.7368 in low reward, p=0.0111; RSP DI = 0.0164 in low reward, p=0.4833, n.s.; YPF DI = 0.0304 in low reward, p = 0.8835, n.s,) We repeated this experiment without testing mice at an early timepoint and again found sustained memory recall for the low reward context in SSFO-

activated but not control mice (Figures SE-G). Taken together, these results demonstrate that the AM-to-ACC projection is not only required for successful memory consolidation, but that activity enhancement at the time of learning can profoundly facilitate consolidation of otherwise unconsolidated memories.

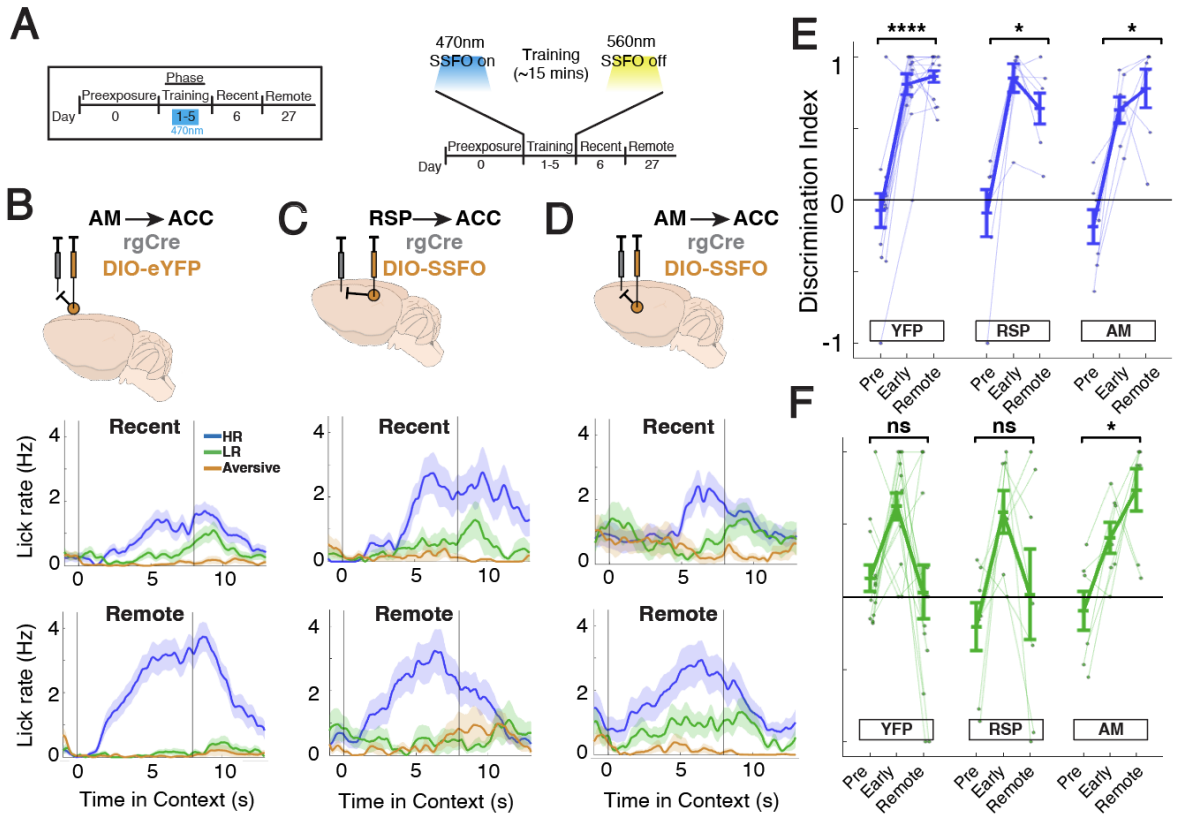

Figure 5.4 | **Excitation of AM-ACC enhances recall for an otherwise unconsolidated memory.** (A) Schematic of experimental design: SSFO-based enhancement of neural excitability during training (T1-T5), followed by testing of recent and remote memory. 470nm light was delivered at the start of each training session to activate the SSFO and then 560nm light delivered at the end to deactivate the SSFO.(B-D) Top: Injection strategy for targeting projections to ACC in YFP control (YFP; I) and SSFO cohorts for the retrosplenial cortex (RSP) projections (RSP-ACC; J) or AM projections (AM-ACC; K). Bottom: Raw lick traces are shown for each mouse in each context on recent and remote retrieval sessions, data are mean (solid line) ± s.e.m (shaded area). (E) Quantification of discrimination between high reward (HR) and aversive (A) contexts on preexposure, recent, and remote sessions for each cohort; YFP (no opsin control, N=14); RSP (RSP-ACC SSFO excitation, N=7); AM (AM-ACC SSFO excitation, N=7). *p<0.05 for YFP, RSP and AM cohorts between preexposure and remote, one-way repeated measures ANOVA with post-hoc Tukey's multiple comparison test. Individual data points shown, with mean ± s.e.m. (F) Same as in (E), but for discrimination between LR and A contexts. *p<0.05 only for AM cohort between preexposure and remote, one-way repeated measures ANOVA with post-hoc Tukey's multiple comparison test. Individual data points shown, with mean ± s.e.m.

Chapter 6

Anteromedial thalamus stabilizes contextual representations in cortex

6.1 Introduction

To gain mechanistic insight into how AM thalamus facilitates memory consolidation, we aimed to perform real-time cellular resolution neural activity imaging of AM thalamus, together with hippocampus and ACC simultaneously during learning and throughout memory consolidation. Existing cellular resolution imaging approaches powerfully enable single region deep brain imaging (Dombeck et al., 2007, Hofer et al., 2009, Ghosh et al., 2011, Aharoni and Hoogland, 2019) or large-scale cortical imaging (Sofroniew et al., 2016, Weisenburger et al., 2019, Yang and Yuste, 2017), but do not provide capabilities for imaging multiple cortical and sub-cortical regions spanning different depths (i.e., thalamus, hippocampus, and cortex) simultaneously during behavior. To provide a solution, we leveraged fiber bundle-based imaging approaches (Helmchen et al., 2001), where the

inherent distance created between the animal and the objective offered a scalable solution toward multi-site imaging. In this section I will detail how we were able, for the first time, to image from three separate brain regions simultaneously in a behaving mouse. I then leveraged this technology to image and manipulate HPC, AM, and ACC, to gain mechanistic understanding into how these regions interact to support memory consolidation.

6.2 Results and Discussion

6.2.1 A fiber bundle-based method for simultaneous multi-region imaging at cellular resolution

We designed a multi-region imaging system where light from multiple fiber bundles (Fujikura, 600 um Diameter, 3.3 um core to core distance) is collected onto a common objective (Nikon 10x, 0.5 NA) and frame projected onto a camera sensor (Photometrics Prime 95b, 95% QE), while optimizing sensitivity, resolution, and robustness to motion-related artifacts from a head-fixed or freely moving animal (Figure 6.1A, Methods). The resulting system was first characterized by imaging sub-diffraction size beads, where reconstruction of the PSF revealed a lateral resolution of 5-10um, comparable to the widely used mini-scope approach (Figure A.7A) (Glas et al., 2019). We further validated the ability of our system to resolve individual cells using resolution test targets (Thorlabs, Figure A.7B). To image in the behaving mouse, we optimized GCaMP injection titers, GRIN-lens based surgical implantations, and the design of an adapter between the animal/GRIN lens and the fiber bundle system (Autodesk Fusion 360, Figure 6.1B).

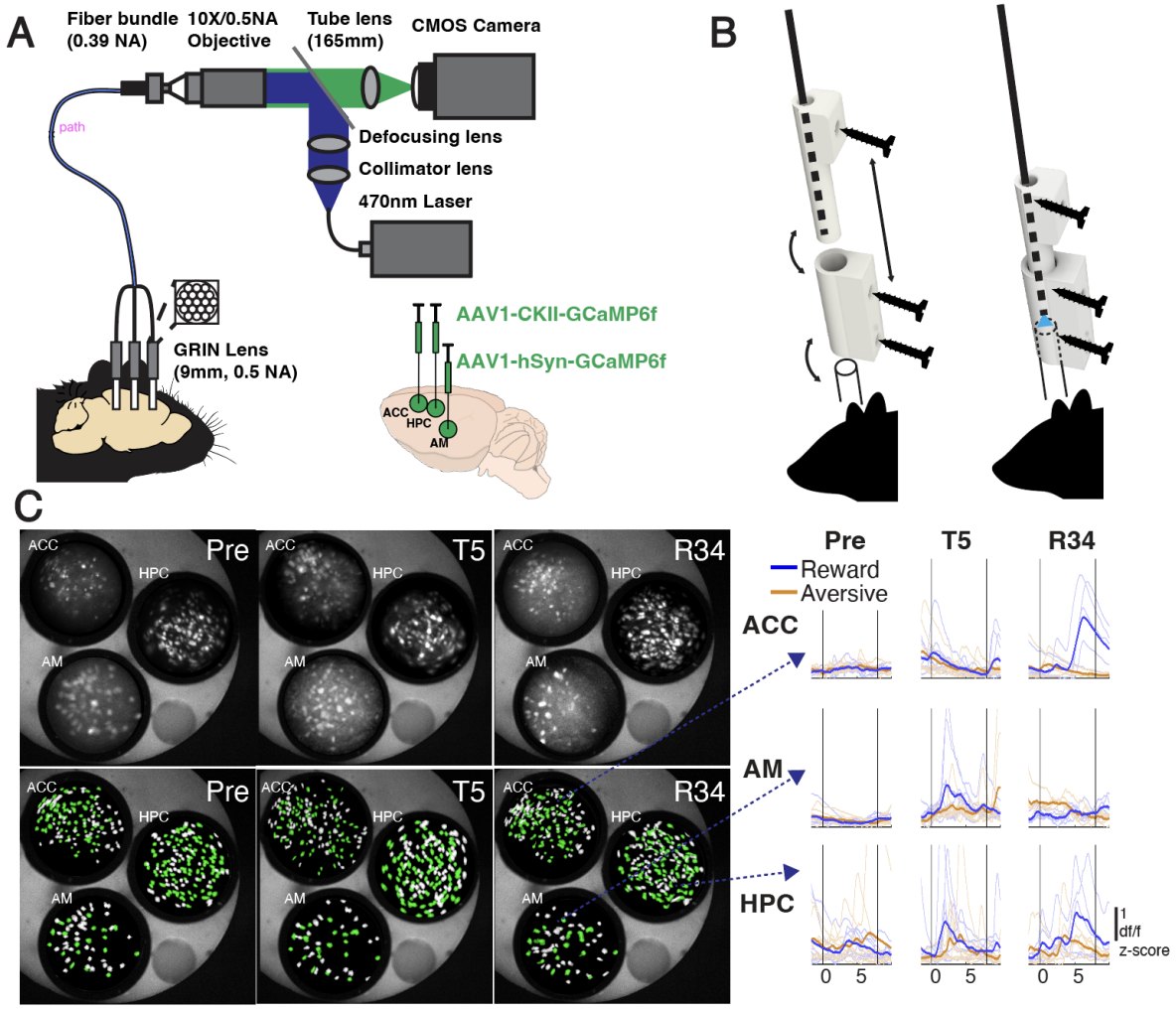

Figure 6.1 | **Longitudinal, simultaneous multi-region imaging design with cellular resolution.** (A) Fluorescence emission from implanted GRIN lenses is imaged by the fiber bundle and collected into a common objective and projected onto a CMOS camera (B) Custom-built apparatus for stabilizing and aligning the fiber bundle-to-GRIN lens connection.(C) Neural sources are tracked simultaneously in anterior cingulate cortex (ACC), hippocampus (HPC), and anteromedial thalamus (AM) for up to 34 days. Shown are neural sources from one mouse, same field of view tracked across preexposure (Pre), training day 5 (T5) and remote retrieval (R34). Sources captured on all days are highlighted in green. Right: Individual and mean z-scored dF, recorded for the same cells in ACC (top), AM (middle), and HPC (bottom), aligned to cue zone entry, and tracked from preexposure through training and remote retrieval. Dashed lines represent the source from (C) of which the dF traces are tracked. Scale: 1 df/f (z-scored).

Put together, our technology provided stable cellular resolution imaging, from the AM, HPC and ACC for up to 34 days (Figures 6.1C). We further assessed and found that the signal-to-noise of neural activity detected from the fiber bundle system was comparable with state-of-the art wide-field recordings using matched sources from the same field-of-view (Figure A.7C). Finally, although we recorded in head-fixed rodents due to the nature of our task, our adaptors provide a stable connection between the GRIN lens and the fiber bundle, and is thus compatible with studies in freely-moving animals. Thus, we developed an optical system, that interfaces seamlessly with the behaving animal, to enable high resolution imaging from multiple brain regions simultaneously and chronically during behavior.

We generated a cohort of mice that were injected with GCaMP6f and implanted with GRIN lenses in AM, HPC, and ACC (Figure A.7D, Methods), and confirmed normal physiological activity of neurons in all regions (Figure A.7E). For targeting ACC, we ensured a field of view primarily consisting of cingulate cortex, rather than the nearby M2 motor cortex, by targeting a field of view as close to the midline as possible, and confirming that motor related signals from neurons in this region are minimal (Figure A.8A). For targeting AM, we ensured that ACC projecting neurons were contained within the imaging field of view, thus minimizing imaging of nearby thalamic nuclei. Implanted mice learned the previously described memory consolidation task well and showed no significant behavioral deficits compared to surgically naïve mice (Figure A.6F). We recorded from all three regions simultaneously during pre-exposure (Pre), early and late training (T1, T5), early retrieval (R6) and intermediate and remote timepoints (R20, R34).

First, looking across all recorded neuronal responses, we observed that even as early as T1 and T5, AM preferentially encodes the HR compared to the LR context, a trend which was noticeably absent in HPC and ACC cells (Figure 6.3A-B). However, by R34, ACC,

but not HPC or AM, showed preferential tuning to HR. We then looked across brain regions for coordinated activity that might suggest interactions occurring on the timescales of systems consolidation. Interestingly, when examining inter-regional activity patterns, we found that context-specific AM-to-ACC activity correlations progressively increased across days, but peaked by R20, and decreased by R34 (Figure 6.2C). We identified the population of ACC cells that were highly correlated with at least one AM cells on R20 (Figure 6.2D; n = 56 cells, 60% of correlated to one AM cell, 20% correlated to two AM cells, and 14% correlated to three or more AM cells). Contextual responses in both regions tended to be higher in the consolidated HR context when compared to the LR context (Fig 6.2D, top and bottom left). When followed out to R34, the same ACC cells tended to significantly increase their preferential tuning to the consolidated memory above that of the remaining cells (Figures 6.2D, bottom right, and Figure 6.2E, Wilcoxin rank-sum $P<0.01$,). Notably, this effect was not observed with ACC cells correlated to HPC cells on R20 (Figure A.8F, Wilcoxin rank-sum p=0.6175).

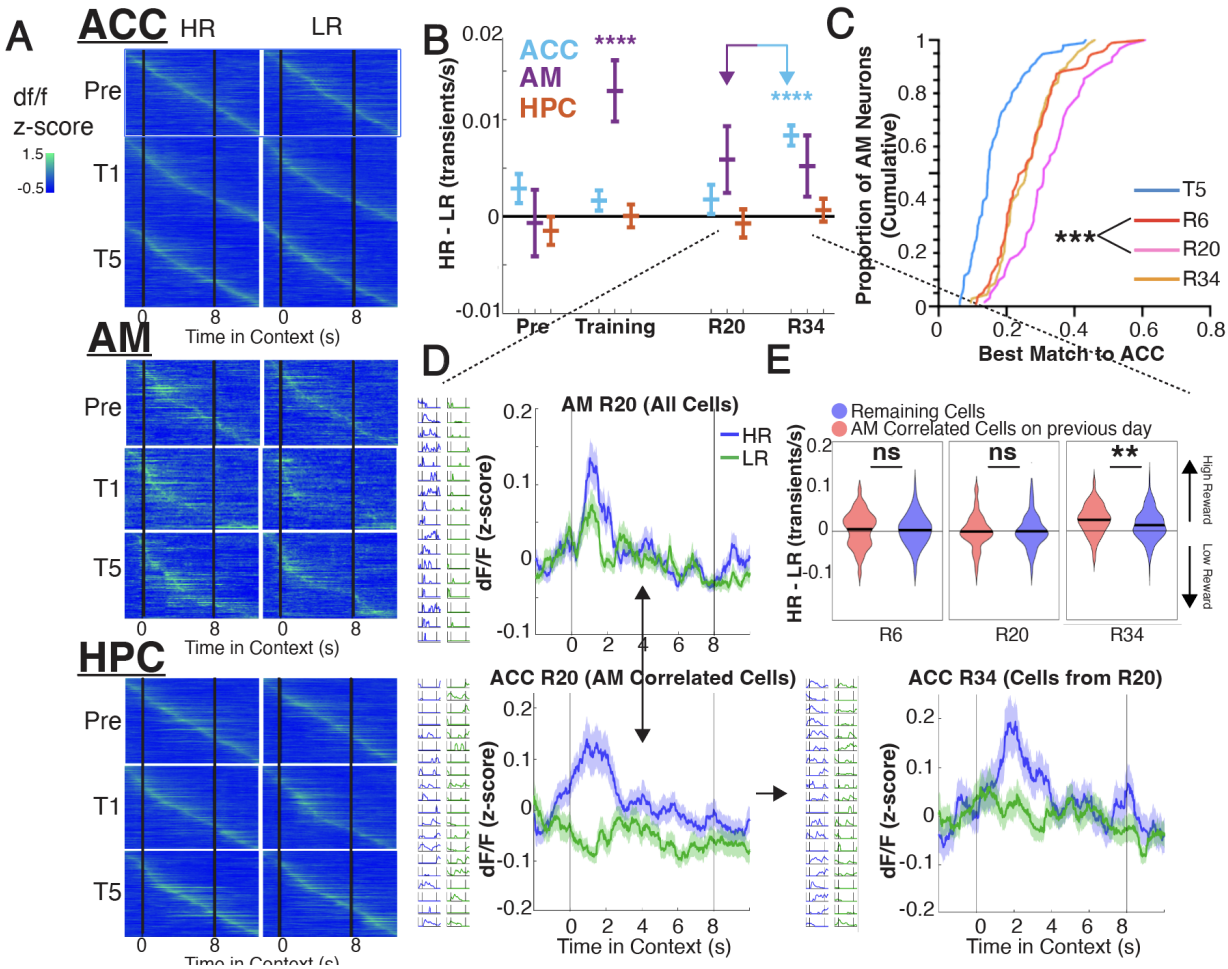

Figure 6.2 | **Contextual tuning shifts across weeks.**

Figure 6.2 (cont.) (A) Mean z-scored dF/F for every recorded cell, aligned to cue-zone entry in high reward (HR; left) and low reward (LR; right) through training (N=3 mice). Number of neurons for Pre, T1, and T5, respectively: ACC: n=426, n= 334, and n=477; AM: n= 94, n=75, and n=111; HPC: n=461, n=457, and n=464. (B) Tuning to high reward vs low reward contexts (see methods) for every recorded cell in ACC, HPC, and AM across days. ***$p<0.001$ for T1 and **$p<0.01$ for T5 and R34, one sample t-test. (C) Cumulative distribution of the best match correlation of ACC cells paired with AM cells across days. ***$p<0.001$, Wilcoxin rank-sum between R6 and R20. (D) AM and ACC correlations on R20 predict tuning in ACC on R34. Top left: cue-zone-aligned mean z-scored dF/F of all AM cells on R20 (n=111 cells). Bottom left: Mean z-scored response of ACC cells which form highly correlated pairs with at least one AM cell. Bottom right: mean response of these same tracked ACC R20 cells on R34. For each mean dF/F trace, representative cells selected from one animal are shown to the left. (E) Distribution of tuning for ACC cells correlated to at least one AM cell on the previous recording session compared to the tuning of all remaining cells. ** $p<0.01$, Wilcoxin rank-sum test.

In addition to increased tuning, we found that within ACC, the intra-region cell-cell correlations increased significantly throughout consolidation (R6 to R34) in HR trials but not LR trials (Figure 6.3A). Interestingly, only on R20 (when AM-ACC correlations peaked), we observed that ACC cells correlated to AM cells tended to be highly correlated with a greater number of other ACC cells than would be expected by chance (Figure 6.3B). These inter-regional correlation structures were not observed with the HPC-to-ACC network (Figure A.8F), and were not due to any appreciable changes in overall event rates in either AM or ACC (Figures A.8A and A.8B). Thus, not only do ACC cells become individually more tuned toward consolidated memories at remote time, but these cells tend to fire more synchronously, with AM-ACC interactions peaking in the days prior to these changes.

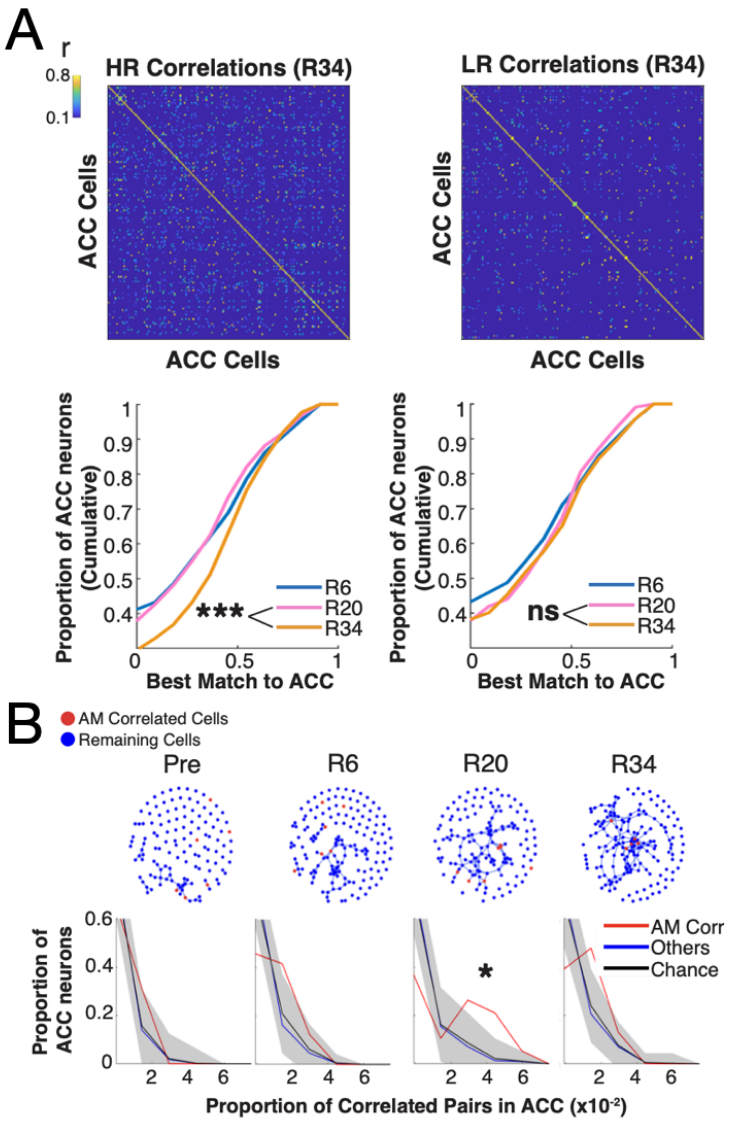

Figure 6.3 | **Network timing in AM and ACC.** (A) Top: Representative correlation matrices within ACC for either HR or LR context, taken from a single animal. Bottom: Cumulative distribution of best match correlation of ACC cell pairs across recording sessions for HR (left) and LR (right).(B) Top: Example from one animal of undirected network graphs of ACC cell correlations. Each node represents an individual ACC cell, and connecting edges represent significant correlations in HR (Pairwise Pearson's r>0.3). Red nodes are the ACC cells most temporally correlated with AM cells (top 5% of Pearson's r) shown in red. Bottom: Quantification of the proportion of pairwise correlations (number of edges for a given cell normalized by the total number of cells for a given recording secession) in ACC for either red nodes (ACC cell that is highly correlated to at least one AM cell) and blue cells (all remaining ACC cells), compared to chance (in black, see methods). Shaded area represents the 95% confidence interval around chance distribution. Significance is indicated by bins above this level.

Taken together, these results suggest a model in which AM performs early selection of salient memories (by T5), and facilitates their re-organization to cortex via progressive increases in inter-regional connectedness with ACC (that peaks by R20), thus coordinating the stability and intra-regional connectedness of memory ensembles within ACC (that peaks at R34). Interestingly, this provides an explanation for how optogenetic manipulations (either inhibition or excitation) during training may still impact circuits at remote time points.

We next sought to prove this relationship through causal manipulation via optogenetics. We developed another cohort of mice with bilateral stGtACR2-based inhibition of AM-to-ACC projections during training (T1-T5) while we imaged in ACC during consolidation (R6 and R34) (Figures 6.4A, A.9A). We found indeed that disruption of AM-to-ACC activity during training again disrupted memory recall at remote but not recent time points (Figure A.9C), and this was associated with loss of contextual responses to the HR context in ACC (Figures 6.4B). Furthermore, inhibition of this projection disrupted the emergence context-specific intra-ACC correlations (Figure 6.4C), which had been a hallmark of consolidation.

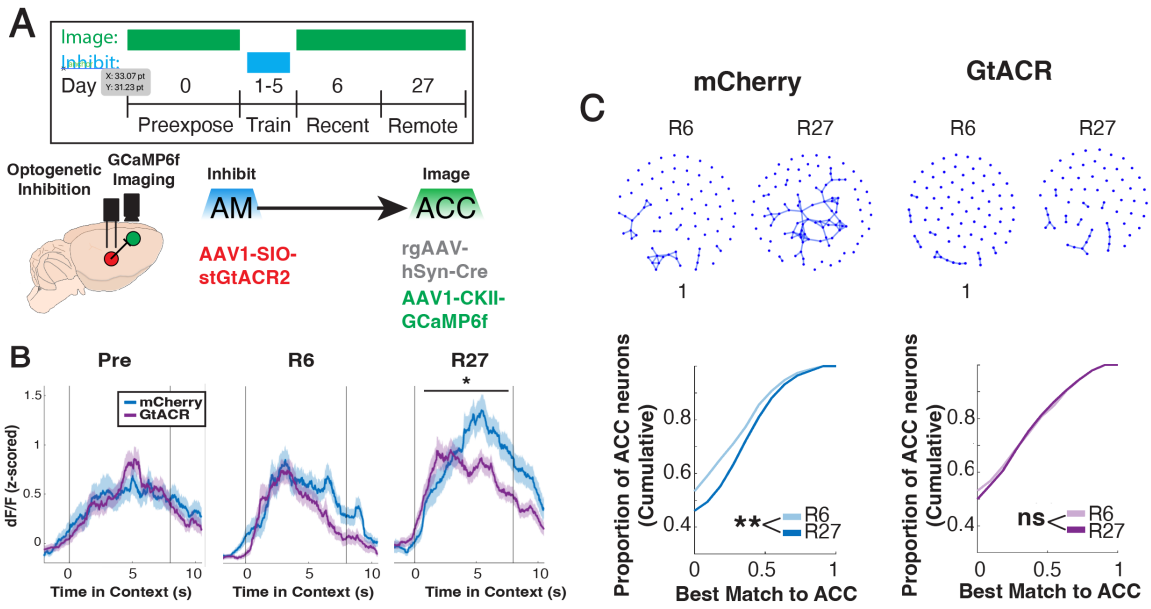

Figure 6.4 | **AM is required to stabilize the tuning and timing of long-term contextual representations in cortex.** (A) Experimental design for optogenetic inhibition and imaging experiment. rgAAV1-hSyn-Cre and AAV1-CKII-GCaMP6f was injected into anterior cingulate cortex (ACC) and AAV1-SIO-stGtACR2 was injected into anteromedial thalamus (AM). Imaging was performed on preexposure, recent and remote retrieval sessions, whereas inhibition occurred during each training session. (B) Mean z-scored dF for context-tuned neurons, aligned to cue-zone entry, compared between mCherry and GtACR mice on preexposure, recent (R6) and remote (R27) retrieval. *p<0.05, two-sample t-test. (C) Top: Examples of undirected network graphs of ACC cell correlations in HR from mCherry (left) and GtACR (right) mice during recent and remote retrieval. Each node corresponds to a cell in ACC and each edge is a highly correlated cell pair (Pairwise Pearson's r>0.3) Bottom: Cumulative distribution of the best-match correlation for every cell in HR from recent to remote retrieval. N=5 mCherry vs 7 GtACR mice. **p<0.01, Wilcoxin Rank-Sum test.

Chapter 7

Conclusion and Future Directions

The idea of memory consolidation first emerged as a way to explain why certain memories change in strength over minutes, days, weeks, and years. In past decades, much progress has been made in detailing the location and timing of the memory trace in the brain. The standard theory of systems consolidation was put forth to explain the curious fact that memories initially depend on the hippocampus, but can eventually be recalled without it (Squire et al., 2015). Much of what is known about systems consolidation relies on lesion studies or observations of the distribution of cell activity markers (such as immediate early genes) in post-mortem brains. Several studies have tracked the longitudinal dynamics of memory representations in individual brain regions (Ziv et al., 2013, Kitamura et al., 2017), an approach that can be made all the powerful by imaging multiple circuits simultaneously as mice consolidate learned contextual associations. Additionally, studies of memory consolidation have historically used fear conditioning paradigms for a behavioral readout of memory retrieval. While powerful, it is important to develop other behavioral models to ensure these results generalize to other forms of hippocampal-dependent memory. The current work makes significant contributions to

the field to address these limitations in several ways.

First, we established an approach to study memory consolidation longitudinally. By using a virtual reality setup, we could precisely align sensory stimuli and behavior with ongoing neural activity or optogenetic interventions. Our task was particularly novel in that rather than using a single start or end point, we successfully probed memory-associated behavior repeatedly across weeks. This allowed us to characterize the state of tuning and functional associativity in neural responses across the brain as the memory trace evolved. The task also required integration of multiple sensory cues, as well as active engagement in virtual space in order to make the appropriate cue-outcome associations. These factors make it much more likely to engage the hippocampal memory system (Squire, 1992), which we confirmed with optogenetic inhibition (Chapter 3). One concern of our behavioral approach might be that by running repeated retrieval trials followed by re-training sessions, we might be inducing extinction or re-consolidation (Nader, 2016). To minimize this effect, we ensured that retrieval and re-training sessions were as short as possible. We also validated that behavior, optogenetic, and imaging experimental outcomes remained the same whether there were intervening retrieval sessions or not (Figures 3.1C, A.1, A.6). Thus we are confident that our results speak to the mechanisms operating during memory consolidation, rather than just extinction or reconsolidation. Using multiple retrieval trials specifically enabled certain findings that required the tracking of neural activity across multiple days (Figure 6.2).

As mentioned in Chapter 1, there is significant ongoing debate in the field of memory consolidation about the role of the hippocampus in remote memory retrieval (Sutherland et al., 2020). On one extreme is the standard model of systems consolidation, which suggests a time-limited role for the hippocampus with no involvement for remote memories (Squire et al., 2015). On the other end is multiple trace theory (MTT), which posits that

the hippocampus is always required for the retrieval of episodic-like memories (Nadel and Moscovitch, 1997). The present work primarily supports the standard model by confirming a time-limited role for the hippocampus in recall for our contextual memory task (Figures 3.3-3.4). In this thesis, I chose to focus my analysis on primarily the AM-ACC circuit. The hippocampus held equally weighted representations of each context (Figures 6.2B, A.8E), but it was difficult to make claims about whether these representations were capable of supporting recall. In future work, it will be necessary to analyze the role of HPC-AM interactions through both casual manipulations and longitudinal recordings to better understand the timing of hippocampal dependency.

In this thesis, I also provided evidence that the AM thalamus acts as a critical gateway for the consolidation of early hippocampal-dependent memories to long-term cortical storage. The AM thalamus is thought to play a role in long term memory based on lesion and inactivation studies (Aggleton and Sahgal, 1993), but the nature of that role has remained somewhat unclear. By tracking neural representations longitudinally over weeks, we were able to identify a memory-related signal in the anterior thalamus which emerged and persisted in the intermediate time window of systems consolidation. Furthermore, inactivation of cortical projections from AM thalamus specifically disrupted consolidation, demonstrating a functional role for that signal. What computations might AM thalamus be performing in order to facilitate consolidation?

AM thalamus plays a known role specifically in modulating attention in memory tasks (Bubb et al., 2021), and may play a more general role in salience selection (Zhu et al., 2018). AM receives input from neuromodulatory and other value-assigning regions of the brain, suggesting it is capable of integrating signals associated with high-value contextual information (de Lima et al., 2017, Harris et al., 2019, Sampathkumar et al., 2021). More salient stimuli are more likely to be remembered in long-term memory (Lisman et al., 2011), so

perhaps AM acts to selectively gate the encoding or preservation of high-value associations in cortical circuits. We provide evidence for this in several ways. First, we demonstrate that enhancement of AM-ACC activity facilitated remote recall for a low-valence contextual memory that would otherwise have not been consolidated (Figure 5.4). A recent study mechanistically supports this finding, by demonstrating that driving AM-ACC projecting cells activates dopaminergic neurons to support learned goal-directed behavior (Yang et al., 2022). Furthermore, our results demonstrate that AM has early preferential tuning to high-valence contexts, even on the first day of exposure (Figure 6.2A-B). Interestingly, inter-regional correlations between AM and ACC cells at intermediate time points (two weeks after training) predicted reliable tuning for the consolidated memory in ACC at the remote timepoint (a "tuning effect"). This supports the idea that AM "tags" certain cortical neurons that are eventually selected to support memory retrieval (Lesburguères et al., 2011). Finally, ACC cells became significantly more correlated with one another by the remote timepoint, and AM cells tended to be correlated with ACC cells that were highly central within the local network (a "synchronicity effect"). Both the tuning and synchronocity effects were crucially dependent on early AM-ACC activity, when salience selection was likely occurring. Thus, AM-to-ACC interactions during training are required for establishing the eventual tuning and synchronicity of cortical neurons associated with successful consolidation and recall (Figure 7.1).

Under this proposed model, representations for both high and low valence memories are formed in HPC and ACC. Selection for consolidation happens at the level of the thalamus, possibly with coincident neuromodulatory input. This preferential encoding drives and shapes cortical ensembles through feed-forward thalamocortical projections, to eventually stabilize and drive recall independently of the hippocampus. Inhibition at the time of learning disrupts the propagation of high-salience contextual information from AM to ACC. On the other hand, excitation via SSFO increases the probability and rate of AM

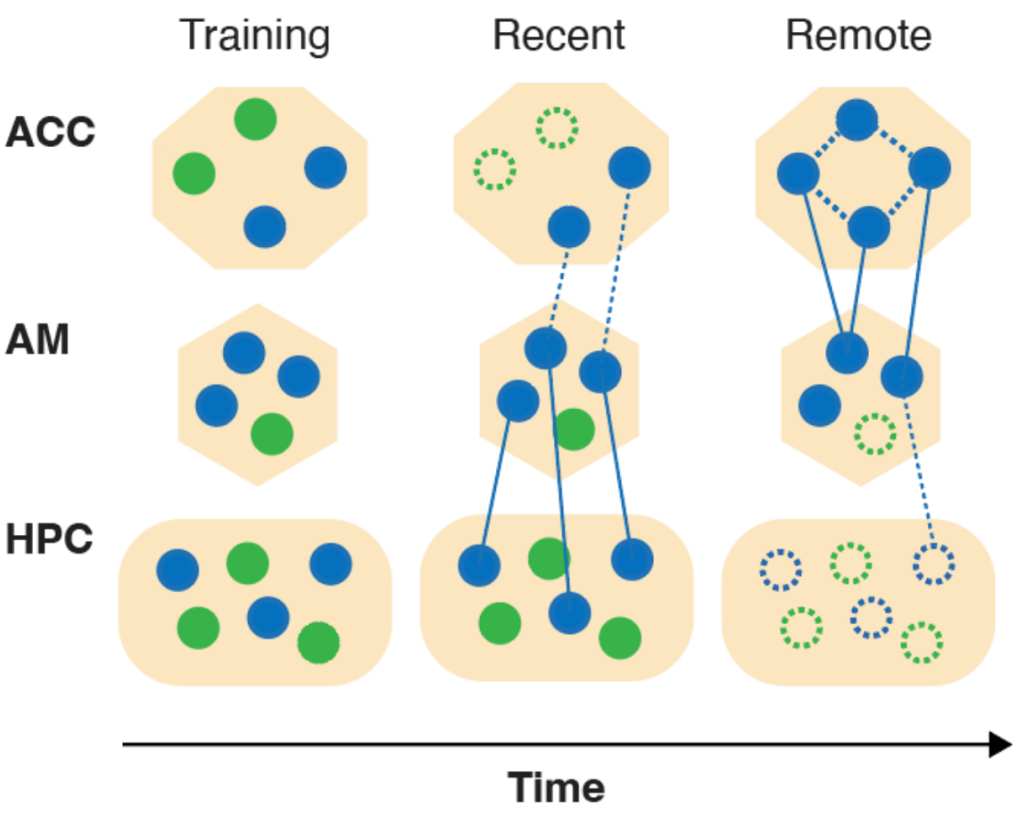

Figure 7.1 | **Proposed model.** AM selects and stabilizes consolidated memory representations in cortex. Selection of information about salient cues by AM during training leads to coordinated responses in ACC at the time of remote retrieval, eventually allowing for recall that is independent of HPC at remote timepoints. Blue: cells tuned to high reward. Green: cells tuned to low reward.

cells firing in response to the low-salience context, leading to associated downstream activation in ACC. Open questions about this model still remain, however. For one, it is still unclear where exactly the memory trace resides in the intermediate window, between the times of hippocampal and cortical dependencies. Is it a gradual transition from the hippocampus to the cortex, or does the AM itself store all the information necessary to drive recall? Based on cell density and distribution of projections in AM (Wright et al., 2010), the latter seems somewhat unlikely. However, future studies should test this by disrupting or enhancing synaptic transmission in AM at various timepoints during the consolidation window; ideally this would be done chronically during wake or sleep (Armbruster et al.,

2007). Sleep is crucial for consolidation (Rothschild, 2019), and the present work only measures neural dynamics during online retrieval. In addition to inhibition experiments, it will be necessary to measure ongoing activity in thalamus during sleep (perhaps with chronically implanted high-density electrode probes, Juavinett et al., 2019) to see whether there is a correlate of hippocampo-cortical reactivation in the thalamus. Though AM displays synchronicity with hippocampal oscillations (Albo et al., 2003), to date no study has chronically studied these interactions, especially during sleep. Does the sharp-wave ripple (Joo and Frank, 2018) pass through the thalamus? If it did, this might provide a pathway for supporting the hippocampo-cortical interactions that occur during sleep and reinforce associations made during learning (Maingret et al., 2016).

Even once the role of AM in consolidation during offline periods is resolved, a major question still remains: why is systems consolidation so slow? In computational models of consolidation, the hippocampus is typically modeled as a ”fast learner” while the cortex is a ”slow learner” (McClelland et al., 1995). It turns out there are beneficial reason for drawing such a distinction. If new information is acquired with too fast a learning rate across the whole system, new associations will disrupt or even eliminate existing ones. Thus it is advantageous computationally to have one network that can rapidly form and eventually forget new memories, and which trains (through reactivation) a separate, slowly-learning network in order to minimize interference between relevant associations. Of note, incorporating an AM-like structure into this model would involve adding a salience signal to each learned association and a prioritization rule (or ”tag”) based on salience for slow learning by the cortex. However, how this slow learning algorithm is enacted in biological systems remains elusive. An explanation for this might come from studying what happens to synaptic connections in offline periods. One theory suggests that during sleep, cortical synaptic weights initially strengthened from learned experiences during waking hours are weakened, in order to achieve homeostatic balance in the excitability of net-

works (Tononi and Cirelli, 2014). If this is the case, cortical learning is constantly working against itself in a competitive fashion. Only those learned associations that are strong enough (or reactivated frequently) will resist overnight synaptic pruning (Li et al., 2017). Perhaps as AM interacts with highly active cortical cells that are central within their local network (Figure 6.3C), marginal differences in synaptic strength are eventually magnified over repeated bouts of sleep. Future studies might use electrophysiological techniques in cortico-thalamic circuits over weeks to understand plasticity changes over time in ACC cells receiving thalamic input versus those that do not.

Furthermore, it will be important to study the roles of the other brain areas, including the other nuclei in the anterior thalamus. Though AD and AV thalamus do not send strong projections to ACC, they do interact through reciprocal connections back to hippocampus-associated structures (Jankowski et al., 2013). What role does the anterior thalamus play as a whole in maintaining memory representations and supporting recall throughout the timeline of systems consolidation? A growing literature also suggests the retrosplenial cortex (RSC) is involved in the long-term storage of hippocampal-dependent memories (Todd and Bucci, 2015). The RSC is particularly interesting anatomically, as it has broad reciprocal connectivity with the hippocampus, ACC, and anterior thalamus (Van Groen and Wyss, 2003). While we found that RSC does not appear to support consolidation for low-salience memories (Figure 5.4), others have shown that is necessary for post-encoding recall of contextual (Keene and Bucci, 2008) and spatial memories (Czajkowski et al., 2014). Other regions of interest include the basolateral amygdala (Paré, 2003) and the entorhinal cortex (Takehara-Nishiuchi, 2014). How can we integrate these previous findings with ours to better understand memory consolidation? One option is the the cortex receives parallel information from each of these circuits, and redundancy is a feature to ensure long-term stability of memory. Another option is that each region provides different information necessary for the eventual binding of memory represen-

tations. In this work, I primarily analyzed the responses to rewarding contextual memories, so the role of AM in fear memories specifically remains unclear; perhaps different memory types are processed through different circuits. The BLA in particular is required for the long-term retention of stress-induced memory retention (Fanselow and LeDoux, 1999). A third option is that these regions (and others) act as sequential gates, with the timing varying over hours, days, and weeks. Future studies should investigate the cross-talk between these regions simultaneously and longitudinally to dissociate the different circuits involved in what is surely a brain-wide phenomenon.

The establishment of our model would not have been possible without the development of a technique for simultaneously imaging multiple regions across the mouse brain. Though imaging techniques utilizing high-resolution fiberoptics have been established (Helmchen et al., 2001), this is the first time multiple fibers have been utilized to gain reliable access to image circuits separated by significant distance across the mouse brain. A major difficulty was minimizing motion artifacts and attaining reliable registration of cells across days. A combination of hardware (Figure 6.1B) and software (see Methods) solutions were required to achieve such stable recordings. Other approaches now exist for multi-region imaging utilizing meso-scale imaging techniques (Sofroniew et al., 2016, Yadav et al., 2022), but our fiber-bundle technique has several benefits. For one, the components are cost-effective and relatively simple to assemble on top of an existing fiber photometry setup. Furthermore, the approach is extremely scalable, with the main limit being the number and size of lenses being surgically implanted inside of the mouse's brain. I estimate that upwards of 6 different regions at various distances and depths across the brain could be imagined simultaneously while the mouse behaves. Additionally, while we opted to use a head-fixed paradigm in order to precisely control the onset of sensory stimuli, our design is compatible with freely-moving animals.

Limitations do exist, and future experiments should work to build on this approach. For one, our microscope uses single-photon epifluorescence for excitation, which has lower spatial resolution and lacks the ability for recording from multiple z-planes compared to state-of-the-art two-photon imaging. Though our goal was to build a simple, scalable technique for multi-region cell-resolution imaging, it is not unfeasible to imagine a two-photon version of this technology that scans rather than epifluoresces (Helmchen et al., 2001). Our imaging experiments were also limited by the sample size (n=3 mice for most results) and the number of cells that could be reliably tracked across days. This latter point could be improved with a larger field of view, and improved hardware and software solutions for reliable registration across days. Future improvements to the design of this technology would allow for better tracking of the stability of memory representations in all three regions; i.e. what percentage of cells remain active in response to memory recall across days, and whether cortical representations are ”tagged” by the early AM selection. The temporal resolution of this technique is also limited by the dynamics of GCaMP. As it stands, the technique likely would not be able to detect precisely-timed neural interactions. This could be solved in the future with rapid voltage sensors (Bando et al., 2019), or by pairing imaging with *in vivo* electrophysiological recordings. Future studies using such an approach with higher temporal recordings will help address outstanding questions such as 1) the plasticity rules between HPC-to-AM that enable gating and selection of salient representations in AM; 2) The modes of firing in thalamic neurons (tonic vs bursting) that may preferentially select feed-forward inhibition vs excitation in cortex (Mukherjee et al., 2021) and 3) the role of cortical feedback in tuning these responses.

Chapter 8

Methods

8.1 Experimental model and subject details

8.1.1 Mice

All procedures were done in accordance with guidelines derived from and approved by the Institutional Animal Care and Use Committees (protocol 19112H) at The Rockefeller University. Animals used were 8-10 weeks-old wild-type male and female (counterbalanced across experimental conditions when applicable) C57BL/6J mice (Jackson Laboratory, Strain 000664) at the time of surgery. Mice were group housed (3-5 per cage) with ad libitum food and water unless mice were water restricted for behavioral assays, in which case they were given 1 mL water a day. Body weight was monitored daily to ensure it was maintained above 80% of the pre-restriction measurement. Surgical procedures and viral injections were carried out in mice under protocols approved by Rockefeller University IACUC and were performed in mice anesthetized with 2% isoflurane using a stereotactic

apparatus (Kopf).

8.2 Method details

8.2.1 Surgical procedures

Puralube vet ointment was applied to the eyes and 0.2mg/kg meloxicam was administered intraperitoneally using a 1mL syringe. Hair from the scalp was trimmed, and the area was sterilized using povidone-iodine swabs and subsequently ethanol swabs. An incision covering the anteroposterior extent was made to allow access to the skull. Injection sites were accessed using a dental drill which made 0.5mm holes through the skull. All virus was injected using a 35G beveled needle in a 10ul NanoFil Sub-Microliter Injection syringe (World Precision Instruments) controlled by an injection pump (Harvard Apparatus) at a rate of 100nl/min. After all viral delivery, an additional 5-10 mins delay was applied to avoid backflush before slowly removing the injection needle. Animals that required cannulas or GRIN lenses were implanted immediately following viral injection. Following surgery, mice were allowed to recover in a single housed cage for up to 12 hours, and were given meloxicam tablets. Mice were typically housed for three weeks to allow for adequate expression before behavioral testing or histology.

Viral injections

- In retrograde tracing experiments, mice were unilaterally injected in ACC (A/P +1.0, M/L, ±0.35, D/V -1.4) with rgAAV-CAG-tdT at a volume of 500 nl (1.0 x 10^{13} vg/mL).
- For multi-fiber photometry experiments, 1µl of AAV1-CaMKIIa-GCaMP6f (UPenn

Viral Core, diluted to 5 x 10^{12} vg/mL) was injected into ACC, HPC (A/P: -1.5, M/L: ±1.5, D/V: -1.6), ENT (A/P: -4.35 , M/L: ±3.75, D/V: -4.0), and BLA (A/P: -1.23, M/L: 2.75, D/V: -4.7) while AAV1-CAG-GCaMP6f was injected into ANT. One week after virus injection, mice were unilaterally implanted with 1.25 mm ferrule-coupled optical fibers (0.48 NA, 400 µm diameter, Doric Lenses) cut to the desired length so that the implantation site is 0.2 mm dorsal to the injection site.

- For cellular imaging, AAV1-CaMKIIa-GCaMP6f (5.0 x 10^{12} vg/mL) was injected into ACC and HPC while AAV1-hSyn-GCaMP6f was injected into AM (5.0 x 1012 vg/mL)
- For optogenetic inhibition of HPC, pAAV1-CaMKIIa-stGtACR2 (1 x 10^{13} vg/mL) was injected into HPC bilaterally. For controls, pAAV1-CaMKIIa-mCherry (7 x 10^{12} vg/mL) was injected.
- For chemogenetic inhibition of HPC and ACC, pAAV9-CaMKIIa-hM4D(Gi) (1 x 10^{13} vg/mL) was injected into ACC or HPC bilaterally. For controls, pAAV9-CaMKIIa-mCherry (1 x 10^{13}vg/mL) was injected bilaterally in either region.
- For optogenetic inhibition of AM-ACC projections, rgAAV-hSYN-Cre (1.20 x 10^{13} vg/mL)was injected into ACC bilaterally and either AAV1-hSyn1-SIO-stGtACR2 (1.50 x 10^{13} vg/mL) or AAV9-hSyn-DIO-mCherry (9.0 x 10^{12} vg/mL) for controls was injected bilaterally into AM.
- In SSFO experiments, rgAAV-hSyn-Cre (1.3 x 10^{13} vg/mL) was injected bilaterally in ACC and pAAV-Ef1a-DIOhChR2(C128S/D156A)-EYFP (Vector BioLabs, 1.0 x 10^{13} vg/mL) bilaterally in AM or RSP (A/P: ±0.40, M/L:-2.0, D/V: -0.7) for behavioral control and pAAV-DIO-eYFP (1.0 x 10^{13} vg/mL) into AM for experimental control.

8.2.2 TRIO tracing

For the "tracing of input-output" (TRIO) tracing of AM-ACC, CAV-Cre (500 nL, 2.5 x 10^{12} vg/mL) was injected into ACC, and a combination of AAV8-CAG-FLEX-TCB/ AAV8-CAG-FLEX-oG-WPRE-SV40 (500 nL each, 2.5x10^{12}) was injected into AM. After two weeks, Env-RV-dG-eGFP (500 nL, 1 x 10^{9} vg/mL) was injected into AM. Five days later, mice were perfused and tracing was confirmed via histology.

8.2.3 Cannula implants

One week after viral injections, mice undergoing photometry or optogenetic experiments were implanted with fiber optic cannulas (Doric Lenses). For photometry, mice were unilaterally implanted with 1.25 mm ferrule-coupled optical fibers (0.48 NA, 400 µm diameter, Doric Lenses) cut to the desired length so that the implantation site is 0.2 mm dorsal to the injection site. For optogenetics, mice were implanted bilaterally with 1.25mm cannulas (0.22 NA, 200µm diameter, Doric Lenses). In both cases, cannula implants were slowly lowered using a stereotaxic cannula holder (Doric) at a rate of 1 mm/min until it reached the implantation site, 0.2 mm dorsal to the injection site. In the case of bilateral AM optogenetic inhibition, one cannula was implanted at a 10 degree angle laterally to the skull in order to prevent stereotactic hindrance. Optic glue (Edmund Optics) was then used to seal the skull/cannula interface and a custom titanium headplate was glued to the skull using adhesive cement (Metabond).

8.2.4 GRIN lens implants

Immediately following viral injections, mice undergoing calcium imaging were implanted with gradient-index (GRIN) lenses. An incision covering the anteroposterior extent was made, and the skin overlying the skull was cleared. The skull was then cleared and textured using a scalpel. Using a dental drill, 1mm diameter holes were made at stereotactically determined sites of implantation. Site of drilling was immediately covered using chilled 1x PBS, and using a sterile 28 G x 1.2" insulin syringe and low pressure vacuum suction, the underlying dura was removed. GRIN lenses (0.6 mm diameter, 7.2mm length, 0.5 NA from Inscopix) were wrapped in a 0.68mm wide custom length stainless steel sleeve (McMaster, catalog 8987K54) using optic glue, made to cover only the part of the lens held external to the brain. With a 0.5mm burr (Fine Science Tools) attached to a stereotaxic cannula holder, the GRIN was slowly lowered into the brain at a rate of 1mm/min, ending 0.2mm dorsal to the injection site. The skull was constantly flushed with chilled 1x PBS. Every time the lens moved 0.8 mm more ventral, it was temporarily retracted 0.4 mm dorsally at the same rate, before continuing down again. We found this especially helpful to maximize the number of observed cells when imaging in very deep regions. The skull-sleeve connection was then sealed with glue, and further secured with adhesive cement. For multi region imaging, the two other GRIN lenses were implanted in the same manner, with consideration to stereotactic hindrance from each additional lens (First AM, then ACC, and finally HPC). A custom titanium headplate was glued to the skull using adhesive cement. Immediately following surgery, mice were injected with 0.2mg/kg dexamethasone subcutaneously to reduce inflammation.

8.3 Histology

Animals were deeply anesthetized with 5% isoflurane before transcardial perfusion with ice-cold PBS and 4% paraformaldehyde in 0.1M PB. Brains were then post-fixed by immersion for 24 hours in the perfusate solution followed by 30% sucrose in 0.1M PB at 4°C. The fixed tissue was cut into 40 µm coronal sections using a freezing microtome (Leica SM2010R), free-floating sections were stained with DAPI (1:1000 in PBST), and mounted on slides with ProLong Diamond Antifade Mountant (Invitrogen). Images were taken on a Nikon Inverted Microscope Eclipse Ti-E with a 4x/0.2 NA objective lens. Whole-slide-images were stitched with NIS-Elements imaging software and further analyzed in ImageJ and MATLAB.

8.4 Virtual Reality Behevior

8.4.1 Design

We used a custom built virtual reality environment, modified from a previously reported version (Rajasethupathy et al., 2015). In brief, a 200-mm-diameter styrofoam ball was axially fixed with a 6-mm-diameter assembly rod (Thorlabs) passing through the center of the ball and resting on 90° post holders (Thorlabs) at each end, allowing free forward and backward rotation of the ball. Mice were head-fixed in place above the center of the ball using a headplate mount. Virtual environments were designed in the virtual reality MATLAB engine ViRMEn (Aronov and Tank, 2014) . The virtual environment was displayed by back-projection onto white fabric stretched over a clear acrylic hemisphere with a 14-inch diameter placed 20 cm in front of the center of the mouse. The screen

encompasses 220° of the mouse's field of view and the virtual environment was back-projected onto this screen using a Vamvo Ultra Mini Portable projector. The rotation of the styrofoam ball was recorded by an optical computer mouse (Logitech) that interfaced with ViRMEn to transport the mouse through the virtual reality environment. A National Instruments Data Acquisition (NIDAQ) device was used to send out TTL pulses to trigger the CMOS camera, laser for optogenetics, and the various Arduinos controlling tones, odors, airpuff, lick ports. Additionally, the NIDAQ recorded the capacitance changes of the lick port when licking occurred and the CMOS camera exposures to align lick rate and neural recording/imaging to trial events.

8.4.2 Behavioral shaping

Starting approximately 3 weeks after mice recovered from surgery, they were put on a restricted water schedule, receiving 1 mL of water in total per day. Body weight was monitored daily to ensure it was maintained above 80% of the pre-restriction measurement.

After a week of water deprivation, mice were habituated to the styrofoam ball for 2 days by receiving their 1 mL of water per day head-fixed. Then mice were put onto a linear track (vertical gray bars) where water release was contingent on walking a short distance to the outcome zone (white horizontal bars) where they received 5 seconds of water delivery. Over the course of a session, and in subsequent days, the distance needed to travel to enter the outcome zone increased. If a mouse took longer than 10 minutes to receive their 1 mL of water on a given day, the distance needed to travel to get water was repeated on the following day until they could reliably walk on the ball for water under 10 minutes. Once mice could walk down the full length of the linear track used in training,

we introduced the inter-trial interval and a timer (5 seconds for photometry experiments, 8 seconds for optogenetics and single-cell imaging experiments) to encourage mice to actively engage with the task. Once all mice from a cohort were able to complete at least 80% of initiated trials, training began.

8.4.3 Behavioral task

In the final version of the task that was used during photometry, optogenetics, and imaging experiments, mice ran down a virtual linear track to reach an outcome zone and used contextual cues presented along the track to predict the reinforcement they will receive (4ul of sucrose water or airpuff). At the beginning of the linear track, mice self-initiate sessions by running through a start zone above a set speed of 12 cm/s, (20% of the ball perimeter in a second). Visual, auditory, and olfactory cues were then presented in succession 1 second after one another. The visual cues consisted of blue stars or yellow triangles designed within the ViRMEN GUI (Aronov and Tank, 2014) and presented along the walls of the linear track. The auditory cues consisted of 5 KHz or 9 KHz tones outputted by a thin plastic speaker (Adafruit) and olfactory cues consisting of alpha-pinene or octanol were diluted with mineral oil to 10% and released by a custom-built olfactometer. Both auditory and olfactory cues were outputted by Arduino code under the control of ViRMEN code. The cues for reward context were blue stars, 5KHz tone, and alpha-pinene while the cues for aversive context were yellow triangles, 9KHz tone, and octanol. For photometry experiments, all cues were turned off after 5 seconds into the context zone. For optogenetics and single-cell imaging experiments, the cue zone was extended to last 8 seconds. Entry into the outcome zone was contingent upon running down a linear distance of 60 cm along the ball within the cue zone time limit. If that distance was not reached, mice would be placed in a 5 second inter-trial interval proceeding the next trial.

The outcome zone consisted of free access to 10% sucrose water presented by a lickometer (reward context) or a 50ms airpuff presented by a pipette tip cut to a fine point 3 inches away from the snout (aversive context). Both reinforcements were outputted by Arduino code under the control of ViRMEN code. After the outcome zone mice were transported to a 5 second inter-trial interval before starting the next trial.

Performance in the task was assessed by average speed (during the first 5 seconds in cue zone) and average anticipatory lick rate (during the last 2 seconds in the cue zone) for all reward and aversive context trials in a given session. Prior to training, mice were given a "pre-exposure" session where they were exposed to each set of cues, with tap water given upon reaching the outcome zone in both. They were then given 5 days of training (referred to as T1-T5), where reinforcement was given in the outcome zone. For the photometry experiment, mice began 5 minutes of retrieval sessions where no reinforcement is given on days 6, 13, 20, 27, 41, and 55 since training began. After each retrieval session, mice underwent 8 trials of each context in a "retraining" session where reinforcement was given again, to avoid memory extinction and loss of engagement in the task. For the optogenetics and imaging experiments with early and remote retrieval sessions, mice were tested with sessions consisting of 4 interspersed trials of each context type (for a total of 12 trials), followed by a re-training session of the same length. For experiments with only remote retrieval, mice received a single session again consisting of 4 trials of each context.

8.4.4 Modified behavior with three contexts

Mice undergo behavioral shaping as outlined above. During pre-exposure and training days, a third low reward (LR) context with non-overlapping cues (green diamond visual

cues, 11 kHz tone, and orange-scented essential oil diluted in mineral oil) was included alongside high reward (HR) (same as "R" context in two-context task) and aversive (A) contexts. Presentation was randomized. In low reward training trials, 10% sucrose water was delivered through the lickport at a rate of 1 drop every second for five seconds. No animal was given more than 1mL of sucrose on a given day, and each session concluded after the completion of 8 trials per context. In SSFO excitation experiments, mice were trained on the task as outlined above for 5 days, then moved onto retrieval sessions on days 6 and 27. For multiple-region GRIN imaging experiments, mice had retrieval sessions on days 6, 20, and 34. Like in other trials, mice exposed given brief re-training sessions with reinforcement to minimize extinction.

8.4.5 Behavioral analysis

In all behavioral experiments, we assessed learning and memory recall by calculating a normalized lick rate difference, which we refer to as the discrimination index (DI). The DI was calculated as follows:

DI = (mean lick rate in reward context - mean lick rate in aversive context)/(mean lick rate in reward context+mean lick rate in aversive context)

A DI of 1 therefore indicates perfect discrimination, while a DI of 0 indicates chance performance. For training sessions, the lick rate was only calculated in the window of time 4 seconds preceding the onset of the outcome zone. On retrieval sessions, we included lick rates during the outcome zone, as no reinforcement is provided but mice still expressed anticipatory licking behavior. Repeated measures ANOVA with Tukey's post hoc test was used to assess learning on later days by comparing to discrimination during pre-exposure.

8.5 Optogenetic inhibition of hippocampus

Mice were injected with AAV1-CaMKII-stGtACR2 bilaterally in HPC, while control cohorts were injected with AAV1-CaMKII-mCherry. Cannulas were implanted directly above the injection sites. After three weeks, mice underwent shaping as described above, then moved onto training. For inhibition during training, light from a 470 nm laser (15 mW at fiber tip) was delivered through a mono fiber optic patch cord for 13 seconds (cue zone followed by outcome zone) upon the animal entering the cue zone, throughout the duration of training (15 minutes). For mice with optogenetic inhibition during retrieval, we administered optogenetic stimulation throughout all retrieval sessions from the beginning of cue zone entry to the end of outcome zone entry.

8.6 Chemogenetic inhibition of hippocampus and ACC

For chemogenetic silencing experiments, we injected AAV9-CaMKIIa-hM4D(Gi) (or AAV9-CaMKII-mCherry for controls) bilaterally into either hippocampus or ACC. For a week prior to the remote retrieval session, mice were habituated to handling and intraperitoneal injections of saline. A solution of clozapine N-oxide (CNO) was prepared at a concentration of 0.5 mg/mL, and mice were injected at a dosage of 5 mg/kg. Behavioral experiments were conducted 45 minutes after injection.

8.7 In Vivo Multi Site Photometry Recordings

8.7.1 Photometry Setup

A custom multi-fiber photometry setup was built as previously (Kim et al. 2016). with some modifications that were incorporated to increase signal to noise, detailed below. Excitation of the 470 nm (imaging) and 405 nm (isosbestic control) wavelengths were provided by LEDs (Thorlabs M470F3, M405FP1) which are collimated into a dichroic mirror holder with a 425 nm long pass filter (Thorlabs DMLP425R). This is coupled to another dichroic mirror holder with a 495 nm long pass dichroic (Semrock FF495-Di02-25x36) which redirects the excitation light on to a custom branching fiberoptic patchcord of five bundled 400 mm diameter 0.22NA fibers (BFP(5)-400/430/1100-0.483-m-SMA-5xMF1.25, Doric Lenses) using a 10x/0.5NA Objective lens (Nikon CFI SFluor 10X, Product No. MRF00100). GCaMP6f fluorescence from neurons below the fiber tip in the brain was transmitted via this same cable back to the mini-cube, where it was passed through a GFP emission filter (Semrock FF01-520/35-25), amplified, and focused onto a high sensitivity sCMOS camera (Prime 95b, Photometrics). The multiple branch ends of a branching fiberoptic patchcord were used to collect emission fluorescence from 1.25mm diameter light weight ferrules (MFC-400/430-0.48-ZF1.25, Doric Lenses) using a mating sleeve (Doric SLEEVE-ZR-1.25). The excitation is alternated between 405nm and 470nm by a custom made JK flip flop which takes the trigger input from the sCMOS and triggers the two excitation LEDs alternatively. Bulk activity signals were collected using Photometrics data acquisition software, Programmable Virtual Camera Access Method (PVCAM).

8.7.2 Photometry Recording

While mice performed the VR-based contextual discrimination task we recorded bulk calcium signals from five regions: ACC, HPC, ANT, BLA, and ENT simultaneously. We recorded at 18 Hz with excitation wavelengths alternating between 470 nm and 405nm, capturing calcium dependent and independent signals respectively, resulting in an effective frame rate of 9 Hz.

8.7.3 Data Processing

For analysis, the images captured by the CMOS camera were post-processed using custom MATLAB scripts. Regions of interest were manually drawn for each fiber to extract fluorescence values throughout the experiment. The 405-nm reference trace was scaled to best fit the 470-nm signal using least-squares regression. The normalized change in fluorescence (dF/F) was calculated by subtracting the scaled 405-nm reference trace from the 470-nm signal and dividing that value by the scaled 405-nm reference trace. The true baseline of each dF/F trace was determined and corrected by using the Matlab function msbackadj, estimating the baseline over a 200 frame sliding window, regressing varying baseline values to the window's data points using a spline approximation, then adjusting the baseline in the peak range of the dF/F signal.

In order to ensure signal fidelity, we excluded individual regional recordings with poor signal-to-noise ratios. A Power Spectral Density (PSD) estimate was calculated for each recording across the entire session. Because low fidelity signals are associated with high frequency noise components (Figure A.2A), a noise estimate was calculated as the PSD in the range of 0.25-0.5x the sampling rate. Peak-to-noise ratio (PNR) was calculated by dividing the max dF/F of this PSD estimate. Plotting the distribution of all signal PNR

revealed an empirically defined cluster of low PNR recordings below a value of 7 (Figure A.2B), which accounted for 6.55% of all recordings, spread out across regions and days. These were subsequently excluded from further analysis.

8.7.4 Bulk neural responses

The adjusted calcium signals from Photometry were aligned to task events (for example, cue presentation, airpuff, lick rate, etc) in ViRMEn by time-stamping behavioral frames captured through the NIDAQ. Photometry signals from all animals from a given region were Z-scored across the entire session. The mean regional responses to task variables (Figures 3C, 4A, and 4C), is the mean of these aligned Z-scored signals across all animals, with s.e.m. calculated across all recorded trials. We then sought to quantify the difference in temporal divergence activity patterns observed in either context. Such differences have been previously described to be similar in magnitude whether mice learn a rewarding and aversive context as to when they learn either in comparison to an otherwise neutral context (Yadav et al., 2022) To calculate the differential response to context entry (Figure 4.4B), for each reward or aversive trial, we calculated the change in Z-scored signal from 0 to 2 seconds into the cue zone. For example, this differential signal may be significant if, on average, the photometry signal in one context moves in either direction (more or less positive) relative to the other context upon entry into the cue zone. To calculate the differential anticipatory response (Figure 4.4D), the summed mean difference between the signal across all reward and fear trials in the anticipatory window (2.5 seconds prior to the end of the cue zone) was compared to the summed mean difference between the signal across both trial types in the first half of the cue zone (0 - 2.5 seconds into the control). This measurement would be significant if the relative difference in magnitude of the context signals diverged as the mouse progressed from context entry toward the

outcome zone.

8.7.5 Linear encoding model

We used a generalized linear model to estimate the encoding of various task parameters by bulk neural activity in each recorded region. In our model, Z-scored dF/F is predicted by a combination of external stimuli, trial-long events, and continuous behavior. External stimuli include the trial-start zone, context-specific cues (reward/fear visual, auditory, and olfactory cues), and training feedback (sucrose or air puff). The predictors for these stimuli were generated by convolving the time course of each with a set of 6 gaussian kernels of various sizes (2-σ width ranging from 1 to 6 seconds, see figure below)

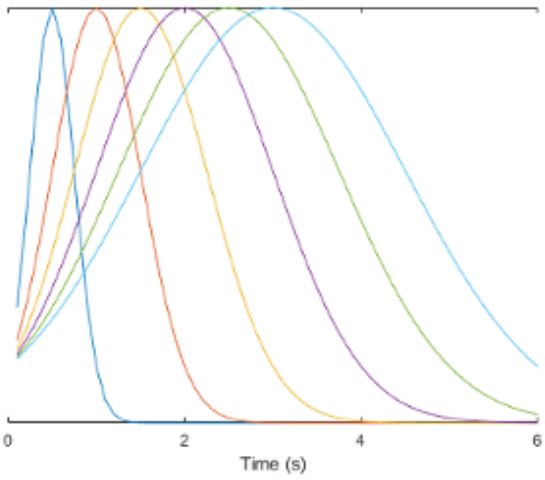

This was to allow for variability in the dynamics of neural responses. This range was determined by assessing the distribution of calcium event widths across all mice and regions (Figure A.3C and A.3D). The trial-long predictor, context identity of the current trial, were either 1 or 0 for all time points in the trial. Continuous behavioral predictors (speed, lick rate, and trial time) were input directly into the model. Finally, we included an L2 penalty (ridge regression) to prevent overfitting. The full equation for the model

was:

$$F = \sum_{i=1}^{N_S} \sum_{k=1}^{6} \beta_{ki}^{S} X_{ki}^{S} + \sum_{i=1}^{N_T} \beta_i^T X_i^T + \beta_0 + \varepsilon$$

where F is dF/F for a given region, $\beta_{ki}{}^{S}$ and $X_{ki}{}^{S}$ are the encoding weights and predictors, respectively, for gaussian kernel k and external stimulus i; $\beta_i{}^{T}$ and Xi^{T} are the weights and predictors for the ith trial-long variables; and ε represents the error. We fit the model on each session using 1000 rounds of 3-fold cross-validation, where the model was trained on a random split of 80% of trials. Accuracy was assessed by calculating the R^2 between the predicted and true dF/F on the held-out trials, after concatenating across each fold.

The proportion of variance explained for a given variable was calculated adapted from previously described methods (Engelhard et al., 2019). Briefly, we first calculated the explained variance of the full model, R^2_f. Then, a partial model was built with a given variable, i, excluded as a predictor and the variance explained for this partial model was calculated $R^2_{p,i}$. The contribution of the selected variable to the variables explained is then calculated as: $(1 – R^2_{p,i} / R^2_f) / \Sigma^n_{j=1}(1 - R^2_{p,j} / R^2_f)$

8.8 Optogenetic inhibition of AM Projections to ACC

Mice were injected with rgAAV-hSyn-Cre bilaterally in ACC and AAV1-hSyn1-SIO-stGtACR2 bilaterally in AM for projection specific expression of GtACR2 in AM. Control cohorts were injected with rgAAV-hSyn-Cre in ACC and AAV9-hSyn-mCherry in AM. Optical cannulas were implanted directly above the injection sites. Mice were trained

on our task as described above while light from a 470nm laser (15 mW at fiber tip) was delivered through the cannulas during the cue and outcome zones of the track.

8.9 Contextual fear conditioning

Mice were injected with rgAAV-hSyn-Cre bilaterally in ACC and AAV1-hSyn1-SIO-stGtACR2 bilaterally in AM for projection specific expression of GtACR2 in AM. Control cohorts were injected with rgAAV-hSyn-Cre in ACC and AAV9-hSyn-mCherry in AM. Optical cannulas were implanted directly above the injection sites. On training day, mice were placed in Context A for a total of 6 minutes while 470nm light was delivered throughout. In that time, they received 4 interspersed foot shocks. Mice were subsequently tested without light the following day and after 3 weeks. Freezing behavior was quantified as the percentage of time immobile in the first minute in Context A as recorded by a near-infrared camera in the conditioning chamber.

8.10 Optogenetic activation of AM projections to ACC

Mice were injected with rgAAV-hSyn-cre bilaterally in ACC and pAAV-Ef1a-DIOhChR2(C128S/D156A)-EYFP bilaterally in AM for projection specific expression of SSFO in the AM. For RSP control mice, pAAV-Ef1a-DIOhChR2(C128S/D156A)-EYFP was injected into RSP and rgAAV-hSyn-cre in ACC. For optical control mice, rgAAV-hSyn-Cre was injected into ACC and pAAV-CAG-DIO-eYFP was injected into AM. Dual fiber optic cannulas were implanted in AM or RSP for the respective cohorts. At the beginning of each training session, a blue 470nm light was on for 5 seconds (at a power of 15 mW

measured at the fiber tip). At the end of 30 minutes, or at the end of 10 completed trials for each context (whichever came first), a secondary pulse of yellow light at 589 nm was administered to deactivate the SSFO and return the membrane potential of transfected neurons to resting values.

8.11 In Vivo Multi-Region Calcium Imaging

After surgical implants of GRIN lenses in ACC, HPC and AM, mice were given one month to recover in their home cage. Mice were selected for behavior and imaging only if multiple clear transients were identifiable in all three regions 3 weeks post surgery.

Microscope A bundle of three imaging fibers with individual diameters of 0.6mm and core-to-core distance of 3.3 µm (Myriad Fibers, FIGH-30-650s) was coupled to the imaging objective (Nikon, CFI Fluor 10X, NA=0.5). The objective path was then passed through a dichroic filter (Semrock FF01-520/35-25) and then frame-projected through a 165mm focal length tube lens (Zeiss) onto the CMOS camera (Photometrics Prime 95B). The excitation arm consists of a 473 nm laser (OptoEngine, BL-II-473/1 100mW) coupled to a collimator (Thorlabs, F230FC-A). A 50 mm lens was then used to focus the beam through an dichroic mirror (Semrock, FF495-Di02-25x36) onto the back focal plane of the objective. The path was manually aligned to ensure uniform illumination of the three fiber bundles. The laser power was adjusted so that 0.25 mW was emitted, measured at the end of each fiber tip, in order to minimize photobleaching over multiple extended recording sessions.

8.11.1 Optical Characterization:

Point spread function estimation: Five microliters of stock solution 0.2-µm-diameter fluorescent beads (Invitrogen, FluoSpheres Sulfate Microspheres, 0.2 µm, yellow-green fluorescent (505/515)) was mixed in a solution of 1.5% aqueous agarose (Sigma). This mixture was then poured onto a glass-bottomed petri dish and was allowed to solidify at room temperature. A single imaging fiber was held above the dish and manually lowered using a linear translation stage (Thoralbs, MT1A) and used to acquire images of the illuminated beads at 5 µm intervals (Figure A.5A). Intensity along X, Y, and Z dimensions were quantified using ImageJ. Linear resolution: A single fiber was used focused above a standardized 1951 USAF Resolution Test Target (Thorlabs). After acquiring, the smallest pair of three lines was identified and linear intensity quantified in ImageJ (Figure A.5B).

8.11.2 SNR comparison

To ensure that the use of multiple fiber cores did not diminish the SNR of recorded Ca2+ transients in vivo, a single mouse was injected with AAV1-CaMKIIa-GCaMP6f in ACC and a 0.6mm GRIN lens (Inscopix) was implanted 0.2mm above the injection site, as described above. After 3 weeks, the mouse was head fixed and imaged using our fiber bundle system at 34 Hz over 5 minutes. The mouse was then imaged through the same objective and imaged with a CMOS camera placed in the widefield path of a Bruker microscope, illuminated with the same laser power and wavelength (0.25 mW, 473nm) again for five minutes. Individual sources were extracted and registered across the fiber bundle and the standard widefield recordings (Figure A.5C, top; see Data Acquisition Post-processing). Recordings of the same cells were overlaid and qualitatively appeared to be similar in quality (Figure A.5C, bottom left). Peak-to-noise ratio was calculated for each

cell for each imaging method and found to be quantitatively similar (R = 0.61) (Figure A.5C, bottom right).

8.11.3 Image acquisition

Prior to each session, mice were headfixed and each GRIN lens was carefully cleaned with 70% ethanol. Custom 3D printed adaptors were first affixed to each lens, and then fibers were manually adjusted vertically while acquiring images until cells were maximally focused. Because both the fibers and lenses had the same diameter of 0.6mm, the design of the adaptors ensured that minimal horizontal adjustments were required to attain the same field-of-view across multiple recordings. Images were collected during behavior at 34 Hz (exposure time 17 ms) using the Photometrics data acquisition software, Programmable Virtual Camera Access Method (PVCAM) at a resolution of 920 pixels/mm.

8.11.4 Paired Optogenetic Inhibition during training and GCaMP imaging during retrieval

During training, bilateral optogenetic inhibition of AM was paired with GCaMP6f imaging through a unilaterally-placed GRIN lens in the ACC (Figure A.7A) during training sessions, using our previously described fiber bundle microscope. Inhibition was achieved with a 473 nm laser (OptoEngine) via a mono fiber patch cord with a minimum power of 15 mW, and was targeted through the bilateral implanted cannulas in AM for the entire time the mouse was in the cue zone (8 seconds). Imaging was performed during the pre-exposure session, R6 and R27 sessions. Imaging laser power was maintained at 0.25 mW to minimize distal inhibition of GtACR. To validate expression and observe the

online effects of AM inhibition on ACC neural activity, an additional recording session was performed after the first pre-exposure session, where imaging was paired simultaneously with inhibition. The mouse was head-fixed in the behavior box in the dark, and eight separate 8-second optogenetic laser pulses occurring 30 seconds apart were delivered while imaging occurred concurrently through the GRIN lens (Figure A.9B).

8.11.5 Source extraction

Each field of view was cropped and motion-corrected using NoRMCorre (Pnevmatikakis and Giovannucci, 2017). A combination of custom scripts and existing packages for 1-photon excitation source extraction (CNMF-E, Zhou et al., 2018) were used to identify and isolate individual cell ROIs and dF/F signals from all three regions separately. Cell identification was verified by manually validating every extracted source. Cell registration across sessions was performed with a combination of custom scripts and existing packages (Cell Reg, Sheintuch et al., 2017).

8.11.6 Calculation of single cell dF/F and transient identification

For each cell detected via automated source extraction, a normalized $\Delta F/F$ was calculated and individual Ca2+ transients were identified as previously described (Rajasethupathy et al., 2015). Briefly, $\Delta F/F$ was defined as: (F - Fbaseline)/Fbaseline, where F is the raw output ("C_raw") from the CNMF-E algorithm, and where Fbaseline is the baseline fluorescence, calculated as the mean of the fluorescence values for a given cell, continuously acquired over a 20 s sliding window to account for slow time-scale changes observed in the fluorescence across the recording session. For all analysis, this dF/F was then normal-

ized by z-scoring the entire time series across a session. To identify statistically significant transients, we first calculated an estimate of the noise for each cell using a custom MATLAB script, with a previously described method. In essence, we identified the limiting noise cutoff level for a given cell using time periods that are unlikely to contain neural events, and then defined a transient as significant if it reached above at least 3σ of this estimated noise level. A custom MATLAB script using the function findpeaks was used to identify any remaining obvious tranisnets not identified by this method (typically when multiple transients occurred in rapid succession). Additional specifications required transients to persist above this noise level for at least 300 ms (roughly twice the duration of the half-life decay time of GCaMP6f). The transient duration was defined as the first and last frames where the dF/F reached 3σ. The value of dF/F was set to zero outside the duration of every identified transient to minimize effects of residual background fluorescence.

8.11.7 Regional context discrimination

To determine the extent to which population activity from regional single-cell recordings could represent contextual information on a given day, we used a linear support vector machine (SVM) to separate population activity between high reward and aversive contexts. First, we aligned the dF/F from every recorded cell from a region and/or experimental condition (for the inhibition and imaging experiments) to the onset of each cue zone of both contexts on each trial. At every frame, the input is an T x N matrix where T is the total number of trials, and N is equal to A nc,r where A is the total number of animals for that day and condition, nc,r is the number of cells for that region and session. The target output at every frame was a T x 1 vector with the context label. An SVM was trained to predict context on each frame from 2 seconds before the cue zone onset until 5 seconds after, using 10-fold cross-validation using the MATLAB function fitcsvm

to calculate model accuracy. The SVM identifies a hyperplane that maximally separates the neural responses between high reward and aversive contexts. The perpendicular to this hyperplane was calculated using coefficients from the model (model.Beta in fitcsvm in MATLAB). For measuring distances between contexts by region (Figure Sx), we calculated the average distance along this perpendicular line, normalized to the baseline distance at zero seconds. For quantifying discrimination during the inhibition and imaging experiments, we selected the maximum value achieved by the decoder at any point in the 8 second cue zone (Figure 7B and 7C).

8.11.8 Correlations

To calculate cell-to-cell correlations (either inter- or intra-regional), we calculated Pearson's R for each pair of time series. To minimize unwanted correlations that may occur from long-tailed Ca2+ transients, we only included the dF/F values from a cell during the rise time and one second after the peak for each transient. We defined the transient rise as the frames from when the dF/F value first rises above the noise threshold (see Calculation of single cell dF/F and transient identification) until the frame when the dF/F reaches a maximal value within the identified transient time window. The rest of the time series was set to zero. When correlations were calculated for a given context (i.e., high reward correlations), the time series for each cell was concatenated to only include the frames that were captured during the cue zone for that context. For calculating correlations of HR-tuned cells, the cue zones of both contexts were concatenated before calculating Pearson's R.

A cell pair was defined as highly-correlated if $R>0.3$. Correlation network graphs were displayed using the MATLAB function graph with a line connecting correlated

cells, and the layout set to force-directed. Best match correlation was defined as the maxmimum R value achieved for a given cell in one region when correlated to cells in another region or with other cells in that same region. To measure the distribution of interconnectedness within a region during a recording session, we calculated the number of intra-regional correlated cell pairs achieved by each cell (network degree/cell) and then normalized by dividing the total number of cells in that recording. When selecting cells that were highly correlated with cells in a different region (AM – ACC or HPC – ACC), we selected cells from the top 5% R-values from each intra-regional cell pair on that day. Chance distributions for Figure 6K were calculated by randomly selecting the same number of cells as there are red cells from the network graph and re-calculating the number of highly correlated cell pairs per cell 1000 times. Significance corresponds to a proportion of the distribution outside of the 95% percentile of this chance level. Distributions include values from all cells from all animals within a given region and/or experimental condition.

8.11.9 Single cell contextual tuning

To calculate the tuning of an individual cell to the high reward over the low reward context for a given session we calculated the difference in number of significant transients occurring during the cue zone in concatenated high reward trials and low reward trials, each normalized by the total time spent in the cue zone. Thus the units are events/second and a positive value corresponds to increased average event rate in the high over the low reward context. For each cell, we also calculated a "shuffled" tuning, where the time between transients across the entire session was randomly shuffled and tuning was re-calculated for a given cell a total of 1000 times. A cell was considered high reward-tuned if the magnitude of its un-shuffled tuning was at least 1 standard deviation above its

shuffled distribution of tunings.

8.12 Statistical Analyses

Sample sizes were selected based on expected variance and effect sizes from the existing literature, and no statistical methods were used to determine sample size a priori. Prior to experiments being performed, mice were randomly assigned to experimental or control groups. The investigator was blinded to all behavioral studies. Data analyses for calcium imaging (in vitro and in vivo datasets) were automated using MATLAB scripts. Statistical tests were performed in MATLAB 2017a, 2021b, or Graphpad Prism. Animals were excluded from experiments using the following criteria: For all behavioral experiments, mice were excluded if by T5, they had a greater rate of anticipatory licking in the aversive condition compared to reward conditions (indicating they had not properly learned the task).

Appendix A

Supplementary Figures

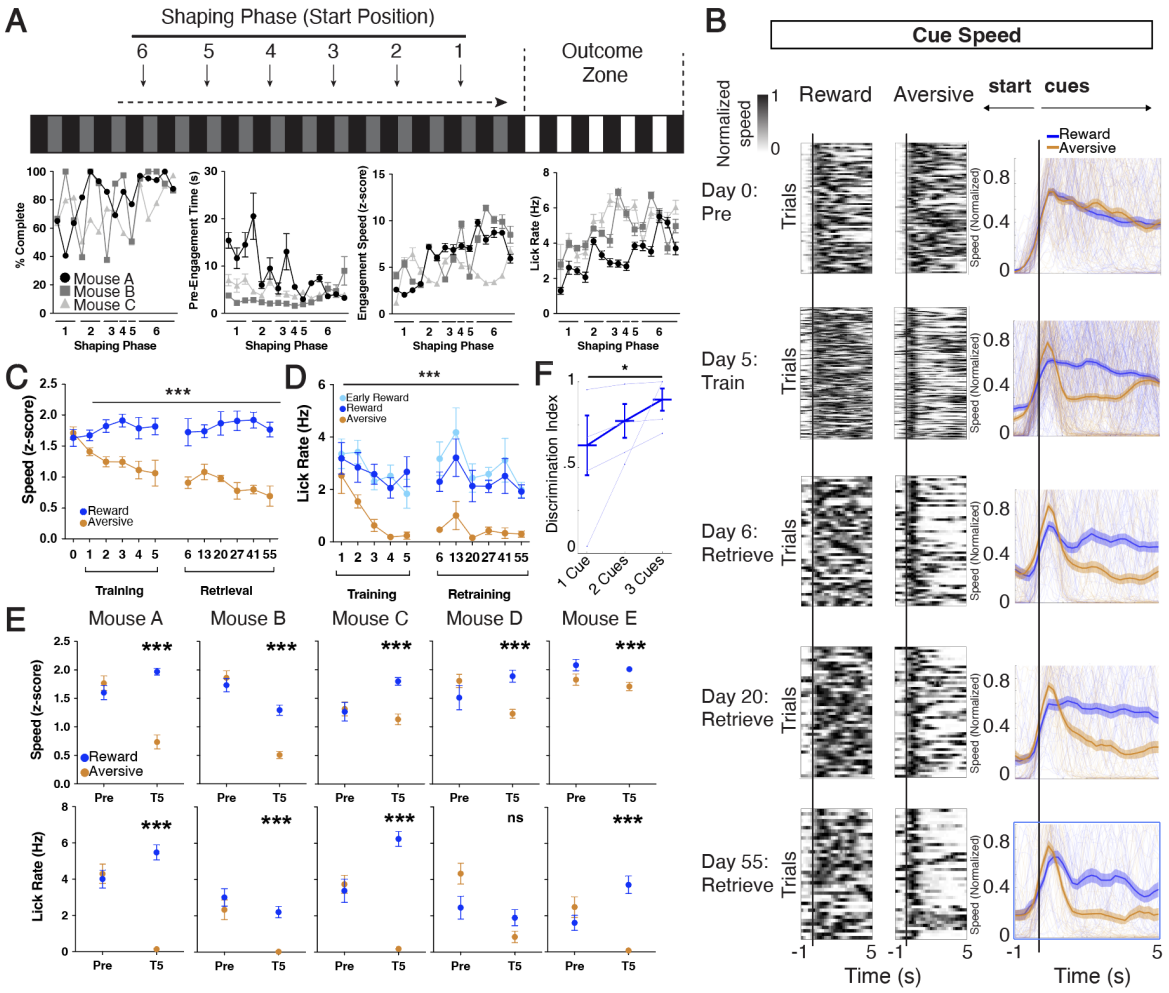

Figure A.1 | **Individual mouse performance and speed contextual discrimination.**

Figure A.1 (A) Lick rate modulation of mice implanted with GRINs in reinforced and probe trials, n=16 mice, (A. Virtual reality linear track design showing starting position of the mouse for each phase of the shaping protocol. Plots for three representative mice during shaping showing percentage of trials complete, time (s) spent prior to engagement, speed (z-score) during engagement, and anticipatory lick rate (Hz) upon entry to outcome zone. (B) Raster of individual trials and plot of trial averages. Speed prior to and during cue zone. Data in heatmaps are normalized to peak speed in the trial. N=5 mice. (C) Average speed in cue zone in each context during preexposure, training, and weekly retrieval sessions throughout consolidation. N=5 mice, ***$p<0.001$ for speed, Two way ANOVA with repeated measures, data are mean ± s.e.m. (D)Anticipatory lick rate (Hz) prior to outcome zone in reward trials at the start of each training session (light blue) is comparable to that of the remainder of the trials in that session (dark blue). Also shown is lick rate on retraining sessions between reward (dark blue) and aversive (orange), following each retrieval session, which have comparable behavioral performance to training sessions. N=5 mice, ***$p<0.001$, Two way ANOVA with repeated measures, data are mean ± s.e.m. (E) Speed (z-score) and lick rate (Hz) in cue zone between reward and aversive, shown individually for each mouse for preexposure and training day 5. ***$p<0.001$, unpaired t-test, data are mean ± s.e.m. (F) Quantification of discrimination between reward and aversive anticipatory lick rates per mouse when 1, 2 or 3 cue modalities are presented after training day 5. N=4 mice. *$p<0.05$ between 1 cue and 3 cues, Dunn's multiple comparison, data are mean ± s.e.m.

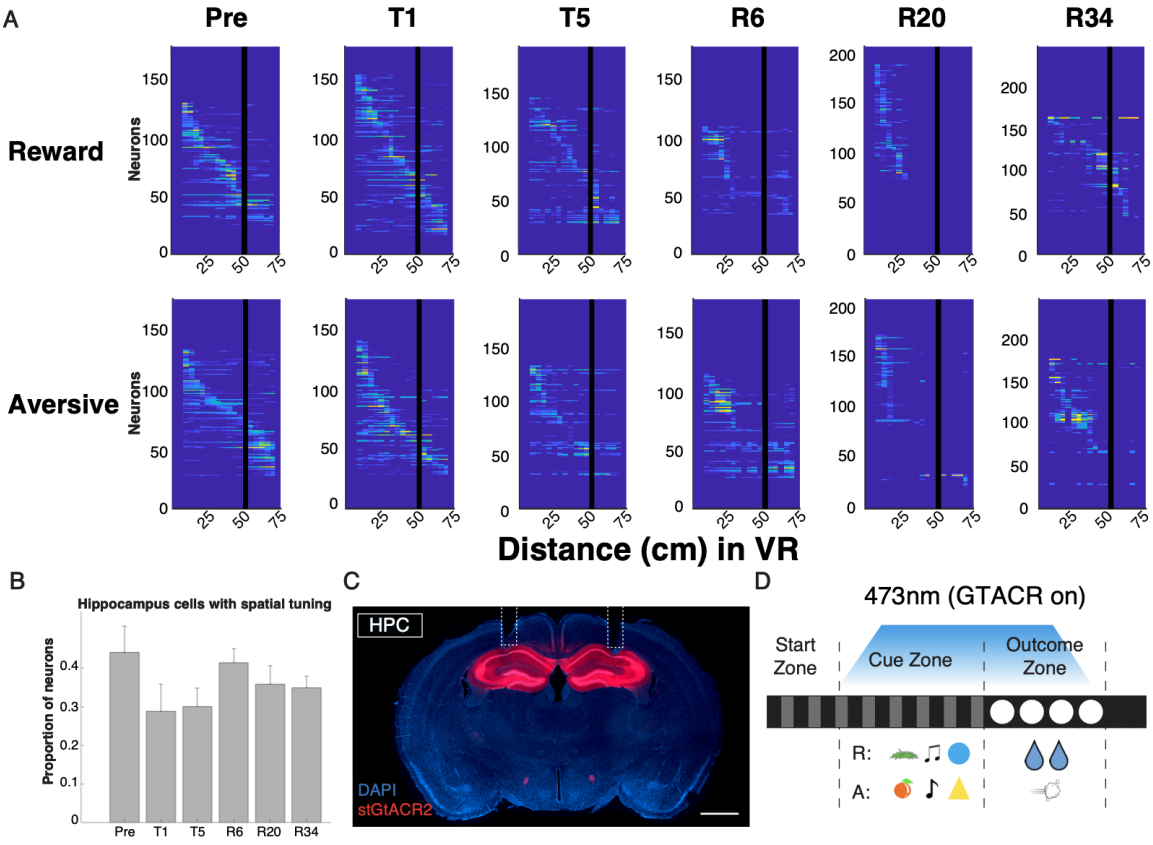

Figure A.2 | **Hippocampus place cell activity and histology for ACC and HPC optogenetic cohorts.** (A) Recorded dF/F from hippocampal cells (see Methods, In Vivo Multi-Region Calcium Imaging) binned by location on the virtual track. (B) Proportion of cells exhibiting spatially-tuned responses, as defined by mean dF/F on the track when binned by spatial location exceeding one standard deviation above mean dF/F during the inter-trial interval (n=3 mice) (C) Coronal sections from animals virally injected with AAV1-CamKii-stGtACR2 bilaterally in HPC. White tracts denote location of fiber optic implants. DAPI is shown in blue and stGtACR2 in red. Scale: 1mm. (D) Schematic showing light for optogenetic inhibition was delivered during cue and outcome periods of the trial.

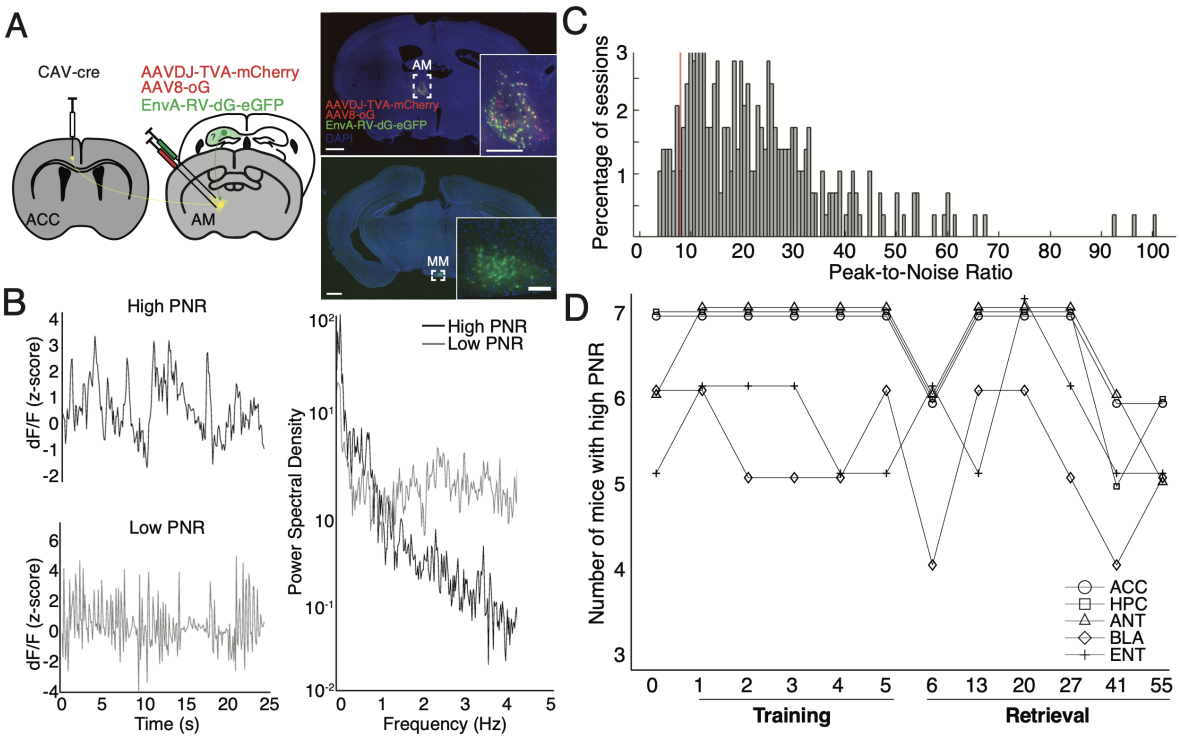

Figure A.3 | **TRIO tracing and signal-to-noise of photometry data.** (A) Strategy for trans-synaptic tracing of input to AM-ACC neurons. CAV-cre was injected into ACC along with AAVs expressing Cre-dependent TVA–mCherry (TC)/rabies glycoprotein (G) into AM, followed by glycoprotein deleted and GFP-expressing rabies viruses (RVdG). Expression in mammillary bodies (MM) is shown. Scale: 1mm or 200um for inserts. (B) Left: Examples of a photometry recording with a high (black) or low (gray) peak-to-noise ratio (PNR). Right: The high PNR recording consists of high amplitude, low-frequency fluctuations lasting several seconds, while the low PNR recording consists of sharp, high-frequency fluctuations.(C) Distribution of PNR for all recording sessions, and empirically selected noise threshold shown in red. (D) Total number of recordings (i.e., number of mice) included from each region and for each session in the final analyses.

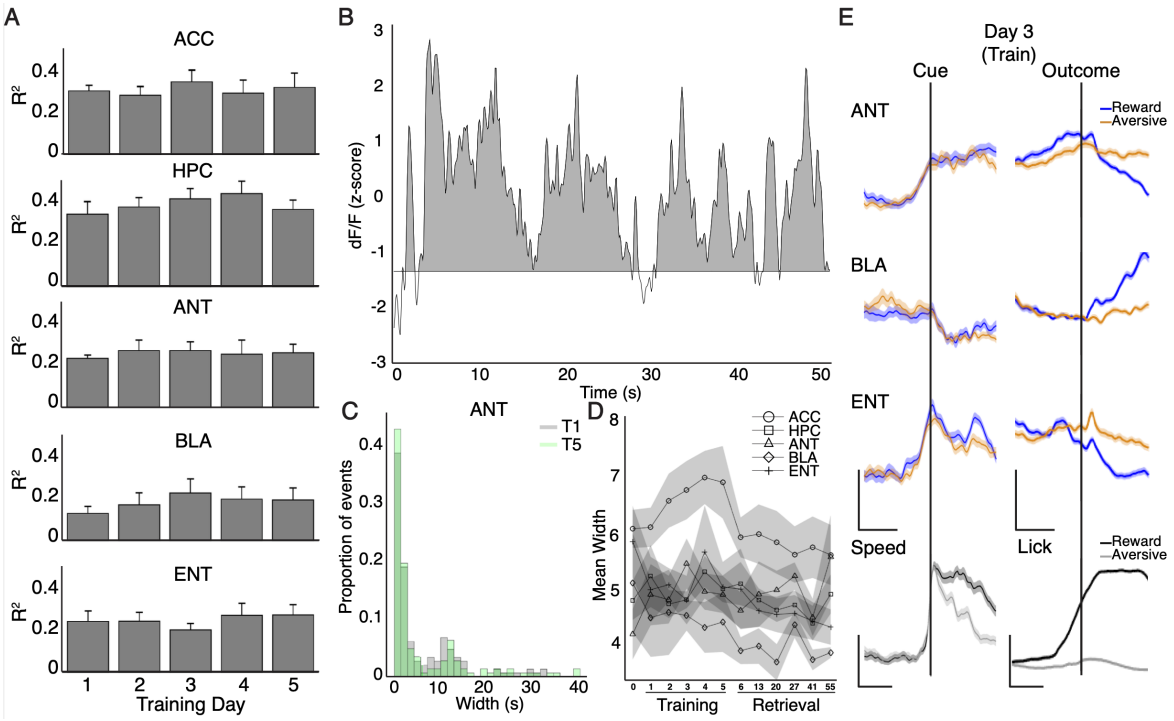

Figure A.4 | **Event rates and regression data for photometry signals.** (A) Mean full-model R2 calculated for photometry recordings from each region during training (see methods). N=7 mice. Data are mean ± s.e.m. (B) Example photometry signal demonstrating large, slow calcium events lasting tens of seconds. (C) Distribution of all photometry signal event durations from ANT on the first (T1) and last (T5) day of training. N=7 mice. (C) Mean calcium event width across mice for each region and recording session. N=7 mice. Data are mean ± s.e.m. (E) Photometry signals (dF/F, z-score) and behavioral variables speed (z-score) or lick rate (Hz) aligned to cue zone or outcome zone entry, respectively for day 3 of training (T3). N=7 mice, dark lines and shaded regions represent mean ± s.e.m.

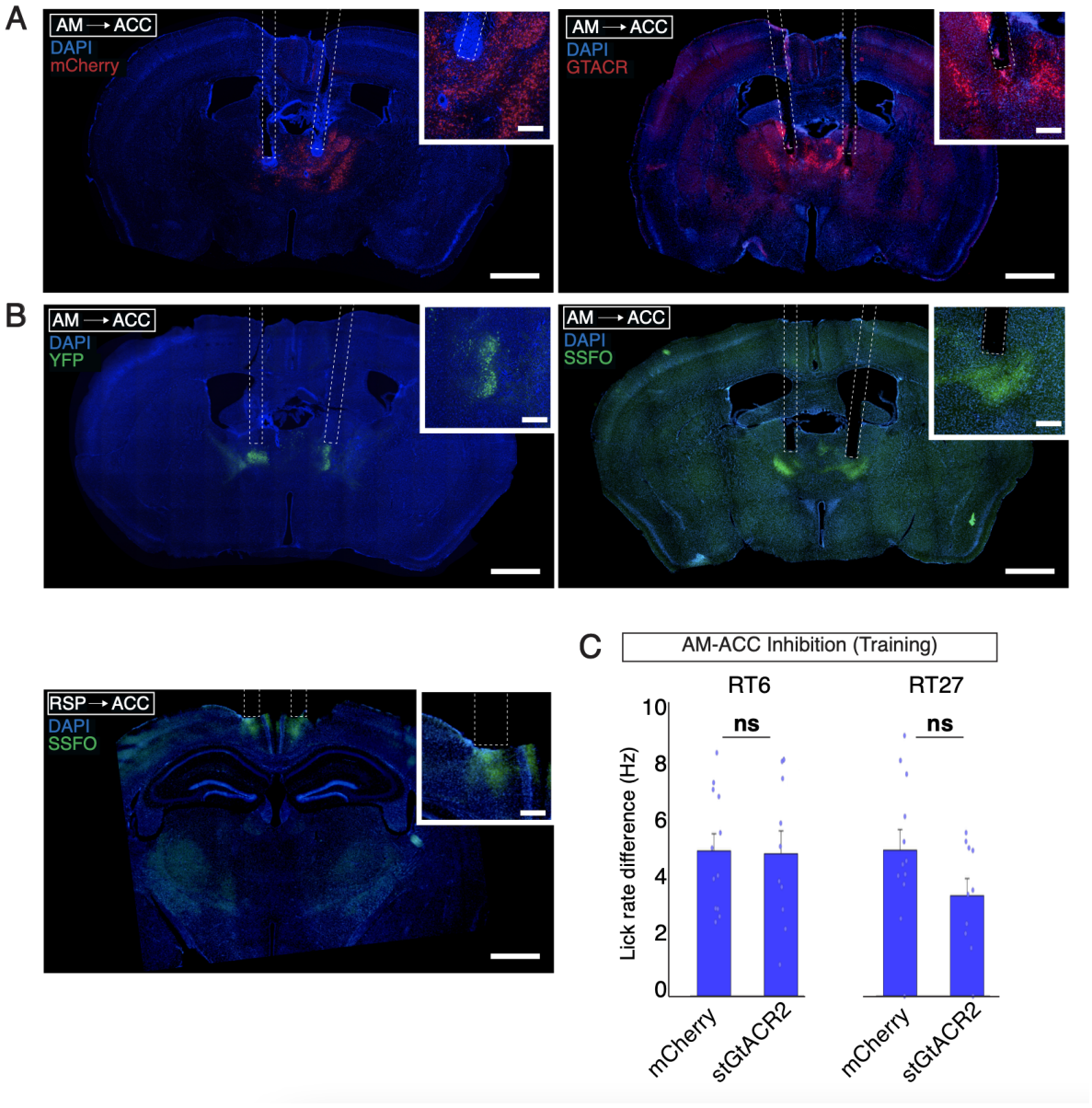

Figure A.5 | **Histology and retraining behavior for optogenetic cohorts.**

Figure A.5 (A) Coronal sections from animals virally injected with rgAAV-hSyn-Cre bilaterally in ACC and either AAV1-SIO-stGtACR2-FusionRed or AAV1-DIO-mCherry bilaterally in AM. White tracts denote location of fiber optic implants. Insert is a zoomed in image of viral expression. DAPI is shown in blue and mCherry or stGtACR2 is shown in red. Scale: 1mm or 200um for insert. (B) Coronal sections from animals virally injected with rgAAV-hSyn-Cre bilaterally in ACC and either Ef1a-DIO-SSFO-EYFP or hSyn1-DIO-eYFP bilaterally in AM or Ef1a-DIO-SSFO-EYFP bilaterally in retrosplenial cortex (RSP). White tracts denote location of fiber optic implants. Insert is a zoomed in image of viral expression. DAPI is shown in blue and YFP or SSFO is shown in yellow. Scale: 1mm or 200um for insert. (C) Behavioral data from AM-to-ACC inhibition during training experiment, quantifying performance on each retraining session following retrieval for all mice in Figures 5A-D, shown as lick rate differences (Hz) in reward vs aversive contexts. N=12 mice for mCherry vs 10 mice for stGtACR2, all $p>0.05$, unpaired t-test. Individual data points shown, as well as mean ± s.e.m.

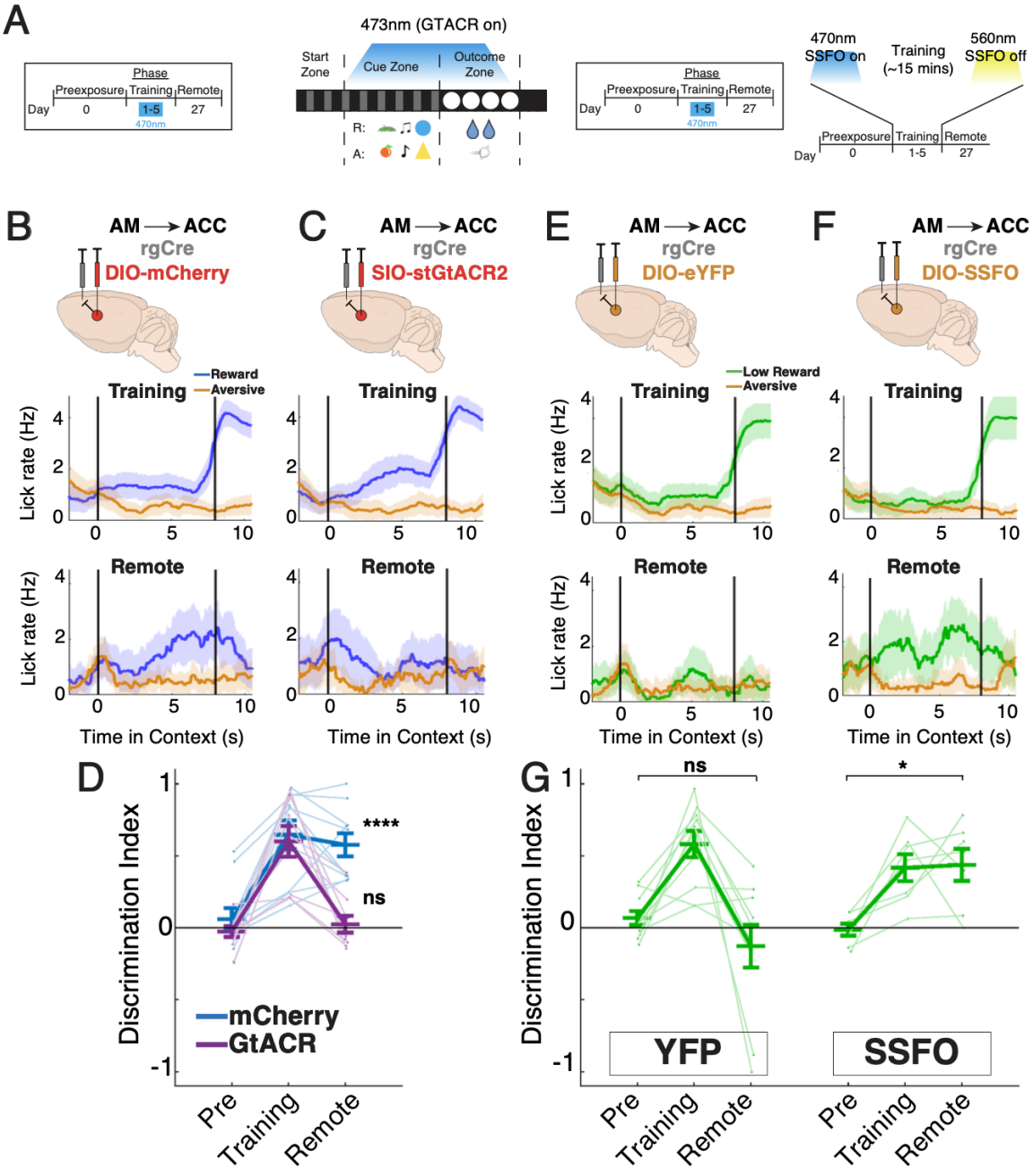

Figure A.6 | **Optogenetic perturbations of AM-ACC activity without recent retrieval and retraining.**

Figure A.6 (A) Schematic of experimental design: stGtACR2-based optogenetic inhibition during training (T1-T5), followed by a test of remote (R27) memory. Light was delivered during cue and outcome periods of the trial.(B,C) Injection strategy for targeting anteromedial thalamus (AM) projections to ACC (AM-ACC) in mCherry control and stGtACR2 opsin cohorts. Raw lick traces in each context on training day 5 and remote retrieval sessions. (D) Quantification of discrimination between reward and aversive lick rates per mouse on preexposure, training day 5, and remote retrieval sessions; mCherry (AM-ACC no opsin control, N=10), GtACR (AM-ACC with opsin, N=9). ****$p<0.0001$ for mCherry between preexposure and remote, one-way repeated measures ANOVA with post-hoc Tukey's multiple comparison test. Individual data points shown, with mean ± s.e.m. (E,F) Injection strategy for targeting AM projections to ACC in YFP control and SSFO opsin cohorts. Raw lick traces in each context on training day 5 and remote retrieval sessions. (G) Quantification of discrimination between low reward (LR) and aversive (A) contexts on preexposure, training day 5, and remote sessions for each cohort; YFP (no opsin control, N=10); SSFO (AM-ACC SSFO excitation, N=6). *$p<0.05$ for YFP and SSFO cohorts between preexposure and remote, one-way repeated measure ANOVAs with post-hoc Tukey's multiple comparison tests. Individual data points shown, with mean ± s.e.m.

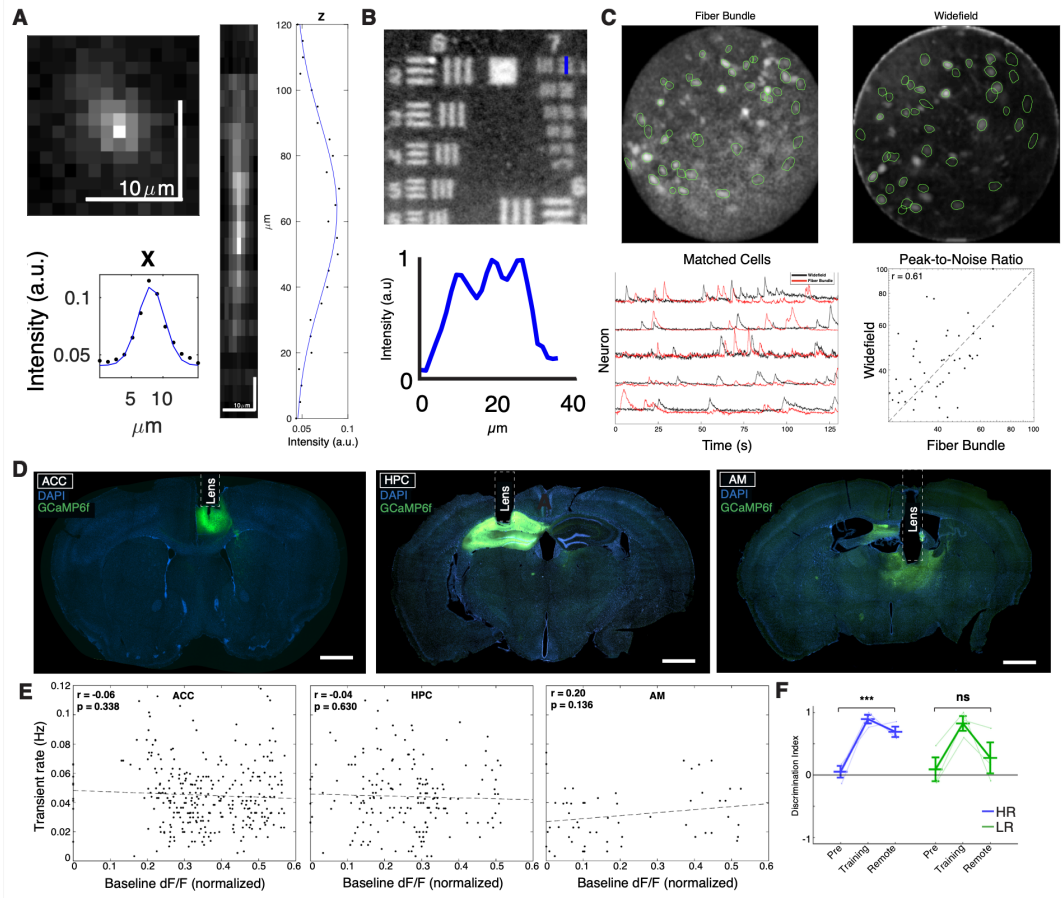

Figure A.7 | **Fiber bundle microscope characterization, in-vivo imaging histology and behavior.** (A) Projections and quantification of a three-dimensional stack of observed fluorescence from a sub-resolution fluorescent microbead acquired using the fiber bundle microscope. (B) Left: Fiber bundle-acquired image of a USAF imaging target. Right: Quantification of intensity along the group with the finest resolved spatial frequency. (C) Top: Snapshot of an in vivo recording of ACC with the fiber bundle microscope (left) and a standard widefield microscope (right), with registered cells circled in green. Bottom left: Overlayed dF/F time series from 5 example cells recorded with the two microscopes. Bottom right: Comparison of estimated Peak-to-Noise ratio (from CNMF-E) of each cell plotted against itself from the two methods. (D) Brain histology from a representative mouse in the 3-way multi-region imaging cohort showing GCaMP6f expression and GRIN lens implantation site in ACC, HPC, and AM. Scale: 1mm. (E) Spontaneous event rate of GCaMP6f-expressing neurons as a function of baseline fluorescence intensity in each region. N=3 mice. Dotted line: best fit line. Lack of correlation suggests that calcium buffering (i.e., increasing levels of baseline GCaMP) in these regions does not affect physiological event rates. (F) Discrimination between high reward (HR) or low reward (LR) and aversive (A) contexts. N=3 mice. *$p<0.05$ for HR between preexposure and remote, one-way repeated measure ANOVA with post-hoc Tukey's multiple comparison test. Individual data points shown, with mean ± s.e.m.

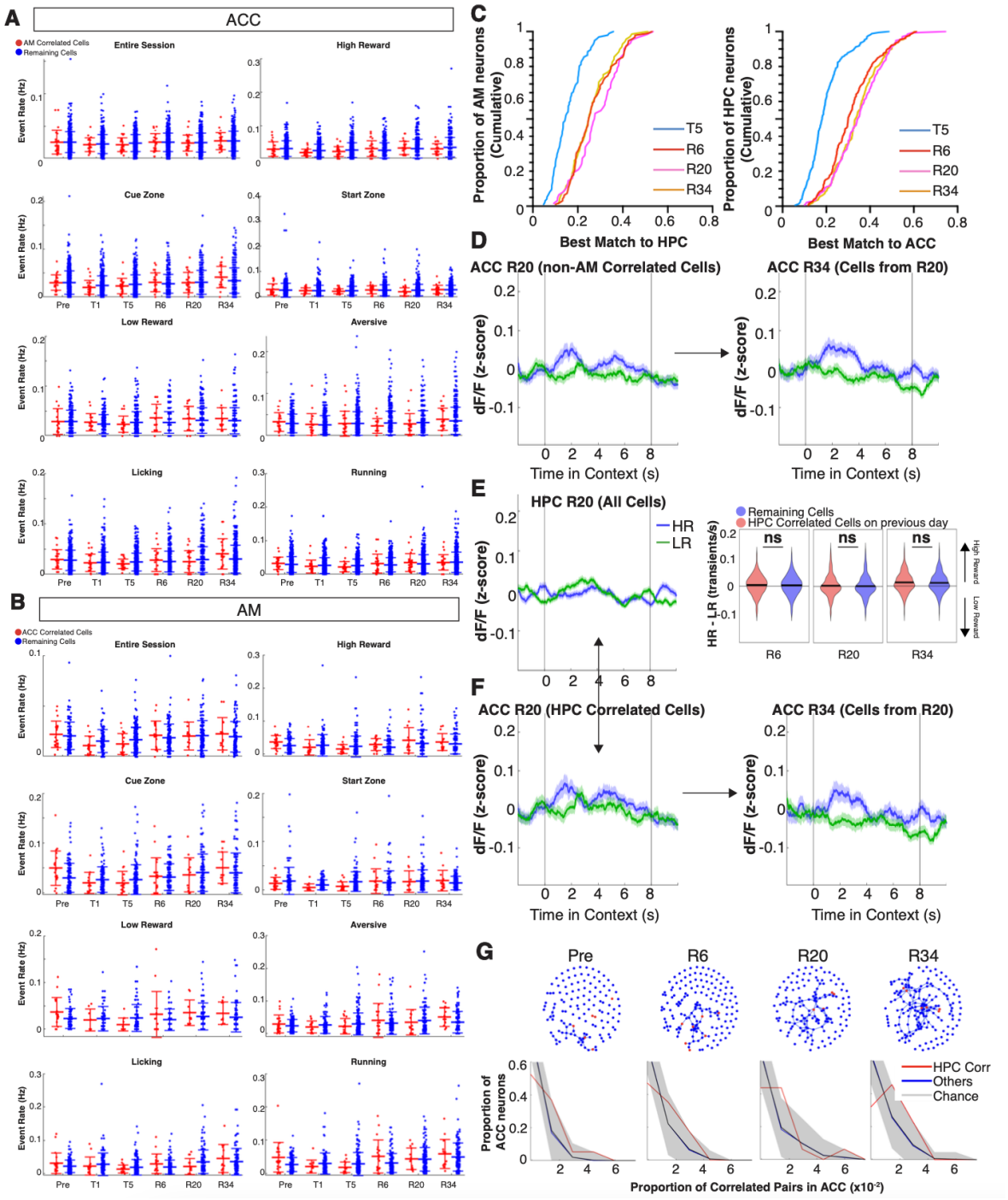

Figure A.8 | **Cross-region event rates, functional correlations, and synchronous activity.**

Figure A.8 (A) Event rate (transients per second) of ACC cells which are highly correlated to AM cells (red, top 5%), and all remaining ACC cells (blue) during context-specific cue zones in the task. For "running" or "licking", transients are counted any time run speed or licking, respectively, are greater than zero. N=all cells from 5 mice. Data are mean ± s.e.m. (B) Same as A.6A, but for the AM cells identified in the top 5% highly correlated AM-to-ACC pairs, compared to all remaining AM cells. N=all cells from 5 mice. Data are mean ± s.e.m. (C) Cumulative distribution of the best match correlation of HPC cells paired with AM cells across days (left) and ACC cells paired with HPC cells (right). N=5 mice. $p>0.05$, two-sample KS test between R6 and R20. D. Left: Cue-zone-aligned mean z-scored dF of all ACC cells on R20 not correlated to an AM cell (n=242 cells). Right: mean response of these same tracked ACC cells on R34. (E) Cue-zone-aligned mean z-scored dF of all HPC cells on R20 (n=518 cells). Bottom left: Mean z-scored response of ACC cells which form highly correlated pairs with at least one HPC cell (n=171, cells across 3 animals. Bottom right: mean response of these same tracked ACC cells on R34. (F) Distribution of tuning for ACC cells correlated to at least one HPC cell on the previous recording session compared to the tuning of all remaining cells. The difference was not significant on R34, R20 or R6. (G) Top: Example from one animal of undirected network graphs of ACC cell correlations (Lines are Pairwise Pearson>0.3) in the reward context across days with ACC cells most correlated with HPC cells (top 5%) shown in red (see methods). Bottom: Distribution of proportion of pairwise correlations in ACC for red cells and blue cells, compared to chance shown in black (see methods). N=5 mice, Shaded area represents 95% confidence interval around chance distribution.

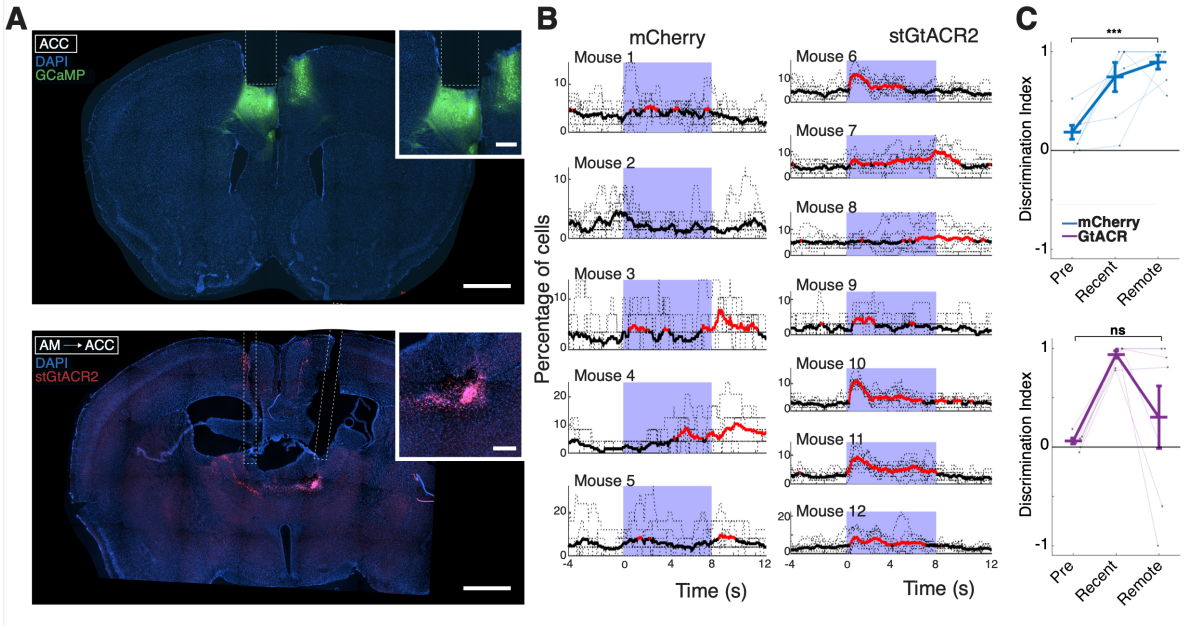

Figure A.9 | **Histology and characterization of paired inhibition and imaging cohort,.** (A) Brain histology from a representative mouse undergoing paired inhibition (AM-to-ACC) and imaging (ACC). Coronal sections show GCaMP6f expression and GRIN lens implantation site in ACC, and stGtACR2-FusionRed expression and fiber optic tracts in AM. Insert is a zoomed in image of viral expression. DAPI is shown in blue, GCaMP6f is shown in green, and stGtACR2 is shown in red. Scale: 1mm or 200um for insert. (B) Percentage of cells having a significant transient event at every frame, averaged across mice, for mCherry and stGtACR2 cohorts. Red denotes time points with synchronous firing greater than 1 s.d. above the mean across 8 pulses. Purple highlights duration of laser on (470nm) for stGtACR2 activation. (C) Discrimination between reward and aversive contexts. ***$p<0.001$ for mCherry between preexposure and remote, one-way repeated measure ANOVA with post-hoc Tukey's multiple comparison test. Individual data points shown, with mean ± s.e.m.

Appendix B

Bibliography

Aggleton, J. P. and Sahgal, A. (1993). The contribution of the anterior thalamic nuclei to anterograde amnesia. *Neuropsychologia*, 31(10):1001–1019.

Aharoni, D. and Hoogland, T. M. (2019). Circuit investigations with open-source miniaturized microscopes: past, present and future. *Frontiers in cellular neuroscience*, 13:141.

Albo, Z., Di Prisco, G. V., and Vertes, R. (2003). Anterior thalamic unit discharge profiles and coherence with hippocampal theta rhythm. *Thalamus & Related Systems*, 2(2):133–144.

Anagnostaras, S. G., Maren, S., and Fanselow, M. S. (1999). Temporally graded retrograde amnesia of contextual fear after hippocampal damage in rats: within-subjects examination. *Journal of Neuroscience*, 19(3):1106–1114.

Armbruster, B. N., Li, X., Pausch, M. H., Herlitze, S., and Roth, B. L. (2007). Evolving the lock to fit the key to create a family of g protein-coupled receptors potently activated by an inert ligand. *Proceedings of the National Academy of Sciences*, 104(12):5163–5168.

Aronov, D. and Tank, D. W. (2014). Engagement of neural circuits underlying 2d spatial navigation in a rodent virtual reality system. *Neuron*, 84(2):442–456.

Atherton, L. A., Dupret, D., and Mellor, J. R. (2015). Memory trace replay: the shaping of memory consolidation by neuromodulation. *Trends in neurosciences*, 38(9):560–570.

Bailey, C. H. and Kandel, E. R. (1993). Structural changes accompanying memory storage. *Annual review of physiology*, 55(1):397–426.

Bando, Y., Grimm, C., Cornejo, V. H., and Yuste, R. (2019). Genetic voltage indicators. *BMC biology*, 17(1):1–12.

Barker, G. R. and Warburton, E. C. (2008). Nmda receptor plasticity in the perirhinal and prefrontal cortices is crucial for the acquisition of long-term object-in-place associative memory. *Journal of Neuroscience*, 28(11):2837–2844.

Barondes, S. H. and Cohen, H. D. (1966). Puromycin effect on successive phases of memory storage. *Science*, 151(3710):594–595.

Bauch, E. M., Bunzeck, N., Hinrichs, H., Schmitt, F. C., Voges, J., Heinze, H.-J., and Zaehle, T. (2018). Theta oscillations underlie retrieval success effects in the nucleus accumbens and anterior thalamus: evidence from human intracranial recordings. *Neurobiology of learning and memory*, 155:104–112.

Bero, A. W., Meng, J., Cho, S., Shen, A. H., Canter, R. G., Ericsson, M., and Tsai, L.-H. (2014). Early remodeling of the neocortex upon episodic memory encoding. *Proceedings of the National Academy of Sciences*, 111(32):11852–11857.

Bliss, T. V. and Lømo, T. (1973). Long-lasting potentiation of synaptic transmission in the dentate area of the anaesthetized rabbit following stimulation of the perforant path. *The Journal of physiology*, 232(2):331–356.

Bontempi, B., Laurent-Demir, C., Destrade, C., and Jaffard, R. (1999). Time-dependent reorganization of brain circuitry underlying long-term memory storage. *Nature*, 400(6745):671–675.

Bubb, E. J., Aggleton, J. P., O'Mara, S. M., and Nelson, A. J. (2021). Chemogenetics reveal an anterior cingulate–thalamic pathway for attending to task-relevant information. *Cerebral Cortex*, 31(4):2169–2186.

Burnham, W. H. (1903). Retroactive amnesia: Illustrative cases and a tentative explanation. *The American Journal of Psychology*, pages 118–132.

Buzsáki, G. (1989). Two-stage model of memory trace formation: a role for "noisy" brain states. *Neuroscience*, 31(3):551–570.

Chamaa, F., Darwish, B., Nahas, Z., Al-Chaer, E. D., Saadé, N. E., and Abou-Kheir, W. (2021). Long-term stimulation of the anteromedial thalamus increases hippocampal neurogenesis and spatial reference memory in adult rats. *Behavioural brain research*, 402:113114.

Cho, Y. H., Beracochea, D., and Jaffard, R. (1993). Extended temporal gradient for the retrograde and anterograde amnesia produced by ibotenate entorhinal cortex lesions in mice. *Journal of Neuroscience*, 13(4):1759–1766.

Cipolotti, L., Shallice, T., Chan, D., Fox, N., Scahill, R., Harrison, G., Stevens, J., and Rudge, P. (2001). Long-term retrograde amnesia... the crucial role of the hippocampus. *Neuropsychologia*, 39(2):151–172.

Cui, G., Jun, S. B., Jin, X., Pham, M. D., Vogel, S. S., Lovinger, D. M., and Costa, R. M. (2013). Concurrent activation of striatal direct and indirect pathways during action initiation. *Nature*, 494(7436):238–242.

Czajkowski, R., Jayaprakash, B., Wiltgen, B., Rogerson, T., Guzman-Karlsson, M. C., Barth, A. L., Trachtenberg, J. T., and Silva, A. J. (2014). Encoding and storage of spatial information in the retrosplenial cortex. *Proceedings of the National Academy of Sciences*, 111(23):8661–8666.

Dash, P. K., Hochner, B., and Kandel, E. R. (1990). Injection of the camp-responsive element into the nucleus of aplysia sensory neurons blocks long-term facilitation. *Nature*, 345(6277):718–721.

de Lima, M. A. X., Baldo, M. V. C., and Canteras, N. S. (2017). A role for the anteromedial thalamic nucleus in the acquisition of contextual fear memory to predatory threats. *Brain Structure and Function*, 222(1):113–129.

Devinsky, O., Morrell, M. J., and Vogt, B. A. (1995). Contributions of anterior cingulate cortex to behaviour. *Brain*, 118(1):279–306.

Dombeck, D. A., Khabbaz, A. N., Collman, F., Adelman, T. L., and Tank, D. W. (2007). Imaging large-scale neural activity with cellular resolution in awake, mobile mice. *Neuron*, 56(1):43–57.

Duncan, C. P. (1949). The retroactive effect of electroshock on learning. *Journal of comparative and physiological psychology*, 42(1):32.

Ebbinghaus, H. (1885). Ueber das gedaechtnis: Untersuchengen zur experimentellen psychologie [on memory: Investigations in experimental psycholog y]. *Leipzig, Germany: Duncker & Humbolt*.

Engelhard, B., Finkelstein, J., Cox, J., Fleming, W., Jang, H. J., Ornelas, S., Koay, S. A., Thiberge, S. Y., Daw, N. D., Tank, D. W., et al. (2019). Specialized coding of sensory, motor and cognitive variables in vta dopamine neurons. *Nature*, 570(7762):509–513.

Fanselow, M. S. and LeDoux, J. E. (1999). Why we think plasticity underlying pavlovian fear conditioning occurs in the basolateral amygdala. *Neuron*, 23(2):229–232.

Flexner, J. B., Flexner, L. B., and Stellar, E. (1963). Memory in mice as affected by intracerebral puromycin. *Science*, 141(3575):57–59.

Foster, D. J. and Wilson, M. A. (2006). Reverse replay of behavioural sequences in hippocampal place cells during the awake state. *Nature*, 440(7084):680–683.

Frankland, P. W. and Bontempi, B. (2005). The organization of recent and remote memories. *Nature reviews neuroscience*, 6(2):119–130.

Frankland, P. W., Bontempi, B., Talton, L. E., Kaczmarek, L., and Silva, A. J. (2004). The involvement of the anterior cingulate cortex in remote contextual fear memory. *Science*, 304(5672):881–883.

Geier, K. T., Buchsbaum, B. R., Parimoo, S., and Olsen, R. K. (2020). The role of anterior and medial dorsal thalamus in associative memory encoding and retrieval. *Neuropsychologia*, 148:107623.

Ghods-Sharifi, S., Onge, J. R. S., and Floresco, S. B. (2009). Fundamental contribution by the basolateral amygdala to different forms of decision making. *Journal of Neuroscience*, 29(16):5251–5259.

Ghosh, K. K., Burns, L. D., Cocker, E. D., Nimmerjahn, A., Ziv, Y., Gamal, A. E., and Schnitzer, M. J. (2011). Miniaturized integration of a fluorescence microscope. *Nature methods*, 8(10):871–878.

Gilmore, A. W., Quach, A., Kalinowski, S. E., González-Araya, E. I., Gotts, S. J., Schacter, D. L., and Martin, A. (2021). Evidence supporting a time-limited hippocampal role in retrieving autobiographical memories. *Proceedings of the National Academy of Sciences*, 118(12):e2023069118.

Girardeau, G., Benchenane, K., Wiener, S. I., Buzsáki, G., and Zugaro, M. B. (2009). Selective suppression of hippocampal ripples impairs spatial memory. *Nature neuroscience*, 12(10):1222–1223.

Glas, A., Hübener, M., Bonhoeffer, T., and Goltstein, P. M. (2019). Benchmarking miniaturized microscopy against two-photon calcium imaging using single-cell orientation tuning in mouse visual cortex. *PloS one*, 14(4):e0214954.

Golob, E. J. and Taube, J. S. (1997). Head direction cells and episodic spatial information in rats without a hippocampus. *Proceedings of the National Academy of Sciences*, 94(14):7645–7650.

Goodridge, J. P. and Taube, J. S. (1997). Interaction between the postsubiculum and anterior thalamus in the generation of head direction cell activity. *Journal of Neuroscience*, 17(23):9315–9330.

Hamann, S. B., Ely, T. D., Grafton, S. T., and Kilts, C. D. (1999). Amygdala activity related to enhanced memory for pleasant and aversive stimuli. *Nature neuroscience*, 2(3):289–293.

Harding, A., Halliday, G., Caine, D., and Kril, J. (2000). Degeneration of anterior thalamic nuclei differentiates alcoholics with amnesia. *Brain*, 123(1):141–154.

Harris, J. A., Mihalas, S., Hirokawa, K. E., Whitesell, J. D., Choi, H., Bernard, A., Bohn, P., Caldejon, S., Casal, L., Cho, A., et al. (2019). Hierarchical organization of cortical and thalamic connectivity. *Nature*, 575(7781):195–202.

Hartley, D. (1791). *Observations on man: his frame, his duty, and his expectations. In two parts*, volume 1. J. Johnson.

Harvey, C. D., Coen, P., and Tank, D. W. (2012). Choice-specific sequences in parietal cortex during a virtual-navigation decision task. *Nature*, 484(7392):62–68.

Harvey, C. D., Collman, F., Dombeck, D. A., and Tank, D. W. (2009). Intracellular dynamics of hippocampal place cells during virtual navigation. *Nature*, 461(7266):941–946.

Hebb, D. O. (1949). *The organization of behavior: a neuropsychological theory*. Science editions.

Helmchen, F., Fee, M. S., Tank, D. W., and Denk, W. (2001). A miniature head-mounted two-photon microscope: high-resolution brain imaging in freely moving animals. *Neuron*, 31(6):903–912.

Hofer, S. B., Mrsic-Flogel, T. D., Bonhoeffer, T., and Hübener, M. (2009). Experience leaves a lasting structural trace in cortical circuits. *Nature*, 457(7227):313–317.

Holscher, C., Schnee, A., Dahmen, H., Setia, L., and Mallot, H. A. (2005). Rats are able to navigate in virtual environments. *Journal of Experimental Biology*, 208(3):561–569.

Ito, H. T., Zhang, S.-J., Witter, M. P., Moser, E. I., and Moser, M.-B. (2015). A prefrontal–thalamo–hippocampal circuit for goal-directed spatial navigation. *Nature*, 522(7554):50–55.

Jankowski, M. M., Ronnqvist, K. C., Tsanov, M., Vann, S. D., Wright, N. F., Erichsen, J. T., Aggleton, J. P., and O'mara, S. M. (2013). The anterior thalamus provides a subcortical circuit supporting memory and spatial navigation. *Frontiers in systems neuroscience*, 7:45.

Jay, T. M., Thierry, A.-M., Wiklund, L., and Glowinski, J. (1992). Excitatory amino acid pathway from the hippocampus to the prefrontal cortex. contribution of ampa receptors in hippocampo-prefrontal cortex transmission. *European journal of neuroscience*, 4(12):1285–1295.

Joo, H. R. and Frank, L. M. (2018). The hippocampal sharp wave–ripple in memory retrieval for immediate use and consolidation. *Nature Reviews Neuroscience*, 19(12):744–757.

Juavinett, A. L., Bekheet, G., and Churchland, A. K. (2019). Chronically implanted neuropixels probes enable high-yield recordings in freely moving mice. *Elife*, 8:e47188.

Kapur, N. (1997). How can we best explain retrograde amnesia in human memory disorder? *Memory*, 5(1-2):115–130.

Keene, C. S. and Bucci, D. J. (2008). Contributions of the retrosplenial and posterior parietal cortices to cue-specific and contextual fear conditioning. *Behavioral neuroscience*, 122(1):89.

Kim, C. K., Yang, S. J., Pichamoorthy, N., Young, N. P., Kauvar, I., Jennings, J. H., Lerner, T. N., Berndt, A., Lee, S. Y., Ramakrishnan, C., et al. (2016). Simultaneous fast measurement of circuit dynamics at multiple sites across the mammalian brain. *Nature methods*, 13(4):325–328.

Kim, J. J. and Fanselow, M. S. (1992). Modality-specific retrograde amnesia of fear. *Science*, 256(5057):675–677.

Kitamura, T., Ogawa, S. K., Roy, D. S., Okuyama, T., Morrissey, M. D., Smith, L. M., Redondo, R. L., and Tonegawa, S. (2017). Engrams and circuits crucial for systems consolidation of a memory. *Science*, 356(6333):73–78.

Konorski, J. (1948). Conditioned reflexes and neuron organization.

Korsakoff, S. S. (1887). Disturbance of psychic function in alcoholic paralysis and its relation to the disturbance of the psychic sphere in multiple neuritis of non-alcoholic origin. *Vestnik Psichiatrii*, 4(2):1–102.

Korsakoff, S. S. (1889). Etude médico-psychologique sur une forme des maladies de la mémoire. *Revue Philosophique*, 28(501):e530.

Lashley, K. S. (1950). In search of the engram.

Lesburguères, E., Gobbo, O. L., Alaux-Cantin, S., Hambucken, A., Trifilieff, P., and Bontempi, B. (2011). Early tagging of cortical networks is required for the formation of enduring associative memory. *Science*, 331(6019):924–928.

Li, W., Ma, L., Yang, G., and Gan, W.-B. (2017). Rem sleep selectively prunes and maintains new synapses in development and learning. *Nature neuroscience*, 20(3):427–437.

Lisman, J., Grace, A. A., and Duzel, E. (2011). A neohebbian framework for episodic memory; role of dopamine-dependent late ltp. *Trends in neurosciences*, 34(10):536–547.

Lisman, J., Schulman, H., and Cline, H. (2002). The molecular basis of camkii function in synaptic and behavioural memory. *Nature Reviews Neuroscience*, 3(3):175–190.

Liu, J., Yu, T., Wu, J., Pan, Y., Tan, Z., Liu, R., Wang, X., Ren, L., and Wang, L. (2021). Anterior thalamic stimulation improves working memory precision judgments. *Brain Stimulation*, 14(5):1073–1080.

Mahn, M., Gibor, L., Patil, P., Cohen-Kashi Malina, K., Oring, S., Printz, Y., Levy, R., Lampl, I., and Yizhar, O. (2018). High-efficiency optogenetic silencing with soma-targeted anion-conducting channelrhodopsins. *Nature communications*, 9(1):1–15.

Maingret, N., Girardeau, G., Todorova, R., Goutierre, M., and Zugaro, M. (2016). Hippocampo-cortical coupling mediates memory consolidation during sleep. *Nature neuroscience*, 19(7):959–964.

Mair, R. G., Burk, J. A., and Porter, M. C. (2003). Impairment of radial maze delayed nonmatching after lesions of anterior thalamus and parahippocampal cortex. *Behavioral Neuroscience*, 117(3):596.

Marr, D. (1970). A theory for cerebral neocortex. *Proceedings of the Royal society of London. Series B. Biological sciences*, 176(1043):161–234.

Marr, D. (1971). Simple memory: a theory for archicortex. *Philos. Trans. R. Soc. Lond. B Biol. Sci.*, 262(841):23–81.

Maviel, T., Durkin, T. P., Menzaghi, F., and Bontempi, B. (2004). Sites of neocortical reorganization critical for remote spatial memory. *Science*, 305(5680):96–99.

McClelland, J. L., McNaughton, B. L., and O'Reilly, R. C. (1995). Why there are complementary learning systems in the hippocampus and neocortex: insights from the successes and failures of connectionist models of learning and memory. *Psychological review*, 102(3):419.

Moreau, P.-H., Tsenkina, Y., Lecourtier, L., Lopez, J., Cosquer, B., Wolff, M., Dalrymple-Alford, J., and Cassel, J.-C. (2013). Lesions of the anterior thalamic nuclei and intralaminar thalamic nuclei: place and visual discrimination learning in the water maze. *Brain Structure and Function*, 218(3):657–667.

Morris, R. G., Garrud, P., Rawlins, J. a., and O'Keefe, J. (1982). Place navigation impaired in rats with hippocampal lesions. *Nature*, 297(5868):681–683.

Mukherjee, A., Lam, N. H., Wimmer, R. D., and Halassa, M. M. (2021). Thalamic circuits for independent control of prefrontal signal and noise. *Nature*, 600(7887):100–104.

Müller, G. E. and Pilzecker, A. (1900). *Experimentelle beiträge zur lehre vom gedächtniss*, volume 1. JA Barth.

Naber, P. A., Lopes da Silva, F. H., and Witter, M. P. (2001). Reciprocal connections between the entorhinal cortex and hippocampal fields ca1 and the subiculum are in register with the projections from ca1 to the subiculum. *Hippocampus*, 11(2):99–104.

Nadel, L. and Moscovitch, M. (1997). Memory consolidation, retrograde amnesia and the hippocampal complex. *Current opinion in neurobiology*, 7(2):217–227.

Nader, K. (2016). Reconsolidation and the dynamic nature of memory. *Novel mechanisms of memory*, pages 1–20.

O'Reilly, R. C. and Rudy, J. W. (2000). Computational principles of learning in the neocortex and hippocampus. *Hippocampus*, 10(4):389–397.

Papez, J. W. (1937). A proposed mechanism of emotion. *Archives of Neurology & Psychiatry*, 38(4):725–743.

Paré, D. (2003). Role of the basolateral amygdala in memory consolidation. *Progress in neurobiology*, 70(5):409–420.

Pergola, G., Ranft, A., Mathias, K., and Suchan, B. (2013). The role of the thalamic nuclei in recognition memory accompanied by recall during encoding and retrieval: an fmri study. *Neuroimage*, 74:195–208.

Pfeiffer, B. E. and Foster, D. J. (2013). Hippocampal place-cell sequences depict future paths to remembered goals. *Nature*, 497(7447):74–79.

Pnevmatikakis, E. A. and Giovannucci, A. (2017). Normcorre: An online algorithm for piecewise rigid motion correction of calcium imaging data. *Journal of neuroscience methods*, 291:83–94.

Radvansky, B. A. and Dombeck, D. A. (2018). An olfactory virtual reality system for mice. *Nature communications*, 9(1):1–14.

Rajasethupathy, P., Sankaran, S., Marshel, J. H., Kim, C. K., Ferenczi, E., Lee, S. Y., Berndt, A., Ramakrishnan, C., Jaffe, A., Lo, M., et al. (2015). Projections from neocortex mediate top-down control of memory retrieval. *Nature*, 526(7575):653–659.

Ramón y Cajal, S. (1894). The croonian lecture.—la fine structure des centres nerveux. *Proceedings of the Royal Society of London*, 55(331-335):444–468.

Remondes, M. and Schuman, E. M. (2004). Role for a cortical input to hippocampal area ca1 in the consolidation of a long-term memory. *Nature*, 431(7009):699–703.

Remondes, M. and Wilson, M. A. (2015). Slow-γ rhythms coordinate cingulate cortical responses to hippocampal sharp-wave ripples during wakefulness. *Cell reports*, 13(7):1327–1335.

Rempel-Clower, N. L., Zola, S. M., Squire, L. R., and Amaral, D. G. (1996). Three cases of enduring memory impairment after bilateral damage limited to the hippocampal formation. *Journal of Neuroscience*, 16(16):5233–5255.

Ribot, T. (1883). The diseases of memory (j. fitzgerald, trans.). *New York: Fitzgerald*.

Robinson, N. T., Priestley, J. B., Rueckemann, J. W., Garcia, A. D., Smeglin, V. A., Marino, F. A., and Eichenbaum, H. (2017). Medial entorhinal cortex selectively supports temporal coding by hippocampal neurons. *Neuron*, 94(3):677–688.

Rothschild, G. (2019). The transformation of multi-sensory experiences into memories during sleep. *Neurobiology of learning and memory*, 160:58–66.

Roy, D. S., Park, Y.-G., Kim, M. E., Zhang, Y., Ogawa, S. K., DiNapoli, N., Gu, X., Cho, J. H., Choi, H., Kamentsky, L., et al. (2022). Brain-wide mapping reveals that engrams for a single memory are distributed across multiple brain regions. *Nature communications*, 13(1):1–16.

Russell, W. R. and Nathan, P. (1946). Traumatic amnesia. *Brain*, 69:280–300.

Rutishauser, U., Mamelak, A. N., and Schuman, E. M. (2006). Single-trial learning of novel stimuli by individual neurons of the human hippocampus-amygdala complex. *Neuron*, 49(6):805–813.

Salmon, D. P., Zola-Morgan, S., and Squire, L. R. (1987). Retrograde amnesia following combined hippocampus-amygdala lesions in monkeys. *Psychobiology*, 15(1):37–47.

Sampathkumar, V., Miller-Hansen, A., Sherman, S. M., and Kasthuri, N. (2021). Integration of signals from different cortical areas in higher order thalamic neurons. *Proceedings of the National Academy of Sciences*, 118(30):e2104137118.

Sanders, H. I. and Warrington, E. K. (1971). Memory for remote events in amnesic patients. *Brain*, 94(4):661–668.

Schwarz, L. A., Miyamichi, K., Gao, X. J., Beier, K. T., Weissbourd, B., DeLoach, K. E., Ren, J., Ibanes, S., Malenka, R. C., Kremer, E. J., et al. (2015). Viral-genetic tracing of the input–output organization of a central noradrenaline circuit. *Nature*, 524(7563):88–92.

Scoville, W. B. and Milner, B. (1957). Loss of recent memory after bilateral hippocampal lesions. *Journal of neurology, neurosurgery, and psychiatry*, 20(1):11.

Serrano, P., Friedman, E. L., Kenney, J., Taubenfeld, S. M., Zimmerman, J. M., Hanna, J., Alberini, C., Kelley, A. E., Maren, S., Rudy, J. W., et al. (2008). Pkmζ maintains spatial, instrumental, and classically conditioned long-term memories. *PLoS biology*, 6(12):e318.

Sheintuch, L., Rubin, A., Brande-Eilat, N., Geva, N., Sadeh, N., Pinchasof, O., and Ziv, Y. (2017). Tracking the same neurons across multiple days in ca2+ imaging data. *Cell reports*, 21(4):1102–1115.

Shibata, H. and Naito, J. (2005). Organization of anterior cingulate and frontal cortical projections to the anterior and laterodorsal thalamic nuclei in the rat. *Brain research*, 1059(1):93–103.

Shimizu, E., Tang, Y.-P., Rampon, C., and Tsien, J. Z. (2000). Nmda receptor-dependent synaptic reinforcement as a crucial process for memory consolidation. *Science*, 290(5494):1170–1174.

Shohamy, D. and Adcock, R. A. (2010). Dopamine and adaptive memory. *Trends in cognitive sciences*, 14(10):464–472.

Siapas, A. G. and Wilson, M. A. (1998). Coordinated interactions between hippocampal ripples and cortical spindles during slow-wave sleep. *Neuron*, 21(5):1123–1128.

Smith, J. F., Alexander, G. E., Chen, K., Husain, F. T., Kim, J., Pajor, N., and Horwitz, B. (2010). Imaging systems level consolidation of novel associate memories: a longitudinal neuroimaging study. *Neuroimage*, 50(2):826–836.

Sofroniew, N. J., Flickinger, D., King, J., and Svoboda, K. (2016). A large field of view two-photon mesoscope with subcellular resolution for in vivo imaging. *elife*, 5:e14472.

Squire, L. R. (1992). Declarative and nondeclarative memory: Multiple brain systems supporting learning and memory. *Journal of cognitive neuroscience*, 4(3):232–243.

Squire, L. R. and Alvarez, P. (1995). Retrograde amnesia and memory consolidation: a neurobiological perspective. *Current opinion in neurobiology*, 5(2):169–177.

Squire, L. R., Genzel, L., Wixted, J. T., and Morris, R. G. (2015). Memory consolidation. *Cold Spring Harbor perspectives in biology*, 7(8):a021766.

Sutherland, R. J., Lee, J. Q., McDonald, R. J., and Lehmann, H. (2020). Has multiple trace theory been refuted? *Hippocampus*, 30(8):842–850.

Takehara, K., Kawahara, S., and Kirino, Y. (2003). Time-dependent reorganization of the brain components underlying memory retention in trace eyeblink conditioning. *Journal of Neuroscience*, 23(30):9897–9905.

Takehara-Nishiuchi, K. (2014). Entorhinal cortex and consolidated memory. *Neuroscience Research*, 84:27–33.

Takehara-Nishiuchi, K., Maal-Bared, G., and Morrissey, M. D. (2012). Increased entorhinal–prefrontal theta synchronization parallels decreased entorhinal–hippocampal theta synchronization during learning and consolidation of associative memory. *Frontiers in behavioral neuroscience*, 5:90.

Taube, J. S. (1995). Head direction cells recorded in the anterior thalamic nuclei of freely moving rats. *Journal of Neuroscience*, 15(1):70–86.

Taube, J. S. (2007). The head direction signal: origins and sensory-motor integration. *Annual review of neuroscience*, 30(1):181–207.

Teng, E. and Squire, L. R. (1999). Memory for places learned long ago is intact after hippocampal damage. *Nature*, 400(6745):675–677.

Tipps, M. E., Raybuck, J. D., Buck, K. J., and Lattal, K. M. (2014). Delay and trace fear conditioning in c57bl/6 and dba/2 mice: issues of measurement and performance. *Learning & Memory*, 21(8):380–393.

Todd, T. P. and Bucci, D. J. (2015). Retrosplenial cortex and long-term memory: molecules to behavior. *Neural plasticity*, 2015.

Tononi, G. and Cirelli, C. (2014). Sleep and the price of plasticity: from synaptic and cellular homeostasis to memory consolidation and integration. *Neuron*, 81(1):12–34.

Tsanov, M., Chah, E., Vann, S. D., Reilly, R. B., Erichsen, J. T., Aggleton, J. P., and O'Mara, S. M. (2011). Theta-modulated head direction cells in the rat anterior thalamus. *Journal of Neuroscience*, 31(26):9489–9502.

Tse, D., Takeuchi, T., Kakeyama, M., Kajii, Y., Okuno, H., Tohyama, C., Bito, H., and Morris, R. G. (2011). Schema-dependent gene activation and memory encoding in neocortex. *Science*, 333(6044):891–895.

Tulving, E., Schacter, D. L., Mclachlan, D. R., and Moscovitch, M. (1988). Priming of semantic autobiographical knowledge: A case study of retrograde amnesia. *Brain and cognition*, 8(1):3–20.

Van Groen, T. and Wyss, J. M. (2003). Connections of the retrosplenial granular b cortex in the rat. *Journal of Comparative Neurology*, 463(3):249–263.

Vann, S. D. and Aggleton, J. P. (2004). The mammillary bodies: two memory systems in one? *Nature Reviews Neuroscience*, 5(1):35–44.

Vann, S. D. and Nelson, A. J. (2015). The mammillary bodies and memory: more than a hippocampal relay. *Progress in brain research*, 219:163–185.

Vetere, G., Restivo, L., Cole, C. J., Ross, P. J., Ammassari-Teule, M., Josselyn, S. A., and Frankland, P. W. (2011). Spine growth in the anterior cingulate cortex is necessary for the consolidation of contextual fear memory. *Proceedings of the National Academy of Sciences*, 108(20):8456–8460.

Vetere, G., Xia, F., Ramsaran, A. I., Tran, L. M., Josselyn, S. A., and Frankland, P. W. (2021). An inhibitory hippocampal–thalamic pathway modulates remote memory retrieval. *Nature neuroscience*, 24(5):685–693.

Viskontas, I. V., McAndrews, M. P., and Moscovitch, M. (2002). Memory for famous people in patients with unilateral temporal lobe epilepsy and excisions. *Neuropsychology*, 16(4):472.

Wang, D. V. and Ikemoto, S. (2016). Coordinated interaction between hippocampal sharp-wave ripples and anterior cingulate unit activity. *Journal of Neuroscience*, 36(41):10663–10672.

Wassum, K. M. and Izquierdo, A. (2015). The basolateral amygdala in reward learning and addiction. *Neuroscience & Biobehavioral Reviews*, 57:271–283.

Weisenburger, S., Tejera, F., Demas, J., Chen, B., Manley, J., Sparks, F. T., Traub, F. M., Daigle, T., Zeng, H., Losonczy, A., et al. (2019). Volumetric ca2+ imaging in the mouse brain using hybrid multiplexed sculpted light microscopy. *Cell*, 177(4):1050–1066.

Willis, T. (1664). *Cerebri anatome : cui accessit Nervorum descriptio et usu.* Typis Tho. Roycroft, Impensis Jo. Martyn Ja. Allestry.

Wiltgen, B. J., Brown, R. A., Talton, L. E., and Silva, A. J. (2004). New circuits for old memories: the role of the neocortex in consolidation. *Neuron*, 44(1):101–108.

Winocur, G. (1990). Anterograde and retrograde amnesia in rats with dorsal hippocampal or dorsomedial thalamic lesions. *Behavioural brain research*, 38(2):145–154.

Winocur, G., Moscovitch, M., and Bontempi, B. (2010). Memory formation and long-term retention in humans and animals: Convergence towards a transformation account of hippocampal–neocortical interactions. *Neuropsychologia*, 48(8):2339–2356.

Winter, S. S., Clark, B. J., and Taube, J. S. (2015). Disruption of the head direction cell network impairs the parahippocampal grid cell signal. *Science*, 347(6224):870–874.

Wirth, S., Avsar, E., Chiu, C. C., Sharma, V., Smith, A. C., Brown, E., and Suzuki, W. A. (2009). Trial outcome and associative learning signals in the monkey hippocampus. *Neuron*, 61(6):930–940.

Wirth, S., Yanike, M., Frank, L. M., Smith, A. C., Brown, E. N., and Suzuki, W. A. (2003). Single neurons in the monkey hippocampus and learning of new associations. *Science*, 300(5625):1578–1581.

Witter, M. P., Doan, T. P., Jacobsen, B., Nilssen, E. S., and Ohara, S. (2017). Architecture of the entorhinal cortex a review of entorhinal anatomy in rodents with some comparative notes. *Frontiers in systems neuroscience*, 11:46.

Wittmann, B. C., Schott, B. H., Guderian, S., Frey, J. U., Heinze, H.-J., and Düzel, E. (2005). Reward-related fmri activation of dopaminergic midbrain is associated with enhanced hippocampus-dependent long-term memory formation. *Neuron*, 45(3):459–467.

Wolff, M., Gibb, S. J., and Dalrymple-Alford, J. C. (2006). Beyond spatial memory: the anterior thalamus and memory for the temporal order of a sequence of odor cues. *Journal of Neuroscience*, 26(11):2907–2913.

Wright, N. F., Erichsen, J. T., Vann, S. D., O'Mara, S. M., and Aggleton, J. P. (2010). Parallel but separate inputs from limbic cortices to the mammillary bodies and anterior thalamic nuclei in the rat. *Journal of Comparative Neurology*, 518(12):2334–2354.

Wu, X. and Foster, D. J. (2014). Hippocampal replay captures the unique topological structure of a novel environment. *Journal of Neuroscience*, 34(19):6459–6469.

Xu, X., Holmes, T. C., Luo, M.-H., Beier, K. T., Horwitz, G. D., Zhao, F., Zeng, W., Hui, M., Semler, B. L., and Sandri-Goldin, R. M. (2020). Viral vectors for neural circuit mapping and recent advances in trans-synaptic anterograde tracers. *Neuron*, 107(6):1029–1047.

Yadav, N., Noble, C., Niemeyer, J. E., Terceros, A., Victor, J., Liston, C., and Rajasethupathy, P. (2022). Prefrontal feature representations drive memory recall. *Nature*, 608(7921):153–160.

Yang, C., Hu, Y., Talishinsky, A. D., Potter, C. T., Calva, C. B., Ramsey, L. A., Kesner, A. J., Don, R. F., Junn, S., Tan, A., et al. (2022). Medial prefrontal cortex and anteromedial thalamus interaction regulates goal-directed behavior and dopaminergic neuron activity. *Nature communications*, 13(1):1–20.

Yang, W. and Yuste, R. (2017). In vivo imaging of neural activity. *Nature methods*, 14(4):349–359.

Yang, Y. and Wang, J.-Z. (2017). From structure to behavior in basolateral amygdala-hippocampus circuits. *Frontiers in neural circuits*, 11:86.

Yizhar, O., Fenno, L. E., Prigge, M., Schneider, F., Davidson, T. J., O'shea, D. J., Sohal, V. S., Goshen, I., Finkelstein, J., Paz, J. T., et al. (2011). Neocortical excitation/inhibition balance in information processing and social dysfunction. *Nature*, 477(7363):171–178.

Yonelinas, A. P., Ranganath, C., Ekstrom, A. D., and Wiltgen, B. J. (2019). A contextual binding theory of episodic memory: systems consolidation reconsidered. *Nature Reviews Neuroscience*, 20(6):364–375.

Zhou, P., Resendez, S. L., Rodriguez-Romaguera, J., Jimenez, J. C., Neufeld, S. Q., Giovannucci, A., Friedrich, J., Pnevmatikakis, E. A., Stuber, G. D., Hen, R., et al. (2018). Efficient and accurate extraction of in vivo calcium signals from microendoscopic video data. *elife*, 7:e28728.

Zhu, Y., Nachtrab, G., Keyes, P. C., Allen, W. E., Luo, L., and Chen, X. (2018). Dynamic salience processing in paraventricular thalamus gates associative learning. *Science*, 362(6413):423–429.

Ziv, Y., Burns, L. D., Cocker, E. D., Hamel, E. O., Ghosh, K. K., Kitch, L. J., Gamal, A. E., and Schnitzer, M. J. (2013). Long-term dynamics of ca1 hippocampal place codes. *Nature neuroscience*, 16(3):264–266.

Zola-Morgan, S., Squire, L. R., and Amaral, D. G. (1986). Human amnesia and the medial temporal region: enduring memory impairment following a bilateral lesion limited to field ca1 of the hippocampus. *Journal of neuroscience*, 6(10):2950–2967.

Zola-Morgan, S. M. and Squire, L. R. (1990). The primate hippocampal formation: evidence for a time-limited role in memory storage. *Science*, 250(4978):288–290.